SPECTROSCOPIC CHARACTERIZATION OF HYDROGEN BONDED AND HALOGEN BONDED INTERACTIONS

A Dissertation

by

KEVIN WAYNE SCOTT, JR.

Submitted to the Office of Graduate and Professional Studies of
Texas A&M University
in partial fulfillment of the requirements for the degree of

DOCTOR OF PHILOSOPHY

Chair of Committee,	Robert R. Lucchese
Committee Members,	Dong Hee Son
	Steven Wheeler
	Mike McShane
Head of Department,	Simon W. North

August 2016

Major Subject: Chemistry

ABSTRACT

Prototypical hydrogen-bonded and halogen-bonded systems give unique insight into the characteristics of weakly interacting systems. Spectroscopic analysis of fundamental, combination, and hot bands of these types of systems has yielded structural properties, molecular dynamics and other molecular parameters. The experimental results from the gas-phase spectroscopy were compared with the results of compound-model morphed potentials.

Experimental spectroscopic analysis was accomplished through the application of a near infrared quantum cascade laser (QCL) based spectrometer to a continuous wave supersonic slit jet expansion with several different combinations of CO and HX (X= F, Cl, Br, I, CN, CCH) species. Spectroscopic analysis of fundamental, combination and hot bands of the CO stretching vibrations provided rovibrational parameters for low frequency intermolecular vibrations. Investigation into the blue frequency shifts in the complexes of the C-O vibrations permitted comparison of the strength and of the resulting effects of the hydrogen and halogen bonding within the systems.

Structural properties and other molecular parameters of OC-HCN were compared with corresponding properties predicted using morphed potentials for the homologous series OC-HX (X = F, Cl, Br, I). Analysis of ν_2, $\nu_2+\nu_7^1-\nu_7^1$, $\nu_2+\nu_7^1$, and $\nu_2+\nu_6^1$ vibrations in OC-HCN enabled the generation of a 5-dimensional semi-empirical intermolecular potential. A five-dimensional compound-model morphed potential was also generated for the halogen-bonded intermolecular interaction OC-BrCl, which could

then be compared with the alternatively hydrogen-bonded dimers OC-HX (X = F, Cl, Br) giving further insight into the nature of these types of interactions.

A new spectrometer was designed to enable the study of DI. The ν_1 spectra of OC-DI and OC-ID, as well as ν_2 of OC-DI and OC-ID have been recorded using a quantum cascade laser pulsed slit supersonic jet spectrometer with an astigmatic multipass cell. The results confirmed the prediction of ground state deuterium isotopic isomerization, originally proposed by using a generated morphed potential.

Finally, another new quantum cascade laser spectrometer was designed to utilize a continuous wave supersonic slit jet expansion with an astigmatic multipass cell. The spectrum of Ar-NO was recorded over the region 1856.8-1887.4 cm^{-1} followed by the recording of the NO-H_2O spectra in this region, both of which had never before been recorded in these regions and are open-shell systems.

ACKNOWLEDGEMENTS

I first would like to express my appreciation for my late committee chair and advisor, Dr. Bevan, for his tutelage and support over the course of the research represented in this work. I also express my deepest thankfulness for Dr. Robert Lucchese, for his willingness to act as my committee chair in Dr. Bevan's stead. I would like to express a special thankfulness all of those who served on my first committee for their assistance and support: Dr. Lucchese, Dr. Son, and Dr. Agnolet, in addition to Dr. Wheeler, as he served as a substitute on multiple occasions. Dr. Agnolet deserves special recognition as he served as my undergraduate advisor in the Physics Department at Texas A&M University. I also sincerely thank all those who served on my final committee: Dr. Lucchese, Dr. Son, Dr. Wheeler, and Dr. McShane, in addition to Dr. Hilty, as he served as a substitute in the final exam. I would like to note and thank Dr. Son, Dr. Hilty, and Dr. North for their assistance in the transition and completion of CHEM 322 during the semester of Dr. Bevan's passing. I also hold immense appreciation and gratitude toward Dr. Mike McShane, who has provided such encouragement, both personally and spiritually, of which, I regret to say, he does not know the full extent.

Fellow research group members, Dr. McElmerry, Dr. Willaert, Dr. Wang, and Sean Springer, in addition to colleague Dr. Rivera-Rivera, have served as invaluable sources of advice, support, assistance and camaraderie, and I thank each of them. I thank the administrators and staff who have assisted in both of my degrees from Texas A&M

University, with specific gratitude for the Department of Chemistry, the Supercomputing Facility, and Organic Chemistry Laboratory Program. I also thank the National Science Foundation and the Robert A. Welch Foundation for their financial support of this research.

I extol and extend my deepest appreciation to my mother and father and my Megan. Their love, patience and support have made the results herein reported possible to obtain. They truly have been wonderful to me, and continually build me up in faith.

Finally, I feel compelled to make a brief statement in regard to Dr. Bevan:

Dr. John W. Bevan was a man whose passion was chemistry. This was most widely seen in his role as an educator, but its depth was not fully realized until one observed his passion at play in his mentoring capacities and scientific investigations.

I first encountered Dr. Bevan in a junior level physical chemistry class. In the first lecture, he was literally overflowing with excitement over the role that quantum mechanics plays in chemistry. Throughout the semester his passion for chemistry shined in every lecture.

In office hours, he would speak with small groups of students for hours on end about applications of spectroscopy and new developments that had the potential to make huge conceptual shifts in our understanding of chemistry. I remember one instance when we were discussing some research that claimed to disprove the Pauli exclusion principle, and Dr. Bevan systematically broke down the arguments and provided an alternative interpretation for the results, including a philosophical debunking of the impetus for the

original misinterpretation of the experimental data. Dr. Bevan had an insatiable passion for chemistry and truly could not help but to share it with his students.

As a graduate student, I saw this passion on a daily basis. His zeal in teaching carried directly over to the research lab as he worked side by side with his students, both graduate and undergraduate alike. His love for chemistry was a noble example and inspiration.

TABLE OF CONTENTS

Page

ABSTRACT ii

ACKNOWLEDGEMENTS iv

TABLE OF CONTENTS vii

LIST OF FIGURES ix

LIST OF TABLES xi

1. INTRODUCTION 1

    1.1 Weak Intermolecular Interactions 1
    1.2 The Forces of Intermolecular Interactions 3
    1.3 The Quantum Cascade Laser 6

2. QUANTUM CASCADE LASER SPECTROSCOPY INVESTIGATIONS INTO HYDROGEN AND HALOGEN BONDED INTERACTIONS 8

    2.1 Background 8
    2.2 Methods 14
    2.3 Results and Discussion 17

3. CONTRASTING HALOGEN-BONDED AND HYDROGEN-BONDED COMPLEXES 25

    3.1 Background 25
    3.2 Methods 31
    3.3 Results and Discussion 34

4. ISOTOPIC ISOMERIZATION: THE DEUTERATION EFFECT IN OC-HI CONFIRMED 43

    4.1 Background 43
    4.2 Methods 47
    4.3 Results and Discussion 50

5. BADGER-BAUER REVISITED: A MODEL 63

5.1 Background 63
5.2 Impact and Application 68

6. INVESTIGATIONS INTO AR-NO AND NO-H_2O 76

6.1 Background for Ar-NO and for NO-H_2O 76
6.2 Methods for Ar-NO Investigations 80
6.3 Methods for NO-H_2O Investigations 82
6.4 Findings from Ar-NO and NO-H_2O Investigations 83

7. CONCLUSION 92

REFERENCES 96

LIST OF FIGURES

Page

Figure 1. Conduction band energy diagram from Faist, et al 7

Figure 2. Diagram of cw QCL supersonic slit jet spectrometer 9

Figure 3. OC-HCN ν_2 broadband spectrum from QCL spectrometer 10

Figure 4. Spectrum of OC-H^{35}Cl recorded using a cw slit jet QCL spectrometer showing the ν_2, CO stretching vibration, $\nu_2 + \nu_5^1 - \nu_5^1$, and $\nu_2 + \nu_3 - \nu_3$ hot bands 17

Figure 5. QCL spectrum of the Q(J) branch of the $\nu_2 + \nu_6^1$ combination band of OC-HCN 21

Figure 6. Jacobi coordinates for OC-BrCl dimer 27

Figure 7. Spectrum of OC-BrCl over the region 2156.0 cm^{-1} to 2158.2 cm^{-1} 34

Figure 8. Illustration of zero point energy effects on deuterium isotopic isomerization in the OC-HI/OC-IH isomers and those predicted for the corresponding OC-DI/OC-ID isomers 46

Figure 9. The path of the pulsed laser to the etalon, reference cell, and astigmatic cell allowing for an immediate measurable comparison of reference to sample on the computer display 48

Figure 10. Experimental spectrum and simulation with a rotational temperature of 8 K and energy difference between isomers of 6 cm^{-1} with a selection of the spectral transitions used to compare peak intensity marked 51

Figure 11. Simultaneous frequency scan in the range of 2147.6 cm^{-1} to 2148.9 cm^{-1} for OC-DI, OC-ID, and OC-HI 52

Page

Figure 12. Correlation for blue shift of CO stretch and dissociation energy D_0 obtained from morphing. Interpolation gives D_0 for H_2O-CO to be 355(13) cm^{-1} 64

Figure 13. Correlation of D_i from *ab initio* morphed potentials and from the model with predicted harmonic frequency shifts in CO for OC-HX (X=F, Cl, Br, CN) 70

Figure 14. Meyer's experimental investigation of Ar-NO via IR-REMPI in the bottom spectrum, with calculated predictions from Klos and Alexander's theoretical studies visualized in the top three spectra..... 77

Figure 15. Full spectrum of Ar-NO over the region 1856.8 cm^{-1} to 1887.4 cm^{-1} investigated with the cw QCL supersonic slit jet spectrometer with an astigmatic multipass cell 83

Figure 16. Segment of Ar-NO spectrum from 1858.9 cm^{-1} to 1859.6 cm^{-1} containing "Band pre-A." 85

Figure 17. Ar-NO spectrum over the region 1865.0 cm^{-1} to 1870.4 cm^{-1} with three observed bands: "Band B," hot band "Band B1," and "Band C."..... 86

Figure 18. Segment of the Ar-NO spectrum over the region 1886.1 cm^{-1} to 1887.3 cm^{-1}, which includes "Band I."..... 87

Figure 19. Experimental spectrum in the 1882 cm^{-1} to 1881 cm^{-1} range for NO-H_2O. Top spectra is Ar-NO complex serving as reference 88

Figure 20. Experimental spectrum in the 1883 cm^{-1} to 1882 cm^{-1} range for NO-H_2O with the top spectrum of Ar-NO serving as a reference..... 89

Figure 21. Spectrum of NO-H_2O complex with suspected P(J) and R(J) type transitions labeled..... 90

LIST OF TABLES

Page

Table 1. Ro-vibrational constants for observed bands in OC-HCl 18

Table 2. Ro-vibrational constants for observed bands in OC-HF 19

Table 3. Ro-vibrational constants for observed bands in OC-HCN 20

Table 4. Ro-vibrational constants in cm^{-1} for OC-BrCl. Global fit with microwave data. All constants are in cm-1 35

Table 5. Experimental data used in the CMM-RC fits for $^{16}O^{12}C$-$^{79}Br^{35}Cl$. All constants are in cm^{-1} 36

Table 6. Optimized values for the morphing parameters for $^{16}O^{12}C$-$^{79}Br^{35}Cl$ 37

Table 7. Anharmonicity constants (X_{ij}) in cm^{-1} for $^{16}O^{12}C$-$^{79}Br^{35}Cl$, calculated using the potential 38

Table 8. Fundamental intermolecular vibrations and D_0 for OC-BrCl, OC-Cl_2 and OC-HX (X = F, Cl, Br), predicted from the morphed potential. All values are in cm^{-1} 40

Table 9. Observed and residual frequencies of OC-DI and OC-ID infrared transitions 53

Table 10. Rovibrational constants determined from the observed infrared transitions of OC-DI and OC-ID and those determined in previous work from the observed infrared transitions of OC-HI and OC-IH 55

Table 11. Peak intensity ratio of OC-DI to OC-ID and OC-HI to OC-IH obtained from comparing certain J transitions 56

Table 12. Frequency shift of the CO stretch and HI(DI) stretch upon complexation and the dissociation energy of the ground and the excited states 57

Table 13. CO blue frequency shifts and dissociation energies from morphed potentials for OC-HX (X = F, Cl, Br, I, CN, CCH). All data in cm^{-1} 69

Table 14. Dissociation energies D_i, parameters g_i, dR_e/dr, and $\Delta\omega_e$ for model calculations on OC-HX (X = F, Cl, Br, CN). All data in cm^{-1} 69

Table 15. CO harmonic blue frequency shifts and dissociation energies from CCSD(T)/aug-cc-pVQZ calculations for OC-HX (X = F, Cl, Br, I, CN, CCH, OH, SH) 71

Table 16. Observed Ar-NO complex band regions over the infrared frequency region of 1856.8 cm^{-1} to 1887.4 cm^{-1} 84

1. INTRODUCTION

1.1 Weak Intermolecular Interactions

Weak intermolecular interactions are the basis for much of the chemistry that affects mankind every day. Much of these intermolecular interactions take place in a biological context within the cells of living organisms, from the manner in which strands of deoxyribonucleic acid (DNA) structure themselves to the mechanism by which enzymes produce adenosine triphosphate (ATP). Lest one become too focused at the cellular level, intermolecular interactions also play a crucial role in the global energy exchange, in particular, these interactions within water-bound complexes. Furthermore, intermolecular interactions govern much of the atmospheric chemistry that contribute yet again to the global energy exchange. Finally, the intermediate complexes in chemical reactions are influenced by these very interactions.

Much of these intermolecular interactions can be termed hydrogen bonding. A similar phenomenon occurs in the case of halogens and is termed halogen bonding. An elucidation of the characteristics of hydrogen and halogen bonding will allow for models to be developed that can shed a predictive light on areas ranging from cellular life to the impact of a particular molecule on global temperature. Therefore, the study and spectroscopic characterization of these interactions pose a significantly urgent task, in order to better understand the recourses that are necessary for rectifying both bodily and environmentally harmful practices.

With this goal in mind, the research that has been accomplished focused on hydrogen and halogen bonded intermolecular complexes, which were studied in the infrared region of the electromagnetic spectrum. Specifically, methods have been employed to produce rovibrationally cold species, including supersonic slit jet expansions. This particular technique allowed for the intermolecular complexes to form and the vibrational energy states to be spectroscopically observed. This observation has provided insight into the structural characteristics of many intermolecular complexes. With this data, trends and relationships have been observed and reported, and from this data, predictive models have been refined to generate the structure and energy of hydrogen bonded and halogen bonded systems. A few of the selected systems of study have been those of the type OC-HX (X= F, Cl, Br, I, CN). This selection can be expanded to deuterated systems of the type OC-DX, and water bonded complexes such as NO-H_2O.

Investigating systems that improve the understanding of the hydrogen and halogen bonding is an endeavor that can fundamentally alter our understanding of how bonding occurs in all systems. It sheds light on the very foundation of how atoms associate with one another, and the study of these specific complexes has particular significance in affecting mankind's understanding of life on both a cellular and global scale.

1.2 The Forces of Intermolecular Interactions

Intermolecular interactions have such distance between the interacting species that electron exchange can be neglected, due to the fact that electron exchange requires an overlap of the molecular wavefunctions, which deteriorates exponentially with large distances. At this non-covalent bonding distance, the general classification of these forces is van der Waals. According to IUPAC, van der Waals is "the attractive or repulsive forces between molecular entities (or between groups within the same molecular entity) other than those due to bond formation or to the electrostatic interaction of ions or of ionic groups with one another or with neutral molecules. The term includes: dipole-dipole, dipole-induced dipole, and London (instantaneous induced dipole-induced dipole) forces."[1]

Because these forces act over larger distances than bond-formation forces and electron exchange can be neglected, it is useful to approach the interaction Hamiltonian as a perturbation of the free molecules.[2] Perturbation theory gives the following wavefunction for the stationary states $\left|\Psi_{n_a}\Psi_{n_b}\right\rangle$:

$$\left|\Psi_{n_a}\Psi_{n_b}\right\rangle = \left|n_a n_b\right\rangle + \sum_{p_a \cdot q_b} \frac{\left\langle p_a q_b \left| H_{ab} \right| n_a n_b \right\rangle}{W_{n_a} - W_{p_a} + W_{n_b} - W_{q_b}} \left| p_a q_b \right\rangle + \cdots$$

The energy can be given by the following, where the summation is over all unperturbed states except $\left|\Psi_{n_a}\Psi_{n_b}\right\rangle$:

$$W^{(2)}_{n_a n_b} = W_{n_a} + W_{n_b} + \left\langle n_a n_b \left| H_{ab} \right| n_a n_b \right\rangle + \sum_{p_a \cdot q_b} \frac{\left\langle p_a q_b \left| H_{ab} \right| n_a n_b \right\rangle^2}{W_{n_a} - W_{p_a} + W_{n_b} - W_{q_b}} + \cdots$$

The first order energy describes the energy from the interaction of permanent electric moments, that is charge, dipole, quadrupole, and so forth. Most notably, this term takes into account dipole-dipole interactions. The second order perturbed energy, from the above equation, gives the induction energy and dispersion energy. This is to say that dipole-induced dipole, or Debye forces are accounted for, as well as the London dispersive forces generated by instantaneous dipole-induced dipole interactions arising from fluctuations in the charge distributions over a particle that produces an electric moment.

The induction energy of particle "a" can be given by the first term of the following equation, and the induction energy of particle "b" can be given by the second term.[2]

$$u_{\text{induction}} = -\sum_{p_a \neq n_a} \frac{\left\langle n_a n_b \middle| H_{ab} \middle| p_a n_b \right\rangle^2}{W_{p_a} - W_{n_a}} - \sum_{q_b \neq n_b} \frac{\left\langle n_a n_b \middle| H_{ab} \middle| n_a q_b \right\rangle^2}{W_{q_b} - W_{n_b}}$$

The dispersion energy is given by the following equation:

$$u_{\text{dispersion}} = -\sum_{\substack{p_a \neq n_a \\ q_b \neq n_b}} \frac{\left\langle n_a n_b \middle| H_{ab} \middle| p_a q_b \right\rangle^2}{W_{p_a} - W_{n_a} + W_{q_b} - W_{n_b}}$$

To give a clear understanding of the distance at which these forces act, we can look at the energy in terms of polarizability, noting the inverse relationship to distance the energy has in the following relationships describing the respective forces:

Dipole-Dipole:

$$U_{\text{DD}}(r) = -\frac{2\mu_1\mu_2}{4\pi\varepsilon_0 r^3}$$

Dipole-Induced Dipole (Debye force):

$$\left\langle U_{\text{ind}}(r)\right\rangle = -\frac{\mu_1^2 \alpha_2}{\left(4\pi\varepsilon_0\right)^2 r^6}$$

Instantaneous Dipole-Induced Dipole (London dispersive force) (approximation given by London formula):

$$U_{\text{disp}}(r) = -\frac{C_6}{r^6} = -\frac{3\alpha^2 I}{4\left(4\pi\varepsilon_0\right)^2 r^6}$$

Finally, hydrogen bonding is an intermolecular force that is directional with an exponential decay as distance increases. Hydrogen bonding requires a hydrogen atom covalently bonded to an electronegative atom that then interacts with an electronegative atom having lone pair electrons accessible. The hydrogen bond is a composite molecular interaction that is a special case of dipole-dipole and overlap interactions. Similarly, halogen bonding is another special case of dipole-dipole and overlap interactions; however, as its name suggests, this bonding involves a halogen atom.

1.3 The Quantum Cascade Laser

Semiconductor lasers are devices that emit electromagnetic radiation by means of **l**ight **a**mplification through **s**timulated **e**mission of **r**adiation (LASER) with the physical properties of semiconductor materials. The p-n junction diode is the source of this radiation with the injection of an electric current through this semiconductor medium. These semiconductor diodes emit radiation through the matching of electron-hole pairs in the semiconductor's band gap, which is the energy gap between the top of the valence energy band and the bottom of the conduction band, or the energy needed to release a valence shell electron from its orbit around the nucleus to allow it to move from atom to atom as a charge carrier within the semiconductor.

The major difference between a traditional semiconductor, injection laser diode and a quantum cascade laser is the use of intersubband transitions, as opposed to the use of interband transitions. By using these intersubband transitions, quantum cascade lasers are able to have a very narrow gain spectrum that is nearly symmetric, and much less sensitive to thermal broadening of the electron distribution.[3] By means of an applied voltage, a conduction band like the one shown in Figure 1 can be formed, where the "electric field exceeds the quasi-electric field of the associated with the conduction band grading."[3] All of this supports the intended goal of increasing the sensitivity of narrow line-width transitions in a spectrometer—be it pulsed or continuous wave—for the infrared region.

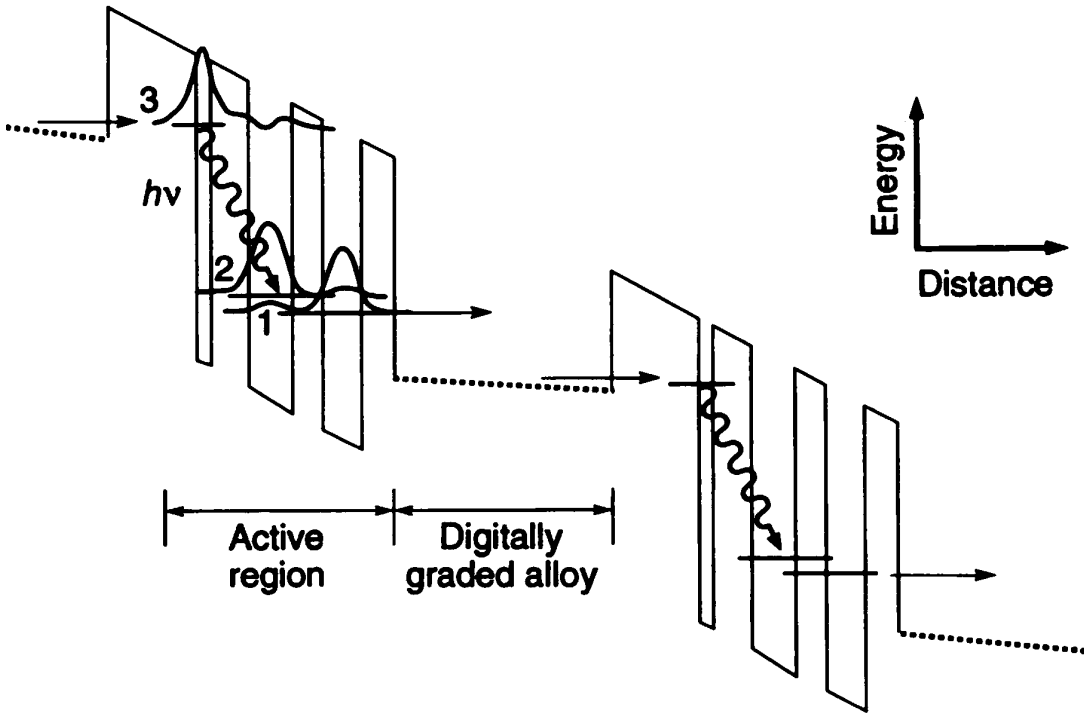

Figure 1. Conduction band energy diagram from Faist, et al.[3]

This laser structure is formed by molecular beam epitaxy with an InGaAs-InAlAs heterojunction material system lattice on an InP substrate.[3] This structure allows for the energy levels to be controlled through engineering of the layer thickness, which also supplies the population inversion in the excited states required for radiation emission. Over the graded portion seen above, electrons relax before tunneling into the excited state. As the electron traverses these states, a photon is emitted for each state. This makes for a stable source that is capable of tremendous power.

2. QUANTUM CASCADE LASER SPECTROSCOPY INVESTIGATIONS INTO HYDROGEN AND HALOGEN BONDED INTERACTIONS*

2.1 Background

In the study of the gas phase species of four-atom OC-HX and five-atom OC-HCN, the following experimental setup was used to investigate the infrared vibrational states. Briefly, Figure 2 shows the continuous wave QCL spectrometer, which contains a Daylight Solutions mode-hop free product, operating over a particular frequency range dependent upon a quantum cascade chip within the QCL head. The reference cell can be filled with a reference gas active in the region over which the investigation takes place. This experimental setup yields such broadband spectra as seen in Figure 3, which shows P and R substructure of OC-HCN in the ν_2 vibration with a signal to noise ratio approximately on the order of one hundred to one. From such a spectra in Figure 3, the structure can be elucidated and structural constants calculated. This data allowed comparison to be made between complexes involving the hydro-halogen species and the pseudo hydro-halogen, HCN.

The investigation of low frequency vibrations in the submillimeter and Terahertz range have a wide range of implications including facilitating spectroscopic studies of

---

* Reprinted from *Chemical Physics*, Volume 409, B. A. McElmurry, L. A. Rivera-Rivera, K. W. Scott, Z. Wang, I. I. Leonov, R. R. Lucchese, and J. W. Bevan, "Studies of Low-Frequency Intermolecular Hydrogen-Bonded Vibrations Using a Continuous Supersonic Slit Jet Mid-Infrared Quantum Cascade Laser Spectrometer," Pages 1-10, Copyright 2012, with permission from Elsevier.

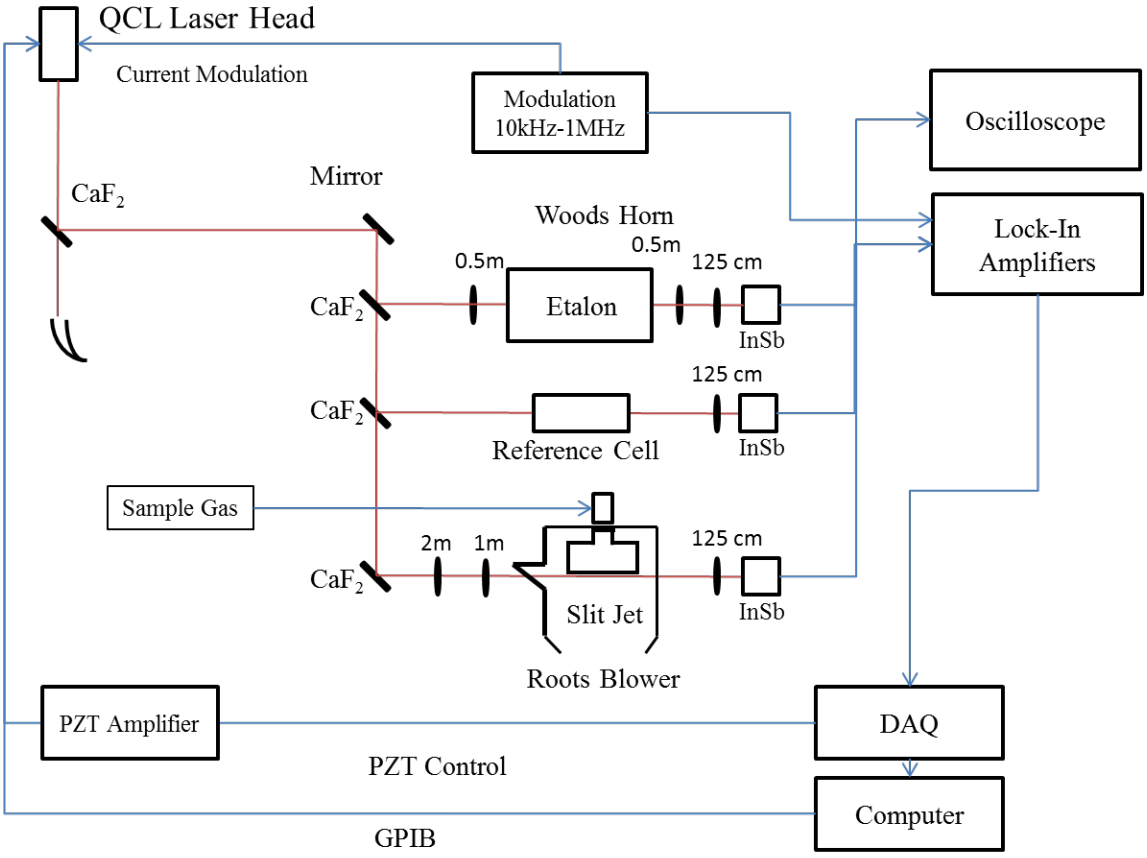

Figure 2. Diagram of cw QCL supersonic slit jet spectrometer.

isomers and conformers greatly extending molecular energy spaces for astrophysical and other studies as well as intermolecular vibrational frequencies so important in characterizing the structures and dynamics of non-covalent interactions. Traditionally, direct observation of such low frequency vibrations in intermolecular complexes has been significantly more difficult to observe than intramolecular vibrations in the mid- or near-infrared range.[4] However, methods developed have made the infrared range, both accessible and increasingly productive as a region for observing the intermolecular

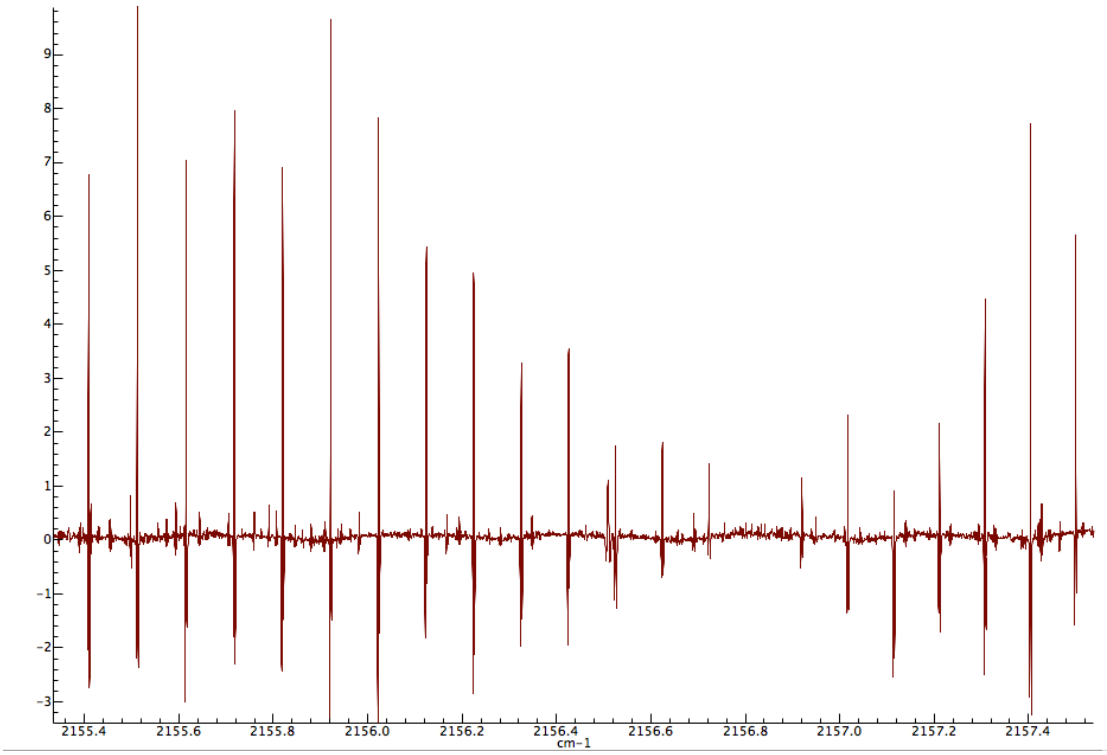

Figure 3. OC-HCN ν_2 broadband spectrum from QCL spectrometer.

vibrational frequencies necessary to characterize non-covalent interactions. Indirect methods such as combination difference approaches have also been developed to facilitate such studies.[5]

In this effort, we report development of the combination difference approach using commercially available quantum cascade mode-hop free infrared tunable lasers used in conjunction with a cw supersonic slit jet spectrometer. Metalorganic chemical vapor deposition (MOCVD) methodologies for InP/InGaAs/InAlAs materials have lead to quantum cascade mode-hop free tunable infrared lasers that now cover the range from

4 to 12 microns while operated under room temperature conditions.[3,6-8] These lasers are based on unipolar multi-subband transitions, in contrast to semiconductor lead salt lasers, which are dependent on electron-hole recombination.[9] The capability of quantum cascade lasers to operate with these relatively narrow continuous wave single frequency characteristics, and to operate with relatively high average powers of 50 mWatts or more, has provided opportunities to apply a range of spectroscopic methods.[10-14] Such investigations can be used to determine accurate ro-vibrational parameters for molecular species in supersonic jet expansions.[15-21]

In the context of current studies, determination of ro-vibrational parameters associated with low frequency intermolecular vibrations in hydrogen-bonded systems will be demonstrated by using prototypical hydrogen-bonded interactions. Such ro-vibrational analyses are ideal for three such systems, OC-HCl, OC-HF, and OC-HCN using a continuous supersonic slit jet infrared QCL spectrometer. The $^{16}O^{12}C$-$^{1}H^{35}Cl$ complex has been the subject of extensive previous investigations using spectroscopic and theoretical methods.[22-37] It thus provides a convenient prototypical system for evaluating instrumental performance characteristics and potential application of mid-infrared QCLs for studies of hydrogen-bonded complexes in cw expansions. The analysis of the ν_2 CO stretching vibration and its $\nu_2+\nu_5^1-\nu_5^1$ and $\nu_2+\nu_3-\nu_3$ hot bands involving the ν_5^1 and ν_3 intermolecular bending and stretching vibrations will be given for OC-HCl. In particular, ro-vibrational parameters of the ground state ν_5^1 vibration can be determined using combination frequency differences.[5] Results are also compared with previous investigations of OC-HCl using a lead salt semi-conductor laser

spectrometer in the linear absorption limit enabling evaluation of performance characteristics in these respective spectrometers.[29] Corresponding ν_5^1 data has not been available for the OC-HF complex, though there have been extensive previous gas phase, theoretical studies, an accurate determination of D_0 as well as generation of a 6-dimensional morphed potential.[22,31,38-56] The frequency of ν_5^1 is expected to be 80(12) cm^{-1} so it should prove a more challenging application of combination difference method used for evaluation of the ν_5^1 in OC-HCl. The applicability of the QCL spectrometer for investigations of non-covalent interactions is further illustrated by analysis of the corresponding ν_2 OC stretching fundamental and its intermolecular hot bands $\nu_2 + \nu_7^1 - \nu_7^1$ and combination $\nu_2 + \nu_7^1$ band in OC-HCN.

OC-HCN has characteristics that represent an interaction between OC and the pseudo-hydrogen halide HCN. The complex has been the subject of extensive theoretical calculation with HCN as hydrogen atom donor.[57] ν_2, ν_4, ν_6^1 and ν_7^1 vibrations have been calculated to be 2134.2 cm^{-1}, 77.6 cm^{-1}, 118.2 cm^{-1} (geared libration) and 51.0 cm^{-1} (anti-geared libration) with intensities of 31.6 km mol^{-1}, 0.39 km mol^{-1}, 17.1 km mol^{-1}, and 8.32 km mol^{-1}, respectively.[57] The OC-HCN complex was initially the subject of previous experimental investigation using microwave spectroscopy where a wide range of ground state isotopomers were studied using pulsed-nozzle Fourier transform (FT) microwave analysis at 6 kHz resolution.[58] Furthermore, the opto-thermal infrared laser spectroscopy of the ro-vibrational substructure of its ν_1 fundamental has been analyzed and used to generate a range of computational

calculations, but there have been few investigations of other vibrations in this system using high resolution infrared spectroscopy.[51,57,59] The OC-HCN complex may also be of broader astrochemical interest because of the relative abundance of both OC and HCN in interstellar clouds; hence, there is an extension of spectroscopic investigations for the complex that could be significant as well.[60,61] Generation of the rovibrational spectrum of the ν_7^1 vibration will permit refinement of searches for this complex in interstellar space in the terahertz spectral range. Microwave analysis indicates that the ground state structure is a quasi-linear complex with R_0 = 4.84484 Å.[58] Infrared investigations have been restricted to the ro-vibrational analysis of the ν_1 vibrational band using opto-thermal spectroscopy.[59] Initial unpublished ground state compound-model morphing (CMM) calculations by the Bevan and Lucchese groups are consistent with D_e = 608(8) cm^{-1}, R_e = 4.843(2) Å, D_0 = 430(8) cm^{-1}, ν_7^1 = 34.6(6) cm^{-1}, ν_4 = 74.9(7) cm^{-1} and ν_6^1 = 99.1(4) cm^{-1}. This optimization was based only on microwave experimental data. Experimental and theoretical studies of this type provide a basis for studying the fundamental nature of CO as an electron donor probing its interactions with different hydrogen bonded donors. Extensions of both experimental and theoretical studies bring greater insight into such fundamental interactions particularly through a natural comparison with the homologous series OC-HX (X = F, Cl, Br, I). There have, however, been insufficient vibrational investigations in the complex to provide such an enhanced analysis. No experimental studies of the fundamental intramolecular CO stretching vibration in OC-HCN exist. Furthermore, no studies of the ro-vibrational energy manifold associated with the intermolecular vibrations of the complex have been

completed thus far. Such information would provide accurate data that gives a basis for refining modeling of the intermolecular potential energy surface in this complex. These studies would also have relevance to studies directed at characterizing the angular characteristics and nature of rigidity in hydrogen bonded complexes.

2.2 Methods

In operating the QCL spectrometer, numerous preparations were made for both the generation of the gas species to be studied, as well as the optical setup required for the use and effective recording of the data obtained.

A schematic of the continuous wave, supersonic slit jet infrared QCL spectrometer is shown in Figure 2 and is based on a modified design to that of a previously constructed lead salt continuous slit jet semiconductor laser spectrometer.[5] The QCL heads utilized in the current investigations were fabricated by Daylight Solutions (San Diego, California) having mode-hop free operational ranges from 2145 cm^{-1} to 2195 cm^{-1} (21045-MHF) and 2194 cm^{-1} to 2285 cm^{-1} (21043-MHF), respectively. The laser controllers were connected via a GPIB interface to the host computer and the output frequency and power of the laser head, in addition to three lock-in amplifiers' settings, could be adjusted by a custom LabVIEW program with integrated virtual interfaces (vi's) from the manufacturer. The laser controller monitored and adjusted the operational parameters such as current to the QCL, the relative temperature of the laser head and the tuning mechanism. Water-cooling was supplied by a Thermo CUBE 200

Watt recirculating chiller (Solid State Systems, Pleasant Valley, NY). The output frequency of the QCL head was controlled by two different methods. Coarse tuning of the output frequency was achieved by controlling a stepping motor that changed the QCL cavity length through a pivoted external cavity grating that sustained a single cavity mode. Fine-tuning used for the spectroscopic measurements was accomplished by application of voltage to a piezo-electric device (PZT) in the 0 to 100 voltage range to mechanically move the grating to cover incremental ranges of about 2.2 cm^{-1}. The voltage applied to the PZT was generated by a NI PCI-6251 analog output and MDT694A piezo controller. Laser output powers in the range 80 to 100 mW were typical once threshold emission had been achieved. Wavelength modulation of the laser source was achieved by the application of a sinusoidal waveform with a frequency of 10kHz to 2MHz (M_F) and a modulation amplitude, M_A, of ±2V DC giving up to 0.05cm^{-1} modulation amplitude in frequency. In these studies, investigations of the effectiveness of frequency modulation measurements were made and found to give optimum sensitivity at M_F=200 kHz and M_A=200mV modulation with second derivative lock-in detection. Frequency tunability and single mode-hop free operation were determined with free-running linewidth of less than 30 MHz. Back reflections were known to produce etaloning and other detrimental effects in the spectral baseline but were minimized using wedged optics and a Wood's horn following careful alignment of the radiation source beam. The output of the laser was first split by a CaF_2 wedge and following a reflection mirror split again into three components using beam splitters as shown in Figure 2. The transmitted beam from the first CaF_2 beam splitter was collected

by a Wood's horn to reduce back reflections and feedback to the QCL chip. The total power used in this experimental setup was estimated to be about 0.8 mW. The detectors used in this study were liquid N_2 cooled InSb detectors (both Graesby Infrared and Infrared Associates) and preamplifiers having a 1MHz bandwidth. The outputs of the detectors were sampled by three EG&G 5302 lock-in amplifiers referenced to the modulation signal. The outputs of the lock-in amplifiers were then digitized and stored in a computer using the LabVIEW program and DAQ interface. The absolute frequency scale of the observed transitions were determined by a combination of passive Fabry-Perot confocal etalon (Spectra-Physics, SP5945) with a FSR of 0.00962456 cm^{-1}, and carbon monoxide (1 Torr, 30 cm path) and nitrous oxide (10 Torr, 10 cm path) reference lines from the HITRAN database. Such measurements were used for calibration of absolute frequencies to an accuracy of ±0.0005 cm^{-1}. The 12 cm long slit jet expansion was formed from a reservoir sample maintained at a total pressure in the range 15 psi to 30 psi consisting of typically 0.5% to 1% HX (X = Cl, F or CN), 5% carbon monoxide mixed in argon carrier and spectra recorded with single pass of the radiation source through the supersonic jet expansion. The vacuum chamber housing the slit expansion was pumped to 600 mTorr by a Leybold RA2001 Roots blower and a Leybold SV630F roughing pump.

2.3 Results and Discussion

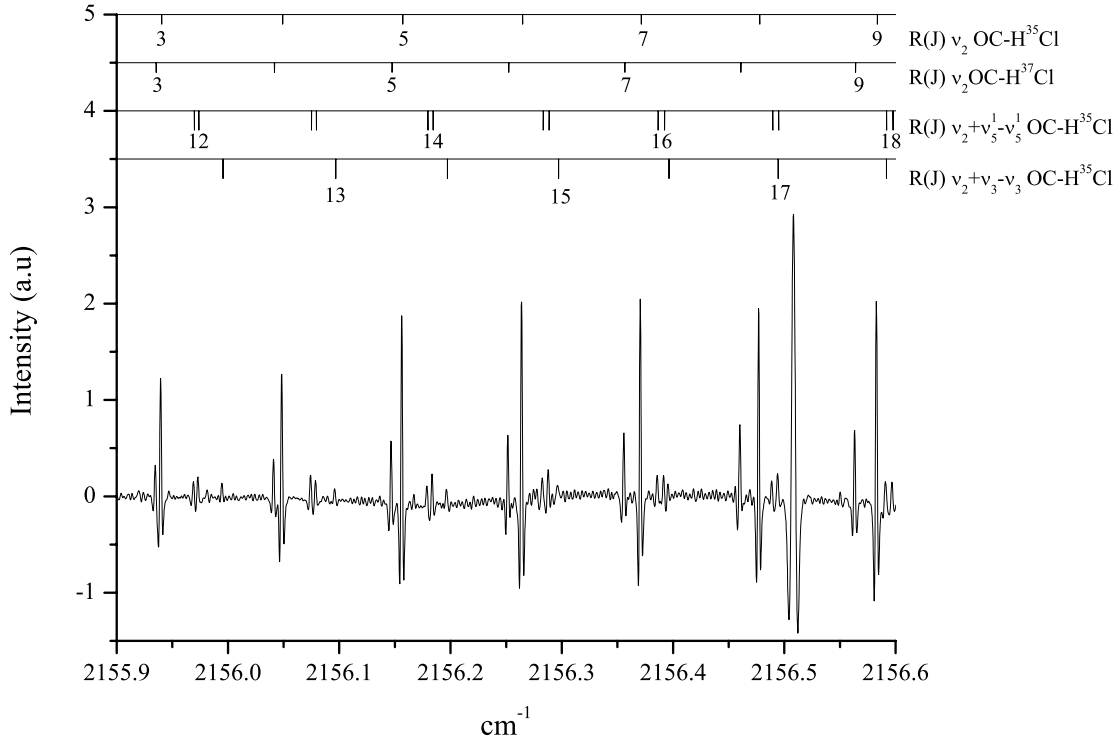

Figure 4. Spectrum of OC-H^{35}Cl recorded using a cw slit jet QCL spectrometer showing the ν_2, CO stretching vibration, as well as $\nu_2 + \nu_5^1 - \nu_5^1$ and $\nu_2 + \nu_3 - \nu_3$ hot bands.

A segment of the recorded spectrum for OC-HCl is presented in Figure 4 for the range 2155.9 to 2156.6 cm^{-1}. The R(4) to R(8) transitions for both OC-H^{35}Cl and OC-H^{37}Cl isotopomers of the ν_2 CO stretching vibration are shown and are consistent with a

previous analyses of this spectrum using a slit jet lead salt semi-conductor spectrometer.[29] In addition, $\nu_2 + \nu_5^1 - \nu_5^1$ and $\nu_2 + \nu_3 - \nu_3$ hot bands were observed and assigned. The former was consistent with a ν_5^1 band origin frequency of 48.99 cm^{-1} and a corresponding predicted ν_3 frequency of 62.43 cm^{-1}. The latter prediction was based on a 4-D CMM potential energy surface for OC-HCl.[37] The measured transition frequencies for these bands were fitted and used to provide the molecular constants given in Table 1 which agree within error with previous results determined using a lead

Table 1. Ro-vibrational constants for observed bands in OC-HCl.

Observable	ν_2 OC-H^{35}Cl	ν_2 OC-H^{37}Cl	$\nu_2 + \nu_5^1 - \nu_5^1$ OC-H^{35}Cl	$\nu_2 + \nu_3 - \nu_3$ OC-H^{35}Cl
ν_0 /cm^{-1}	2155.500175(81)	2155.505481(97)	2154.551155(87)	2154.627385(86)
B' /cm^{-1}	0.0554811(43)	0.0542171(43)	0.0563031(35)	0.0543061(45)
D' /cm^{-1}	1.85(20) × 10^{-7}	2.09(21) × 10^{-7}	1.870(64) × 10^{-7}	2.702(86) × 10^{-7}
q' /cm^{-1}			1.489(23) × 10^{-4}	
B'' /cm^{-1}	0.0557646(44)	0.0544949(45)	0.0565681(33)	0.0545695(43)
D'' /cm^{-1}	1.82(19) × 10^{-7}	2.04(20) × 10^{-7}	1.849(56) × 10^{-7}	2.589(76) × 10^{-7}
q'' /cm^{-1}			1.476(22) × 10^{-4}	

salt semi-conductor slit jet spectrometer.[5] The rotational intensity distributions are consistent with an effective temperature distribution of 12(2) K. Table 2 includes ro-vibrational data fitted for the OC-HF complex in the ν_2 fundamental region as well as hot band $\nu_2 + \nu_5^1 - \nu_5^1$ and $\nu_2 + \nu_5^1$ combination band. Using combination differences, the corresponding ν_5^1 intermolecular bridge band origin frequency was determined to be 81.96825(12) cm^{-1} above the ground state from this data. The fitted ro-vibrational parameters for the observed vibrational bands are given in Table 3. A segment of

Table 2. Ro-vibrational constants for observed bands in OC-HF.

Observable	ν_2	$\nu_2 + \nu_5^1 - \nu_5^1$	$\nu_2 + \nu_5^1$
	OC-HF	OC-HF	OC-HF
ν_0 /cm^{-1}	2167.69833(19)	2166.41714(17)	2248.38604(26)
B' /cm^{-1}	0.1015555(71)	0.1023860(70)	0.1023860(70)
D' /cm^{-1}	3.17(19) × 10^{-7}	3.55(16)× 10^{-7}	3.55(16)× 10^{-7}
q' /cm^{-1}		-3.212(23)x10^{-4}	-3.212(23)x10^{-4}
B'' /cm^{-1}	0.1021997(72)	0.1030257 (65)	0.1021997(72)
D'' /cm^{-1}	3.17(17) × 10^{-7}	-3.58(13) × 10^{-7}	3.17(17) × 10^{-7}
q'' /cm^{-1}		-3.20(24)× 10^{-4}	

ν_5^1 = 81.96890(33) cm^{-1}

Table 3. Ro-vibrational constants for observed bands in OC-HCN.

Observable	ν_2	$\nu_2 + \nu_6^1$	$\nu_2 + \nu_7^1 - \nu_7^1$	$\nu_2 + \nu_7^1$
	OC-HCN	OC-HCN	OC-HCN	OC-HCN
ν_0 /cm^{-1}	2156.82167(11)	2251.17882(14)	2153.16319(15)	2190.80061(15)
B' /cm^{-1}	0.04905039(57)	0.0489774(11)	0.0498477(15)	0.0498477(15)
D' /cm^{-1}	1.1482(88)× 10^{-7}	1.540(19) × 10^{-7}	2.331(35) × 10^{-7}	2.331(35) × 10^{-7}
q' /cm^{-1}		3.598(45) × 10^{-5}	1.495(11) × 10^{-4}	1.495(11) × 10^{-4}
B'' /cm^{-1}	0.04924416(27)	0.04924416(27)	0.0500535(17)	0.04924416(27)
D'' /cm^{-1}	1.126(9) × 10^{-7}	1.126(9) × 10^{-7}	1.440(35)× 10^{-7}	1.126(9) × 10^{-7}
q'' /cm^{-1}			1.562(11) × 10^{-4}	

$\nu_7^1 = 34.63742(18)$ cm^{-1}

the $\nu_2 + \nu_6^1$ spectrum from 2250.92 cm^{-1} to 2251.25 cm^{-1} is shown in Figure 5, illustrating primarily the assigned Q(J) transitions. The intensity distribution of the observed bands is consistent with an effective rotational temperature distribution of 12 K.

Comparison of the ν_2, $\nu_2 + \nu_3 - \nu_3$, and $\nu_2 + \nu_5^1 - \nu_5^1$ OC-HCl spectra recorded using the current QCL slit jet spectrometer with a previously constructed lead salt slit jet spectrometer gives insight into potential applications of the former for investigation of non-covalent interactions. The performance characteristics of QCL lasers have been

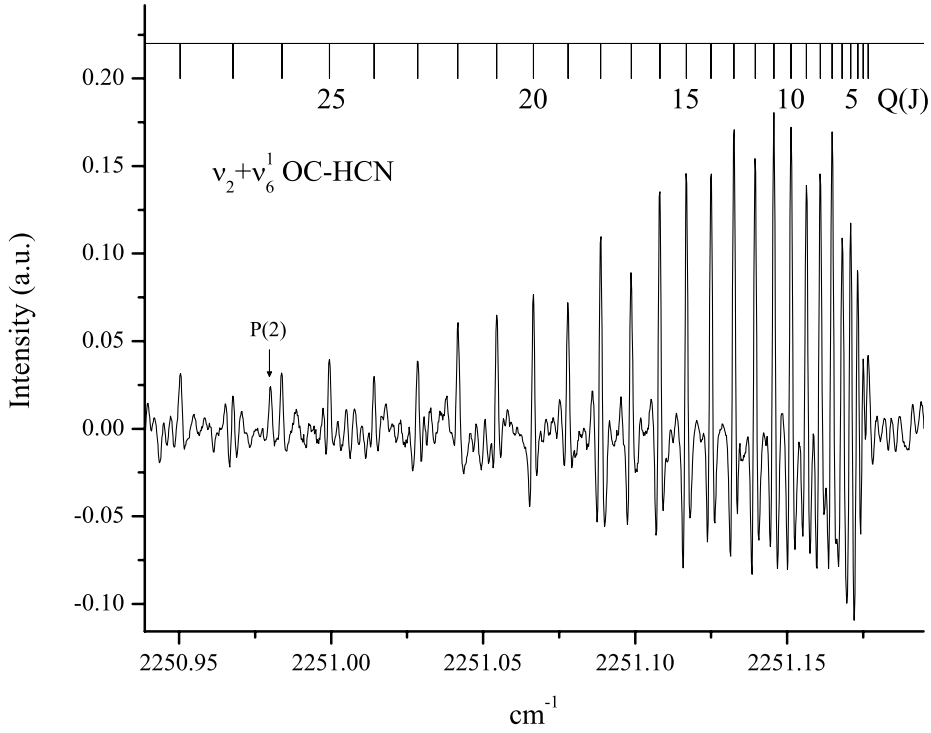

Figure 5. QCL spectrum of the Q(J) branch of the $\nu_2 + \nu_6^1$ combination band of OC-HCN.

greatly extolled including potential of frequency coverage from the THz to 3 microns using different individual broadband mode-hop free tunability regions, over 30 cm^{-1}, or more, in the mid-infrared (sometimes up to 120 cm^{-1}). Possibilities of relatively high average cw powers in the range 30 mWatts to 200 mWatts are also attractive. The latter characteristics are particularly advantageous for nonlinear techniques and other applications such as in opto-thermal spectroscopy. However, in the current context of linear absorption applications, the real issue is one of ultimate sensitivity as measured by

signal/noise ratio. In prior studies, it was found that when using high frequency wavelength modulation spectroscopy that S/N ratio was still determined by 1/f noise at fundamental modulation frequencies of 1 MHz.[5] At the higher modulation frequencies used, this corresponded to a sensitivity of 2 parts in 10^7 for single pass absorption in the linear limit. In the corresponding QCL experiments, which involved temperature modulation, it was found that the optimum sensitivity occurred at about 200 kHz and there was little improvement in transferring from first to second derivative detection. This contrasts with the corresponding characteristics associated with lead salt second derivative detection where an improvement by a factor of 8 was measured when operated at a fundamental modulation of 200 kHz. A direct comparison of sensitivity based on observation of spectra of ν_2, $\nu_2 + \nu_3 - \nu_3$, and $\nu_2 + \nu_5^1 - \nu_5^1$ OC-HCl spectra indicate that the sensitivity of the current spectrometer using second derivative detection is still a factor of 50 less sensitive than the optimum that was observed using the lead salt semiconductor technology. It is pertinent to point out that broadband tuning of the current QCL spectrometer is based on mechanical tuning of the external cavity grating in contrast to semiconductor lead lasers which have no moving parts involved in such tuning, a distinct advantage in performance reproducibility. The latter affects reproducibility, particularly for co-addition purposes. In the current QCL spectrometer, back reflection can also produce etaloning in the spectral baseline but this was minimized using wedged optics and careful alignment of the source beam as it passed through the optical path. Some residual etaloning in the baseline was also attributed to the cavity length of the chip. We expect that the current limitation in sensitivity can be

improved by application of molecular modulation methods or zero-based detection methods and such investigations were underway at the passing of Dr. Bevan.

The data spectral characterization of the species studied with the QCL spectrometer provided results, which allow for the structural characterization of the species. A continuous supersonic slit jet QCL spectrometer was constructed and successfully used to investigate the CO stretching vibrational bands and associated intermolecular hot and combination bands for three prototypical hydrogen bonded complexes, OC-HCl, OC-HF and OC-HCN. Most importantly, the QCL spectrometer permitted the investigation of low frequency bridged intermolecular hydrogen bonded vibrations in all three of these complexes. In the case of OC-HF, it allowed evaluation of the ν_5^1 band origin to be 81.96825(12) cm^{-1} above the ground state. With extension of the operating wavelength range of commercially available mode-hop free QCLs, this spectrometer has useful potential capabilities for investigation of low frequency vibrations in a wide range of non-covalent interactions. This research provided the first observation and ro-vibrational analysis of the ν_2, and intermolecular ν_7^1 hot and combinations bands in OC-HCN complex. This analysis also permitted an initial prediction of transitions associated with the ν_7^1 vibration, which can be used for investigating the possible existence of the OC-HCN complex in interstellar space. These spectroscopic investigations also have enabled the generation of a 5-D morphed potential for the OC-HCN complex. D_e of the OC-HCN complex (650(8) cm^{-1}) is between that predicted from morphed potentials for OC-HCl (725.6(50) cm^{-1}) and OC-HBr complex (564(5) cm^{-1}). The corresponding value of D_0, however, is predicted to be 463(8) cm^{-1}

compared with 397(5) and 322(6) cm^{-1} for OC-HCl and OC-HBr respectively. The D_0 value thus lies between that of OC-HF (742.5(50)) cm^{-1} and that of OC-HCl. In addition, the OC-HCN complex has a predicted r_{C-H} value at its global minimum of 2.572(2) Å, significantly larger than the corresponding predicted values of 2.061, 2.370 and 2.484 Å for OC-HF, OC-HCl and OC-HBr.

3. CONTRASTING HALOGEN-BONDED AND HYDROGEN-BONDED COMPLEXES*

3.1 Background

A similar experimental investigation of the complex OC-BrCl in the gas phase with the QCL spectrometer produced spectra from which the following constants could be calculated. This particular complex presents the unique opportunity to study the halogen bond in a pure sense, without a directly competing hydrogen bond alternative configuration. Furthermore, this study allowed several intriguing observations, specifically that the series of OC-Cl_2, OC-Br_2, and OC-BrCl does not follow the parallel series of OC-HX. This would indicate that there is some factor or factors standing in contrast between the two series, in spite of the similar linearly bound structure, and similar electron donation of the CO molecule.

The concept of the halogen bond has recently been the subject of renewed interest, of late, that even led to a refined definition of this type of interaction by an IUPAC Task Group (project 2009-032-1-200).[62-64] This is in no small part due to the proposed significance of such bonding in the rational design of halogenated ligands as inhibitors and drugs, and in biomolecular engineering, as well as material science. In

---

* Reprinted from *Chemical Physics*, Volume 425, L. A. Rivera-Rivera, K. W. Scott, B. A. McElmurry, R. R. Lucchese, and J. W. Bevan, "Compound Model-morphed Potentials Contrasting OC-$^{79}Br^{35}Cl$ with the Halogen-bonded OC-$^{35}Cl_2$ and Hydrogen-bonded OC-HX (X = ^{19}F, ^{35}Cl, ^{79}Br)," Pages 162-169, Copyright 2013, with permission from Elsevier.

previous literature, the halogen bond was described as paralleling the hydrogen bond with a major difference existing in a propensity to more non-linearity in the hydrogen bond.[65-68] Systematic studies of such interactions under effectively collisionless conditions have made important contributions to such characterizations. The recorded pulsed-nozzle FT microwave spectrum of OC-BrCl has given a detailed characterization of the complex in its ground state.[69] Rotational constants B_0, the centrifugal distortion constants D_J and halogen nuclear quadrupole coupling constants c_{aa}(X), where X = Cl or Br, were interpreted to give the properties of this weakly bound complex. It was found that the molecule was linear through isotopic substitution data, and the ground state had the atomic arrangement OC-BrCl, with the Br atom forming the intermolecular bond to carbon. The r_s values for the distances r(C-Br) and r(BrCl) reflected limitations imposed by the small coordinates that had to be considered. Specifically, the effect of bond shrinkage resulting from isotopic substitution at the Br nucleus indicated that a_{Br} was underestimated because the bromine atom was close to the center of mass of the complex.[69] It was also concluded from a proposed model that there was probably only a small increase in r(BrCl) upon formation of the complex. Furthermore, an interpretation of the c_{aa}(X) values concluded that the electric charge distribution in BrCl was also only slightly perturbed indicating that this complex can not be regarded as a typical B-XY charge transfer complex.[69]

Application of a compound model morphed potential enabled a detailed study of the intermolecular interaction for halogen bonding in OC-Cl_2 and a quantitative comparison of its molecular dynamics and other properties with the hydrogen bond OC-

HCl.[20] The results pertained to complexes having comparable D_0 values giving further perspectives on the nature of bonding in these interactions. Comparison of results from respective potentials indicated that the halogen component bond had more restricted angular amplitude and greater directionality in the case of OC-Cl_2, whereas the hydrogen bond potential is characterized by a greater degree of coupling.[20] The latter was further supported by determination of respective anharmonic coupling terms in both systems. These results also correlated with the significantly greater contribution of zero point energy in the case of OC-HCl (329(10) cm^{-1}) relative to OC-Cl_2 (147(10) cm^{-1}). Furthermore, the predicted vibrational ground state structure of the OC-Cl_2 complex from the morphed potential is $\overline{\theta}_2 = \cos^{-1}\left(\left\langle \cos^2\theta_i \right\rangle^{1/2}\right) = 175.4°$, whereas the corresponding value for OC-HCl is $\overline{\theta}_2 = 162.2°$. The values of $\overline{\theta}_1$ were found to be

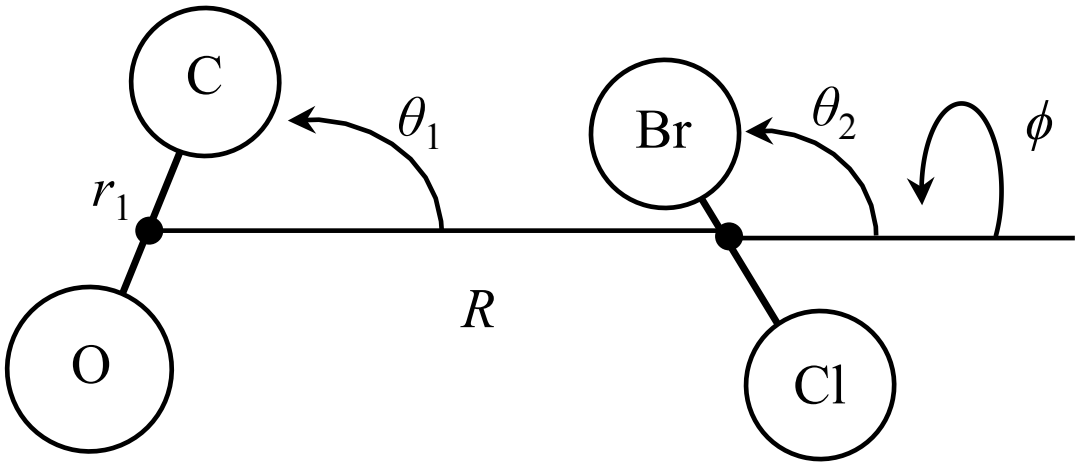

Figure 6. Jacobi coordinates for OC-BrCl dimer.

more comparable indicating that the amplitude of the CO bending motion in both complexes was almost the same. The angles are defined in Figure 6. Consequently, the Cl_2 monomer, in the halogen-bonded complex OC-Cl_2, underwent significantly smaller excursions (and is in this sense more rigid and consequently more directional) than the HCl monomer, in the hydrogen-bonded complex OC-HCl.[20]

In other spectroscopic studies in Ar and N_2 matrices, infrared spectra have been recorded for complexes of OC-XY including $^{12}C^{16}O$, $^{13}C^{16}O$ and $^{12}C^{18}O$ isotopomers. For the $^{12}C^{16}O$ isotopomer, the CO-XY complexes (form 2) have also been reported.[70] Quantum calculations for linear complexes have also been completed for OC-Cl_2 and CO-Cl_2 applying B3LYP, CCSD/B3LYP and CCSD(T)/B3LYP methods.[70] The experimentally observed blue frequency shift observed in these studies for the OC stretch in OC-BrCl was found to be 2147.95 cm^{-1} in Ar matrix (CO monomer 2138.5 cm^{-1}) and 2138.05 cm^{-1} for the corresponding isotopomer OC-ClBr. For CO-Cl_2 2134.1 cm^{-1}, CO-Br_2 2132.8 cm^{-1}, CO-BrCl 2131.5 cm^{-1} values were determined and compared with the corresponding monomeric CO at 2138.5 cm^{-1} indicating shifts due to matrix effects as the free monomer was observed at 2143.29156(8) cm^{-1}. These corresponding shifts for $\Delta\nu$ (CO) which are found to be +2.1 cm^{-1} (for OC-Cl_2), +5.4 cm^{-1} (for OC-Br_2), +9.5 cm^{-1} (for OC-BrCl), and -0.5 cm^{-1} (for OC-ClBr) and for form 2 are -4.4, -5.5, -7.0, and -3.3 cm^{-1} give information on the nature of such interactions.

Romano and Downs extended the previous matrix studies and molecular calculations with investigation and further matrix studies of both OC and CO complexes

in ICl and IBr, as well as corresponding studies of the XY stretching vibrations for OC-Cl_2 and OC-BrCl and OC-ICl.[71] DFT calculations on these systems included binding energies, frequency shifts, and bond lengths. Two families of these linear complexes were found to exist according to whether the C or the O atom of the CO binds to the dihalogen. With heteronuclear dihalogens XY, this binding may occur to either of the dihalogen atoms, giving four possible isomeric forms. In addition to the ν(CO) modes of the various complexes, these IR measurements have been used to identify ν(XY) stretching modes for the complexes of the type OC-XY. The structures, vibrational properties, and binding energetics of the complexes were analyzed in light of related studies.

This research provided new perspectives on pairwise halogen bonding by enabling the generation of a semi-empirical 5-D compound model morphed potential of OC-BrCl. The highly accurate CMM potential became available for a simple prototypical pairwise halogen bond involving a bromine interaction as well as for a halogen diatomic with significant dipole moment. This investigation under isolated conditions has direct relevance to conclusions based on previous gas phase and condensed phase investigations particularly associated with the strength and directionality of halogen bonding.[62-69] These studies are also relevant to previous microwave studies that concluded limited electron transfer and change in the Cl_2 bond length on complexation in OC-Cl_2.[72] Electrostatic forces were expected to make minor contributions to the bonding of this latter complex in which polarizability and the resulting London dispersive forces were expected to dominate. Electrostatic forces,

however, are expected to make significant contributions to intermolecular interactions in the OC-BrCl complex. A similar situation was found to occur in OC-HCl, yet both OC-Cl_2 and OC-HCl were predicted to have comparable ground dissociation energies, D_0 of 397(5) cm^{-1} and 397(2) cm^{-1} respectively. The Cl_2, the electron acceptor in OC-Cl_2, does not have a dipole moment and the contribution of electrostatic forces to this interaction are restricted. From this perspective, the OC-BrCl complex provides a convenient system for investigation and comparison. The BrCl has a permanent dipole moment of 0.67 Debyes, such that the OC-BrCl complex should have a significant electrostatic contribution to the halogen bonded interaction, making the complex significantly more strongly bound, reflecting a contrast to the D_0 in OC-Cl_2. Furthermore, just as a comparison of OC-Cl_2 with the hydrogen bond OC-HCl provided quantitative perspectives on the D_0, D_e and other properties, a comparable study of OC-BrCl with hydrogen bonded complexes including OC-HF is equally insightful. The nature of the angular molecular dynamics involving the BrCl component in the OC-BrCl is also of particular interest due to the contributions of the heavy bromine atom in the molecular motions in this complex.

3.2 Methods

The spectrometer is described in detail earlier in this work and in previous publications; thus, only a brief discussion will be presented here.[5,73] In short, two Daylight Solutions mode-hop free, quantum cascade lasers operating over the respective frequency ranges of 2140 cm^{-1} to 2195 cm^{-1} and 2194 cm^{-1} to 2280 cm^{-1} were employed to record the observed spectra. The laser output was split using three CaF_2 beam splitters and directed respectively to a passive Fabry-Perot etalon (Spectra Physics SP495, 0.00962456 cm^{-1} FSR), a N_2O/CO reference cell, and a cw supersonic jet. Wavelength modulation of the laser output was achieved by application of a sine wave to the current modulation port of the laser head. The modulation frequency (F_M) and amplitude (M_A) were adjusted to give the optimum signal-to-noise ratio in the spectrum, with typical values F_M ~200 kHz and M_A ~150 MHz. Lock-in amplifiers using first and second derivative detection were utilized to sample the output of the respective detectors. The output radiation from the QCL's could be tuned through the application of a voltage to a PZT integrated into the laser head. The lasers were scanned using a custom LabVIEW program with data acquisition as well as GPIB control of the laser head. Coarse tuning is achieved using the laser head controllers and a 621B-MIR laser wavelength meter. Fine tuning of the laser is controlled by a voltage generated from the data acquisition board and amplified to drive an integrated PZT to give spectral coverage of ~2 cm^{-1}. Voltage steps of 0.01V were used to record 10000 data points with an effective instrumental linewidth of 30 MHz. The estimated absolute accuracy of measured transitions was

± 0.001 cm^{-1}. A CaF_2 window was mounted at the Brewster angle before the laser beam entered the supersonic jet expansion to minimized back reflections. The slit used to generate the expansion measured 5 inches by 25 μm and the optical beam was positioned between 1 mm to 2 mm from the opening of the slit. Frequency calibration of observed transitions were determined as described previously.[5,73]

In order to prepare the samples of BrCl, I initially poured liquid bromine into a glass cylinder with a Teflon "screw stopper" and equipped with a side arm connected to a system of lines leading to a gas cylinder and a vacuum pump. Subsequently, the glass cylinder was immersed in liquid nitrogen above the level of the bromine within, until the bromine was converted entirely to the solid state. The glass cylinder was then evacuated to less than one Torr, effectively removing the air above the solid bromine. The gas cylinder was evacuated independently and sealed from the vacuum pump to the lines connecting the gas cylinder and the glass cylinder containing the solid bromine. The solid bromine was allowed to warm to room temperature and return to the liquid phase and subsequently evaporate overnight through diffusion into the mixing cylinder. An equi-molar amount of chlorine gas was then added to the mixing cylinder and BrCl allowed to form by exchange over a 24 hour period. Subsequently carbon monoxide gas was added and finally an appropriate amount of argon carrier gas. The composition of the final reservoir gas mixture was 93% argon, 5% carbon monoxide, 1% chlorine, and 1% bromine, which was then expanded into the continuous wave, slit jet expansion previously described.

A resulting short wavenumber scan (~ 2 cm^{-1}) of the recorded spectrum of OC-BrCl is shown in Figure 4. The measured line frequencies were fitted using PGOPHER.[74] Six infrared bands were fitted using the following general expression

$$\nu = \nu_0 + B'\left[J'\left(J'+1\right)-l'^2\right] \pm \frac{q'}{2}\left[J'\left(J'+1\right)\right] - D_J'\left[J'\left(J'+1\right)-l'^2\right]^2$$
$$-B''\left[J''\left(J''+1\right)-l''^2\right] \pm \frac{q''}{2}\left[J''\left(J''+1\right)\right] - D_J'\left[J''\left(J''+1\right)-l''^2\right]^2,$$

where ν_0 is the band origin, B is the rotational constant, D_J is the centrifugal distortion constant and q is the Coriolis coupling constant for the respective vibrational states. The l and q terms in the above equation are used as appropriate, for the Σ ground and ν_1 states and Π states ν_5^1.

The recorded infrared spectra of OC-BrCl are characteristic of a linear complex, having abundances determined primarily by those of the monomer components $^{79}Br^{35}Cl$, $^{81}Br^{35}Cl$, $^{79}Br^{37}Cl$, and $^{81}Br^{37}Cl$. These correspond to a ratio of $^{79}Br/^{81}Br$ of 50.7 : 49.3 % and $^{35}Cl/^{37}Cl$ of 75.8 : 24.2%. The recorded spectra involve the effective CO stretching vibration ν_1, a $\Sigma \leftarrow \Sigma$ transition, and $\nu_1 + \nu_5^1 - \nu_5^1$, $\Pi \leftarrow \Pi$ bands. I have reported analysis of the ν_1 of OC-$^{79}Br^{35}Cl$, OC-$^{81}Br^{35}Cl$, OC-$^{79}Br^{37}Cl$, and OC-$^{81}Br^{37}Cl$. In addition, I have reported analyses of $\nu_1 + \nu_5^1 - \nu_5^1$ for OC-$^{79}Br^{35}Cl$ and OC-$^{81}Br^{35}Cl$. A search for the corresponding $\nu_1 + \nu_5^1$ combination bands proved unsuccessful.

3.3 Results and Discussion

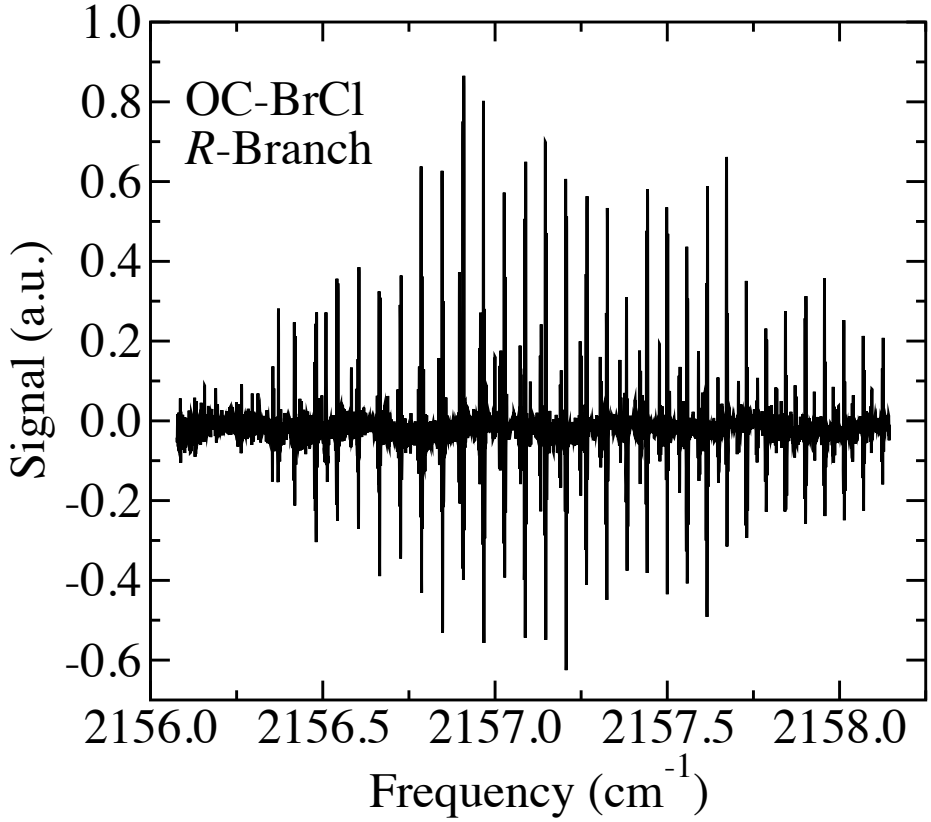

Figure 7. Spectrum of OC-BrCl over the region 2156.0 cm^{-1} to 2158.2 cm^{-1}.

Figure 7 shows a segment of scan of OC-BrCl spectrum which corresponds to the transition associated with the $\Sigma \leftarrow \Sigma$ ν_1 CO stretching vibration and its $\nu_1 + \nu_5^1 - \nu_5^1$, intermolecular low frequency hot band. Series of transitions associated with $^{79}Br^{35}Cl$, $^{81}Br^{35}Cl$ isotopomers for the $\Sigma \leftarrow \Sigma$ and $\Pi \leftarrow \Pi$ bands are given in the supplementary data for the publication.[75] Corresponding transitions of the $^{79}Br^{37}Cl$, $^{81}Br^{37}Cl$ in the ν_1

vibration are also given in the supplementary data. Other isomer transitions are apparent in the spectrum have not been presented because they are not poignant to current analysis. The ro-vibrational parameters for the analyzed spectra are given in Table 4.

Table 4. Ro-vibrational constants in cm^{-1} for OC-BrCl. Global fit with microwave data.[69] All constants are in cm^{-1}.

		ν_0	B	D_J	q
OC-^{79}Br^{35}Cl	GS		0.0314664434(13)	2.0376(22)e-8	
	ν_5^1		0.0315198(14)	1.994(44)e-8	-1.192(25)e-4
	ν_1	2156.16755(13)	0.03135603(68)	2.001(48)e-8	
	$\nu_1+\nu_5^1$	2155.69282(11)	0.0314171(15)	1.949(53)e-8	-1.174(24)e-4
OC-^{81}Br^{35}Cl	GS		0.0314631271(16)	2.0383(22)e-8	
	ν_5^1		0.0315240(38)	1.94(20)e-8	-7.02(30)e-5
	ν_1	2156.17044(13)	0.03135908(36)	2.053(18)e-8	
	$\nu_1+\nu_5^1$	2155.69737(12)	0.0314225(38)	1.95(19)e-8	-7.03(29)e-5
OC-^{79}Br^{37}Cl	GS		0.0308501155(90)	1.947(15)e-8	
	ν_1	2156.17181(15)	0.03074894(45)	1.943(29)e-8	
OC-^{81}Br^{37}Cl	GS		0.0308481976(67)	1.974(11)e-8	
	ν_1	2156.17462(16)	0.03074696(47)	1.958(28)e-8	

Table 5. Experimental data used in the CMM-RC fits for $^{16}O^{12}C$-$^{79}Br^{35}Cl$. All constants are in cm^{-1}.

Observable[a]	$V^{(0)}_{\text{CMM-RC}}$	$V^{(4)}_{\text{CMM-RC}}$ [b]	Exp.[c]	σ
B (GS)/10^{-2}	3.035	3.145	3.147	0.001
D (GS)/10^{-8}	1.7	2.1	2.2	0.1
B (v_5^1)/10^{-2}	3.044	3.155	3.151	0.001
v_1	2154.20	2156.17	2156.17	0.01
B (v_1)/10^{-2}	3.025	3.133	3.136	0.001
D (v_1)/10^{-8}	1.8	2.2	2.2	0.1
$v_1 + v_5^1 - v_5^1$	2153.75	2155.69	2155.69	0.01
B ($v_1 + v_5^1$)/10^{-2}	3.034	3.142	3.141	0.001
RMS	124.7	1.7		

[a] GS = ground state. [b] The "(4)" indicates the number of morphing parameters in the fit. [c] This data correspond to an individual fit of the $^{16}O^{12}C$-$^{79}Br^{35}Cl$ isotopomer.

The experimental data used to morph the intermolecular potential energy surface of OC-$^{79}Br^{35}Cl$ are presented in Table 5, and the values of morphing parameters, C_α, are given in Table 6. The adiabatic interaction potential energy surface of $^{16}O^{12}C$-$^{79}Br^{35}Cl$, with CO in its ground vibrational state is characterized by a linear global minimum $^{16}O^{12}C$-$^{79}Br^{35}Cl$ having R_e = 4.270(7) Å and D_e = 778(70)cm^{-1}. Also the potential surface

has a secondary linear minimum $^{12}C^{16}O$-$^{79}Br^{35}Cl$ with R_e = 4.159(4) Å and D_e = 412(25) cm^{-1}. Moreover, the morphed potential predicts, for $^{16}O^{12}C$-$^{79}Br^{35}Cl$, a D_0 value of

Table 6. Optimized values for the morphing parameters for $^{16}O^{12}C$-$^{79}Br^{35}Cl$.

α	$C_\alpha^{(0)}$	$C_\alpha^{(4)}$	σ
1	1.0	1.1130	0.0090
2	1.0	1.5227	0.0674
3	1.0	0.9214	0.0255
4	0.0	0.0308	0.0018

605(70) cm^{-1}, ν_3 = 58(3) cm^{-1} (the intermolecular stretching vibration), ν_5^1 = 31(1) cm^{-1} (the intermolecular low frequency bend), and ν_4^1 = 104(4) cm^{-1} (the intermolecular high frequency bend).

The predicted vibrational ground state structure of the OC-$^{79}Br^{35}Cl$ complex from the morphed potential is: $\overline{\theta}_i = \cos^{-1}\left(\left\langle \cos^2\theta_i \right\rangle^{1/2}\right)$ for i = 1 and 2, $\overline{\theta}_1$ = 13.3°, $\overline{\theta}_2$ = 174.1°, R = 4.307 Å, and r(C-Br) = 3.005 Å (3.026 Å correcting for $\overline{\theta}_1$ and $\overline{\theta}_2$). These structural parameters agree very well with the values: $\overline{\theta}_1$ = 10°, $\overline{\theta}_2$ = 175°, R = 4.306 Å, and r(C-Br) = 3.004 Å determined from the microwave analysis.[69] Corresponding values

for OC-$^{35}Cl_2$ are $\overline{\theta}_1$ = 15.1°, $\overline{\theta}_2$ = 175.4°, R = 4.777 Å, and r(C-Cl) = 3.136 Å (3.162 Å correcting for $\overline{\theta}_1$ and $\overline{\theta}_2$).[20] These structural parameters indicate that the amplitude of the bending motion in the ground state of the monomer components in both OC-$^{79}Br^{35}Cl$ and OC-$^{35}Cl_2$ complexes are almost the same.

Table 7. Anharmonicity constants (X_{ij}) in cm^{-1} for $^{16}O^{12}C$-$^{79}Br^{35}Cl$, calculated using the $V^{(4)}_{\text{CMM-RC}}$ potential.[a]

X_{ij}	1	3	4	5
1	-13.32	-0.61	-1.17	-0.48
3		-1.87	-1.70	-2.54
4				-2.75
5				-0.14

[a] g_{55} = 0.17 cm^{-1}.

In Table 7, the anharmonicity constants for $^{16}O^{12}C$-$^{79}Br^{35}Cl$ are given. This information was generated by predicting the appropriate wavenumbers, which were then fit to the following energy expression:

$$G\left(v_1, v_2, v_3, v_4^{l_4}, v_5^{l_5}\right) = \sum_i \omega_i \left(v_i + d_i/2\right) + \sum_i \sum_{i \geq j} X_{ij} \left(v_i + d_i/2\right)\left(v_j + d_j/2\right) + \sum_{i \geq j} g_{ij} l_i l_j ,$$

where ω_i is the harmonic frequency, d_i is the degeneracy factor, X_{ij} are the anharmonic constants, and g_{ij} is the l-dependent term of the bending vibrational modes. The value of X_{11} of -13.32 cm^{-1} indicates very small change in the anharmonicity of CO in the complex when compared to the free CO, which is characterized by anharmonicity of -13.24 cm^{-1}. It is observed that the values of X_{11} of -13.36 in OC-$^{35}Cl_2$ and X_{11} in $^{16}O^{12}C$-$^{79}Br^{35}Cl$ are the same within error.[20] This indicates a very small change in the anharmonicity for CO on complexation in both relative to that of the free CO. It is of interest that combination bands between the OC stretch and the low frequency n_5 intermolecular vibration have been relatively easy to observe experimentally for OC-Cl_2, OC-HCl and OC-HF. However, this was not so in the case for OC-BrCl, even though its anharmonic constant X_{15} is comparable to that in OC-Cl_2 and the corresponding hot bands were observable in both. Additionally, it is noticeable that the values for the intermolecular anharmonicity X_{34} are relatively large in the case of the hydrogen bonded complexes compared to the significantly smaller magnitudes characteristic of the halogen bonds.

In Table 8, we compare the fundamental intermolecular vibrations and D_0 values of OC-BrCl with OC-Cl_2 and OC-HX (X = F, Cl, Br), predicted from the morphed potential. In terms of D_0 value the OC-BrCl complex is stronger bound than the other complexes except for OC-HF. In contrast, in terms of ν_3 (the intermolecular stretching vibration) and ν_5^1 (the intermolecular low frequency bend) OC-BrCl is comparable to OC-Cl_2. Lastly, in terms of ν_4^1 (the intermolecular high frequency bend) OC-BrCl has a larger value than OC-Cl_2 but smaller than OC-HX.

Upon comparing the nature of bending motions in the ground state of OC-HF and OC-BrCl, it can be observed that the extent of the wave function in the CO bending coordinate is similar in both OC-BrCl and OC-HF. However, the BrCl monomer in the halogen-bonded complex OC-BrCl undergoes significantly smaller bending excursions than does the HF monomer in OC-HF complex. This effect is primarily a consequence of the mass differences in these two systems.

Table 8. Fundamental intermolecular vibrations and D_0 for OC-BrCl, OC-Cl_2 and OC-HX (X = F, Cl, Br), predicted from the morphed potential. All values are in cm^{-1}.

Complex	D_0	ν_3	ν_4^1	ν_5^1	Reference
$^{16}O^{12}C$-$^{79}Br^{35}Cl$	605(70)	58(3)	104(4)	31(1)	This Work
$^{16}O^{12}C$-$^{35}Cl_2$	397(5)	56.43(4)	85.43(4)[a]	25.99(2)	[20]
$^{16}O^{12}C$-HF	742.5(50)	107.99(2)	368.18(7)	81.98(2)	[56]
$^{16}O^{12}C$-$H^{35}Cl$	397.1(5)	62.88(3)	201.21(4)	48.99(3)	[20]
$^{16}O^{12}C$-$H^{79}Br$	322(3)	48.2(1)	157(1)	39.66(2)	[76]

[a] In $^{16}O^{12}C$-$^{35}Cl_2$ the ν_4^1 state is relabeled ν_b^1.[20]

It has also been previously noted that the order of the intermolecular binding strength, as measured by k_s for OC-Cl_2 < OC-BrCl < H_3N-Cl (the k_s values are 3.6, 6.3 and 12.7 N m^{-1}); the order of shrinkage corrections as described earlier, however, leads

to the lengthening of *ca*. 0.003, 0.017 and 0.0188 along this series and can be compared with the currently predicted k_s values determined from the corresponding morphed potentials (the k_s values are 3.9, and 4.3 N m^{-1}) for the first two members of the series. Furthermore these values can be compared with the corresponding values of D_0 and D_e evaluated from the corresponding morphed potentials. The previous use of the X(^{35}Cl) leads to the upper limit of $\phi_{av} = \cos^{-1} (\cos^2\phi)^{1/2} = 10.2°$.[69] The value for ϕ_{av} was selected to be most likely 5° +/- 2° which can be compared with the corresponding value 5.9° determined from the current morphed potential.[69] The estimated equilibrium values of $X_{aa}(^{79}Br)$ and $X_{aa}(^{35}Cl)$ in OC-BrCl suggest in the previous microwave study that only an additional *ca*. 3% contribution from the ionic structure in the formation of the complex, even if all the change in electric field gradient at the halogen atoms were attributed to this effect. Upon those grounds, it was considered unlikely that charge transfer, either within BrCl or from CO to BrCl, is of appreciable magnitude when OC-BrCl is formed.

Recorded infrared spectra of the halogen bonded complex OC-BrCl has been recorded in a supersonic jet and combined with previously available microwave spectroscopic data to generate a 5-D compound model morphed potential of the complex. This potential predicts a D_0 of 605(70) cm^{-1} significantly larger than OC-Cl_2 and OC-HCl but less than OC-HF (732 cm^{-1}). This prediction is consistent with the magnitude of a proper n_{CO} blue shift on complexation which increases from 6.252984(14) cm^{-1} to 12.89643(28) cm^{-1} for OC-Cl_2 and OC-BrCl respectively, values different from the 2.1 and 9.5 cm^{-1} determined from matrix studies. The value predicted for R_{CM} in OC-BrCl on the basis of the morphed potential is fully consistent with the

model proposed to correct for the effect of small coordinate determination based on microwave data.[69] Our r_e structural parameters of the complex determined from the present morphed potential functions agree with the previous conclusions that the changes in r(CO) and r(BrC1) implied by the uncorrected r_s-type coordinates a_i are probably too large since the application of only small shrinkages of the expected magnitude is sufficient to bring these quantities near to the free monomer values.[69] Furthermore, the isomerization energy of the minimum for OC-BrCl to that in CO-BrCl is predicted to be 336 (95) cm^{-1} and compares with corresponding isomerization energy of 215(10) cm^{-1} for OC-Cl_2, CO-Cl_2 isomerization.

4. ISOTOPIC ISOMERIZATION: THE DEUTERATION EFFECT IN OC-HI CONFIRMED*

4.1 Background

Isotopic substitution frequently provides powerful and widely applied approaches to the investigation of a large range of physical and chemical phenomena.[77] These have greatly enhanced fundamental understanding, characterization and prediction of the properties of matter while playing a major role in rapidly developing fields such as structural biology; nano- and bio-technology.[77-82] The latter have varied from structural effects in biologically significant interactions, isotopic effects in atmospheric ozonolysis to enzymatic rate effects.[83-85] Considerable attention has concentrated on the influence of deuterium and tritium isotopic substitution due to the inherently light mass of hydrogen and the consequent influence of relatively large mass substitution dependence particularly related to zero point energy effects. As a consequence of such extensive applications, investigations of anomalous isotope effects have now become the subject of intense interest and considerable focus.[86-89] Such effects are particularly prominent when involved in non-covalent interactions where the influence of large amplitude anharmonic vibrations and the frequent existence of different low energy isomeric

---

* Reprinted from *Chemical Physics Letters*, Volume 619, K. W. Scott, B. A. McElmurry, I. I. Leonov, R. R. Lucchese, and J. W. Bevan, "Experimental Confirmation of Ground State Isotopic Isomerization from OC-HI to OC-ID," Pages 174-179, Copyright 2015, with permission from Elsevier.

configurations can manifest themselves in many phenomena whether in the gas or condensed phases. The initial investigations of deuterium substitution effects in hydrogen bonded materials by Ubbelohde and his coworkers have long been the subject of study, particularly with respect to the isotopic dependence on the hydrogen bond length and the influence of multidimensional quantum dynamics.[90-93] Moreover, application of high resolution spectroscopic techniques to the systematic study of a range of prototypical isolated gas phase systems have proven particularly effective in giving more detailed insight following deuterium substitution in medium to weakly bound hydrogen bound dimers.[94] In-depth investigation of relatively small isolated molecular interactions are well known to provide definitive and accurate experimental data on phenomena that have wide ranging relevance but are inherently dependent on quantal effects even under macroscopic conditions. A combination of high-resolution gas phase and supersonic jet/molecular beam spectroscopic methods and application of theoretical and modeling approaches can be particularly effective for phenomenologically more detailed investigations. This is especially so when extraneous complications characteristic of condensed phase or matrix interactions are minimized and many properties can be measured with exquisite accuracy and facilitate direct comparison with theoretical and molecular computational methods. The interplay between these and condensed phase investigations can thus give important new insights into fundamental characteristics of non-covalent interactions. Indeed, such approaches can suggest new directions in investigations of related structural changes associated with isotopic substitution in isolated non-covalent interactions. A particularly unique example is the

anomalous isotopic structural change on condensed phase deuteration that has been reported by Mootz and Schilling.[95] Here, deuterium substitution has been proposed to fundamentally change hydrogen bonding in trifluoracetic acid tetrahydrate from a cationic layer structure of hydrogen bonded ($H_3O^+ \cdot 3H_2O$) enclosing F_3CCOO^- anions to a molecular hydrogen bonded $(D_2O)_n$ layer enclosing F_3CCO_2H.[95]

This result suggested potential investigations of related structural changes associated with isotopic substitution in isolated non-covalent interactions. In a previous investigation of deuteration of OC-HI using potential morphing, calculations predicted that its ground state hydrogen bound molecular system OC-HI is converted upon deuteration to a deuterated ground state with van der Waals structure OC-ID, which can be categorized as halogen bonding.[96] In this case, at absolute zero temperature, the ^1H isotope ground state structure would then be hydrogen bound whereas the corresponding ^2H isotope structure would be halogen bonded giving rise to a profound anomalous geometric isotope effect. Differential isotopic zero point energy effects have been attributed to initiating such a significant change in structure in the weakly bound limit. This is a consequence of the shallower nature of the hydrogen bound interaction at its potential minimum (frequently, a consequence of greater quartic character of the potential) relative to that which corresponds to the van der Waals global minimum (Figure 8).

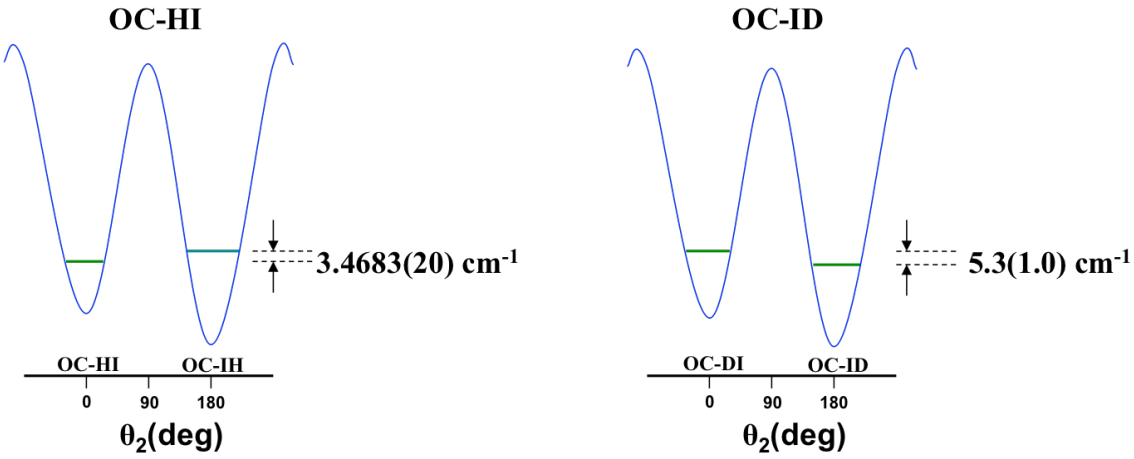

Figure 8. Illustration of zero point energy effects on deuterium isotopic isomerization in the OC-HI/OC-IH isomers and those predicted for the corresponding OC-DI/OC-ID isomers.

OC-HI and its isotopomers have been the subject of previous study using pulsed nozzle FT microwave spectroscopy as well the common isotopic species of OC-HI using an infrared diode laser cw slit supersonic jet spectrometer.[5,97] In the case of cw expansions, use of isotopic species such as DI would be prohibitively expensive. Attempted determination of the isomerization energy using such microwave spectroscopic intensity measurements gave a value of -1.0 cm^{-1} in the right direction to that predicted but the measurement was inconclusive.[5,97] We now report construction of a quantum cascade laser pulsed slit jet supersonic spectrometer that enables a cost effective and reliable evaluation of isomerization energies. Most importantly, intensity measurements on resolved transitions in the ν_1 $^{16}O^{12}C$-DI : $^{16}O^{12}C$-ID and ν_2

$^{16}O^{12}C$-HI : $^{16}O^{12}C$-IH can now be made in a simultaneous expansion that permits determination of the isomerization energy for the respective isomeric species centered around 4.66 mm. The n_2 spectra of $^{16}O^{12}C$-DI, $^{16}O^{12}C$-ID have also been recorded using the quantum cascade laser pulsed slit supersonic jet spectrometer but in this case, the laser was centered around 6.26 mm to provide the first rovibrational spectroscopic constants for the weak DI stretching vibrations in OC-DI or OC-ID.

4.2 Methods

A schematic of the pulsed slit jet infrared QCL spectrometer is shown in Figure 9 and is a design incorporating an astigmatic AMAC-76LW absorption cell (Aerodyne Research) to create a multi-pass system within the vacuum chamber. The QCLs utilized in the current investigations were fabricated by Daylight Solutions (San Diego, California) having operational ranges from 1970 cm^{-1} to 2206 cm^{-1} (21047-MHF) and 1529 cm^{-1} to 1655 cm^{-1} (21062-MHF) respectively. The laser controller was connected via GPIB interface to the host computer and the output frequency and power of the laser head could be set by a custom LabVIEW program with integrated visual interfaces from the manufacturer. Water cooling is supplied by a Thermo CUBE 200 Watt recirculating chiller (Solid State Cooling Systems, Wappingers Falls, NY). There are two ways to control the QCL's output frequency. This frequency is concurrently controlled by a stepping motor for coarse tuning and a piezo-electric micro-positioner (PZT) for fine-tuning through approximately 2 cm^{-1}. The voltage applied to the PZT was generated by

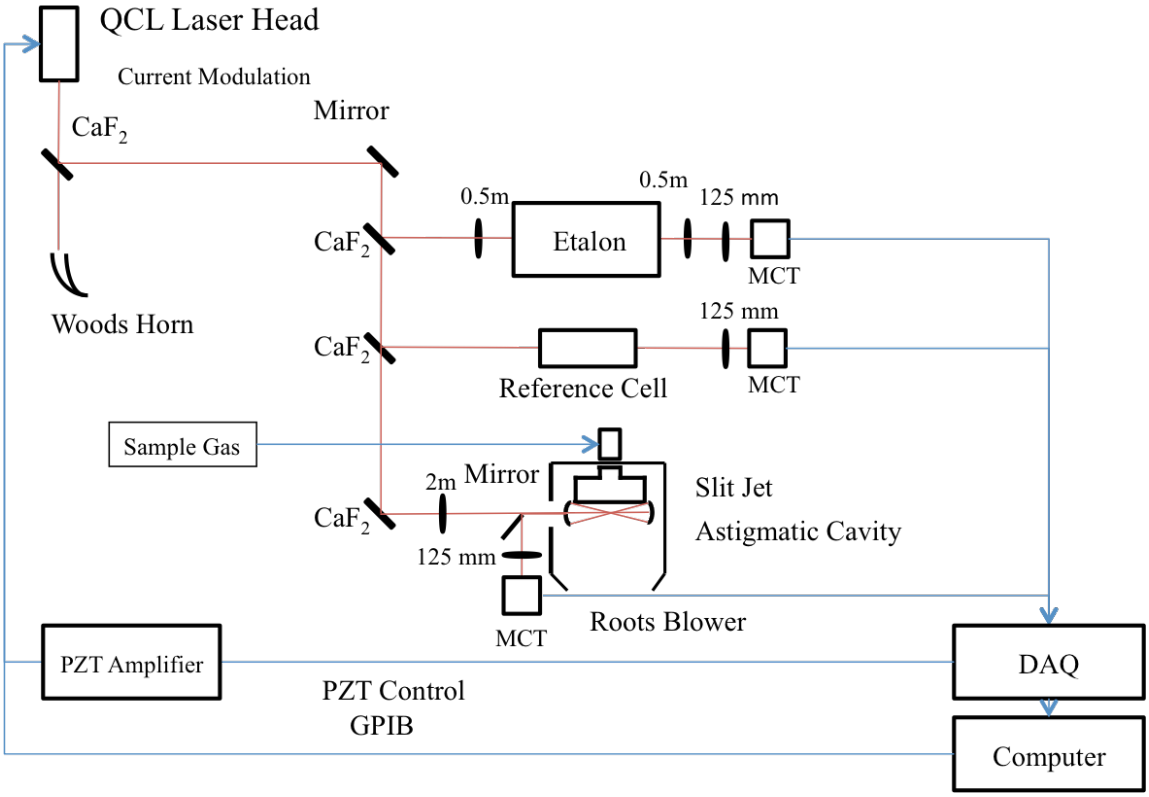

Figure 9. The path of the pulsed laser to the etalon, reference cell, and astigmatic cell allowing for an immediate measurable comparison of reference to sample on the computer display.

a NI PCI-6251 analog output and MDT694A Piezo controller. Laser output powers of 80 to 100 mW are typical. Back reflections are known to produce etaloning and other detrimental effects in the spectral baseline but was minimized using wedged optics. The output of the laser was first split by a CaF_2 wedge and split again twice more using beam splitters as shown in Figure 7. The total power used in the current experiment is estimated to be about 1 mW. The detectors used in the present study are two LN_2 cooled

MCT detectors and preamplifiers having a 1MHz bandwidth. The output of the detectors are digitized and stored in the computer using the LabVIEW program and DAQ interface. The absolute frequency scale of the observed spectrum was determined by a combination of 500 MHz germanium etalon and reference lines from the HITRAN database of carbon monoxide (CO at 1 Torr, 30 cm path) and nitrous oxide (N_2O at 10 Torr, 10 cm path) and nitrogen dioxide (NO_2 at 1 Torr, 10 cm path). The 6 cm long slit jet expansion was formed from a reservoir sample maintained at a total pressure in the range 70 psi to 85 psi consisting of typically 0.5% to 1% DI (Cambridge Isotope Laboratories), 5% carbon monoxide mixed with 94% argon carrier and spectra recorded with a multi-pass path for the radiation source through the supersonic jet expansion. The AMAC-76LW multi-pass cell was composed of two astigmatic mirrors, one containing a center hole allowing the radiation to enter and exit the cavity. The vacuum chamber housing for the slit expansion and multi-pass cavity was pumped to 60 mTorr by an Edwards roughing pump (E2M275). A diffusion pump (VHS-400) obtained a vacuum pressure operating range of 2E-6 to 5E-4 Torr. The gas entry into the vacuum chamber was pulsed with a solenoid valve (Parker General Valve, Series 9) by an Iota One valve driver box triggered by the DAQ, allowing the LabVIEW program to be used to control both the length of the pulse during which the gas was allowed to enter the chamber, and the timing of the pulsed gas expansion with the desired frequency position of the QCL range.

4.3 Results and Discussion

A total of 154 transitions were observed for OC-ID and OC-DI in both the ν_1, carbon monoxide stretch, and the ν_2, DI stretching regions. Transitions associated with the carbon monoxide stretch in the complex were significantly stronger than the DI stretch due to the larger transition dipole moment associated with that vibration, which can be seen in Figure 10 and Figure 11. Fifty-seven lines were observed for ν_1 of OC-ID; forty-five were observed for ν_1 OC-DI; twenty-three were observed for ν_2 OC-ID; and twenty-nine were observed for ν_2 OC-DI. There are gaps in the series due to spectral overlap with intense monomeric transitions of carbon monoxide and water in certain spectral regions. In addition to these newly observed transitions, we also observed transitions associated with OC-HI and OC-IH in the expansions due to incomplete deuteration of the sample cylinder, regulator and sample line.

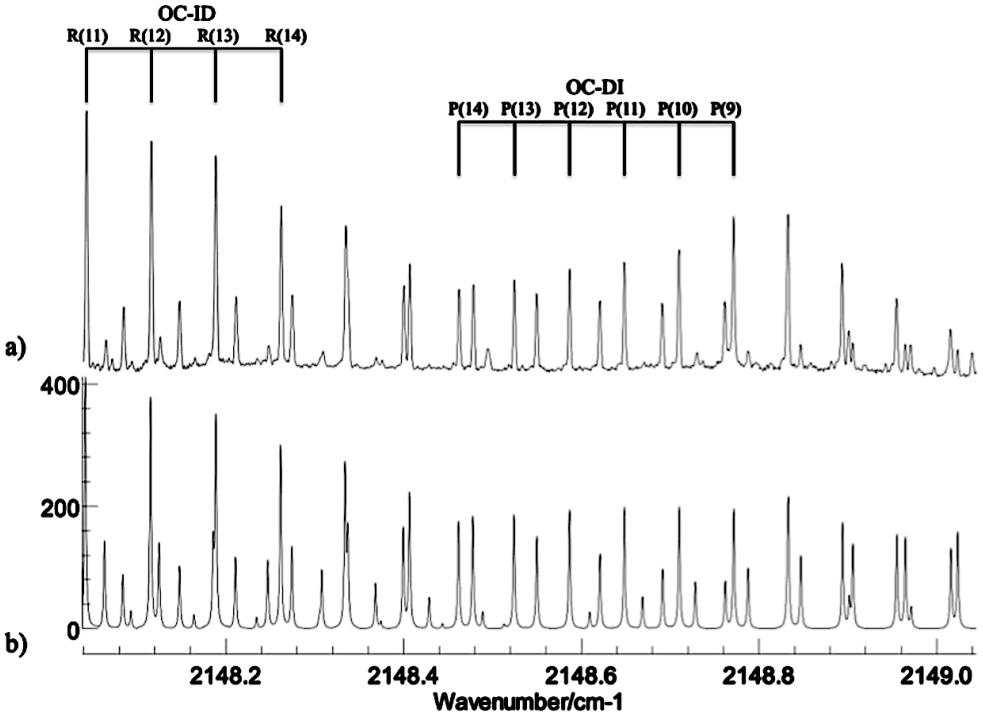

Figure 10. Experimental spectrum and simulation with a rotational temperature of 8 K and energy difference between isomers of 6 cm^{-1} with a selection of the spectral transitions used to compare peak intensity marked.

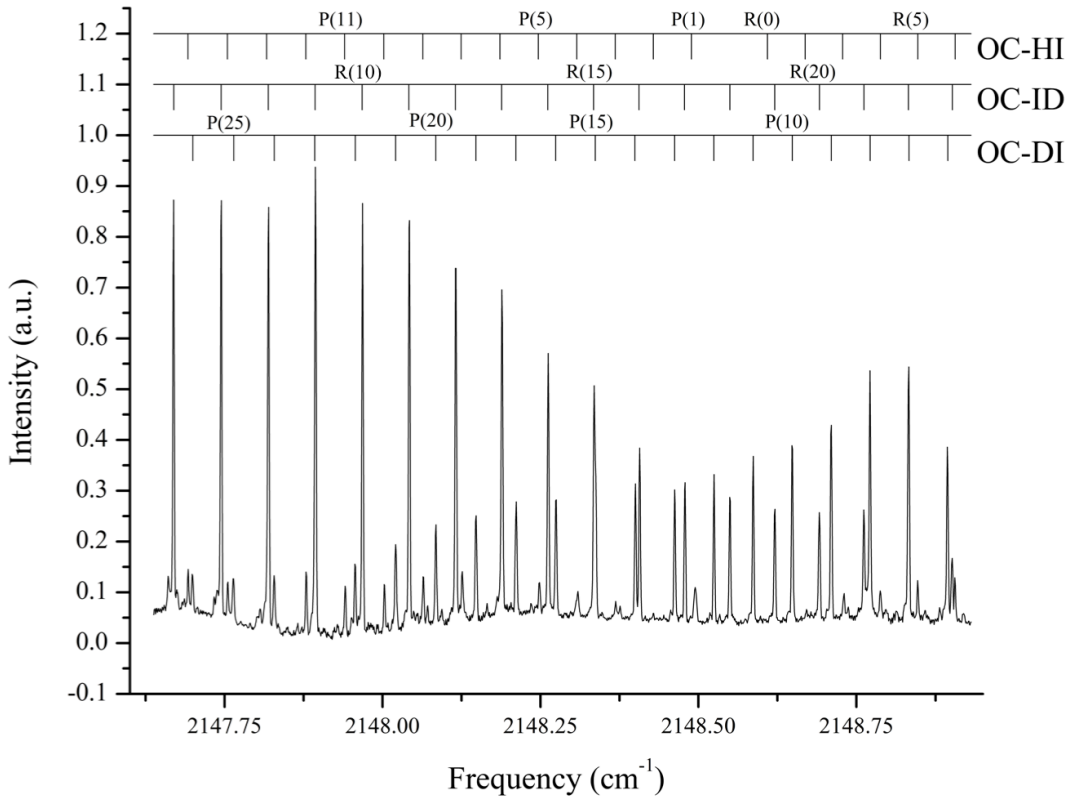

Figure 11. Simultaneous frequency scan in the range of 2147.6 cm^{-1} to 2148.9 cm^{-1} for OC-DI, OC-ID, and OC-HI.

All data including intensity measurements were treated using the PGOPHER program (C.M. Western, University of Bristol), employing a Hamiltonian consistent with a linear molecule.[74] Determination of rovibrational constants included the newly generated infrared data as well as previously generated pure rotational transitions with quadrupole substructure. In total 179 available transitions here were in the global fit of

all available data to an RMS deviation of 0.0006 cm^{-1} fitted using band origin, rotational constant, B, and centrifugal distortion, D_J for observed infrared transitions (Table 9, Table 10). Based on the simulation and comparisons with the observed intensity data (Figure 10, Table 11), we estimate that the effective rotational temperature of the expansion to be 8±1 K and the energy difference between the OC-ID and OC-DI isomers being 6.0±1.0 cm^{-1}.

Table 9. Observed and residual frequencies of OC-DI and OC-ID infrared transitions.

	OC-DI ν_1		OC-DI ν_2		OC-ID ν_1		OC-ID ν_2	
	Observed	O-C	Observed	O-C	Observed	O-C	Observed	O-C
P(1)					2147.0563	-18		
P(2)					2146.9800	-4		
P(3)			1597.9326	9	2146.9027	2		
P(4)	2149.0158	-2			2146.8254	10		
P(5)	2148.9550	-1	1597.8097	11	2146.7470	10	1594.2897	0
P(6)	2148.8943	1	1597.7470	6	2146.6681	9	1594.2137	1
P(7)	2148.8330	0	1597.6838	0	2146.5887	5	1594.1379	2
P(8)	2148.7709	-8	1597.6205	-3	2146.5095	4	1594.0623	1
P(9)	2148.7101	1	1597.5557	-15	2146.4301	5	1593.9868	0
P(10)	2148.6477	-6	1597.4924	-8	2146.3505	7	1593.9114	-5
P(11)	2148.5860	-4	1597.4282	-5	2146.2703	3	1593.8367	-5
P(12)	2148.5241	-2	1597.3637	-2	2146.1903	5	1593.7624	-4
P(13)	2148.4624	4	1597.2987	3	2146.1100	7	1593.6881	-7
P(14)	2148.3999	4	1597.2323	-3	2146.0289	3	1593.6148	-3
P(15)			1597.1666	4	2145.9478	1	1593.5421	3
P(16)	2148.2741	2	1597.0996	4	2145.8664	-1	1593.4698	9
P(17)	2148.2113	4	1597.0322	4	2145.7850	-1	1593.3960	-3
P(18)	2148.1479	2	1596.9638	0	2145.7035	0	1593.3240	-2
P(19)	2148.0842	0	1596.8955	3	2145.6217	0		
P(20)	2148.0210	3			2145.5405	10		
P(21)	2147.9568	-1			2145.4574	2		
P(22)					2145.3751	5		

Table 9. Continued.

	OC-DI ν_1		OC-DI ν_2		OC-ID ν_1		OC-ID ν_2	
	Observed	O-C	Observed	O-C	Observed	O-C	Observed	O-C
P(23)	2147.8286	-3			2145.2916	-3		
P(24)	2147.7639	-7			2145.2081	-7		
P(25)	2147.6991	-11			2145.1248	-8		
P(26)					2145.0413	-8		
R(0)								
R(1)					2147.2904	9		
R(2)	2149.4371	11			2147.3660	0	1594.9072	-5
R(3)	2149.4953	1	1598.3469	-17	2147.4427	4	1594.9869	9
R(4)	2149.5540	-1	1598.4054	-10	2147.5171	-12	1595.0648	2
R(5)	2149.6127	-2	1598.4635	-2	2147.5926	-13	1595.1431	-3
R(6)	2149.6714	-1	1598.5212	6	2147.6688	-6	1595.2212	-12
R(7)	2149.7296	-2	1598.5777	8	2147.7438	-6	1595.3019	2
R(8)	2149.7879	0	1598.6337	9	2147.8185	-7	1595.3816	4
R(9)	2149.8459	0	1598.6895	13	2147.8929	-8	1595.4615	5
R(10)	2149.9036	1	1598.7437	6	2147.9672	-7	1595.5421	11
R(11)	2149.9611	2	1598.7976	2	2148.0416	-2		
R(12)	2150.0184	3	1598.8509	-3	2148.1151	-2		
R(13)	2150.0754	3	1598.9041	-4	2148.1880	-5		
R(14)	2150.1321	2	1598.9565	-7	2148.2618	4		
R(15)	2150.1886	1	1599.0085	-8	2148.3351	11		
R(16)	2150.2447	0			2148.4067	5		
R(17)	2150.3007	-1			2148.4785	4		
R(18)	2150.3564	-2			2148.5499	3		
R(19)	2150.4118	-3			2148.6199	-8		
R(20)	2150.4671	-3			2148.6918	2		
R(21)	2150.5227	3			2148.7622	1		
R(22)	2150.5776	5			2148.8330	9		
R(23)	2150.6316	0			2148.9017	-2		
R(24)	2150.6862	3			2148.9703	-8		
R(25)	2150.7400	1			2149.0398	-2		
R(26)	2150.7940	4			2149.1082	-4		
R(27)					2149.1764	-3		
R(28)					2149.2446	1		
R(29)					2149.3130	12		
R(30)					2149.3781	-5		
R(31)					2149.4456	5		

Observed-Calculated (O-C) is multiplied by 10^{+4} for clarity.

Table 10. Rovibrational constants determined from the observed infrared transitions of OC-DI and OC-ID and those determined in previous work from the observed infrared transitions of OC-HI and OC-IH.[5,96,97]

	OC-DI		OC-ID	
	ν_1	ν_2	ν_1	ν_2
ν_0 (cm^{-1})	2149.25720(18)	1598.11303(27)	2147.13549(14)	1594.67408(30)
B" (MHz)	899.4750(9)	899.4750(9)	1159.9309(7)	1159.9309(7)
D_j " (kHz)	2.234(7)	2.234(7)	3.954(12)	3.954(12)
B' (MHz)	896.450(43)	892.90(13)	1155.839(25)	1163.53(16)
D_j ' (kHz)	2.321(62)	3.45(38)	4.095(27)	2.96(53)
	OC-HI		OC-IH	
	ν_1	ν_2	ν_1	ν_2
ν_0 (cm^{-1})	2228.31996(11)	2148.54904(3)	2222.6684(1)	2146.68233(16)
B" (MHz)	900.9524(6)	900.9519(6)	1158.67342(5)	1158.65(12)
D_j " (kHz)	2.522(6)	2.515(6)	4.5143(6)	4.60(8)
B' (MHz)	890.692(19)	898.280(2)	1164.781(14)	1154.44(12)
D_j ' (kHz)	2.442(20)	2.611(2)	4.489(14)	4.69(8)

The 154 observations obtained with the pulsed jet spectrometer are given in Table 9. With these observations, we were able to determine the rovibrational constants of OC-DI and OC-ID (Table 10). From previous analysis of ν_1 for OC-HI, the band origin, rotational constant, B'', and centrifugal distortion, D_J'', were reported as 2228.31996(11) cm^{-1}, 900.9524(6) MHz, and 4.522(6) kHz, respectively.[5,96,97] Similarly, for OC-IH ν_1, the band origin, rotational constant, B'', and centrifugal distortion, D_J'', were reported as 2222.6684(1) cm^{-1}, 1158.67342(5) MHz, and 4.5143(6) kHz, respectively.[5,96,97] The values for both upper and lower states of both ν_1 and ν_2 of

OC-HI and OC-IH are provided in Table 10 for a fuller comparison with rovibrational constants in the deuterated species recorded. In Table 10, it is pertinent to note that the ν_1 and ν_2 vibrational quantum labeling for the CO and DI stretching vibrations are interchanged by convention from the labels for the CO and HI stretching vibrations due to the large frequency shift on deuteration.

Table 11. Peak intensity ratio of OC-DI to OC-ID and OC-HI to OC-IH obtained from comparing certain J transitions.

J Transition	Peak Height Ratio: OC-DI : OC-ID	Peak Height Ratio: OC-HI : OC-IH
9	0.46	-
10	0.45	-
11	0.44	-
12	0.45	1.84
13	0.44	1.97

Table 11 gives a peak intensity ratio ($I_{P(J)}/I_{R(J)}$) 0.45(1) for J = 9 to 13 for the deuterated isomers OC-DI and OC-ID, which correlates with certain spectral transitions labeled in Figure 8. This contrasts with the corresponding peak intensity ratio ($I_{P(J)}/I_{R(J)}$) average value of 1.91(6) given in Table 11 for the corresponding hydrogen isomers, OC-HI and OC-IH, which we determine free from spectral overlap with other transitions.

Table 12. Frequency shift of the CO stretch and HI(DI) stretch upon complexation and the dissociation energy of the ground and the excited states.

Complex	CO stretch[a] frequency shift (blue shift) [$\Delta\nu/cm^{-1}$]	XI (X=H, D) stretch[b] frequency shift (red shift) [$\Delta\nu/cm^{-1}$]	D_0'' /cm^{-1}	D_0' /cm^{-1}
OC-HI	5.28	-1.26	213	214.26
OC-IH	3.41	-6.91	209	215.91
OC-DI	5.99	-1.65	238	239.65
OC-ID	3.86	-5.09	243	248.09

[a] CO monomer stretch frequency from [98]

[b] HI and DI monomer stretch frequency from [99]

In Table 12, the frequency shifts of the different isotopomers and isomers are given relative to monomeric CO and HI (DI) and can be compared with the corresponding values of ground and excited state dissociation energies determined using compound model morphing methods (columns 4 and 5).

Rovibrational infrared spectroscopy of fundamental vibrational bands as well as combination bands and hot bands have previously been demonstrated to provide significant information concerning the energy manifold of isomers OC-HI/OC-IH.[5,96,97] Infrared studies that had been applied to OC-HI included using a tunable infrared diode laser and high frequency modulation detection. In this case, a cw slit supersonic jet

expansion was used to generate an effective rotational temperature of 13 K based on its rotational intensity distribution. Such investigations unequivocally showed that the ground state was the OC-HI isomer, and application of a precise 3.4683(80) cm^{-1} combination difference frequency analysis provided a very accurate and definitive determination of the isomerization relative to the OC-IH isomer. In previous studies, fundamental vibrations associated with both the intramolecular ν_2 DI and ν_2 CO stretching vibrations in OC-DI/ID were not recorded due to expense of using enriched isotopes in these previous studies. It was thus not possible to utilize intensity measurements to determine the OC-DI to OC-ID isomerization energy using this previous cw supersonic jet infrared method and consequently to confirm the prediction from potential morphing for ground state isotopic isomerization.[96]

The ν_2 spectra of $^{16}O^{12}C$-DI and $^{16}O^{12}C$-ID, as well as ν_1 spectra of $^{16}O^{12}C$-DI, $^{16}O^{12}C$-ID have now been recorded using a newly constructed quantum cascade laser pulsed slit supersonic jet spectrometer centered around 4.57 mm and 6.26 mm, respectively and exploiting its lower gas consumption associated with its advantageous duty cycle. Rovibrational analyses of these spectra have now been completed. Most importantly, intensity measurements of rovibrationally resolved transitions in ν_2 $^{16}O^{12}C$-HI : $^{16}O^{12}C$-IH and ν_1 $^{16}O^{12}C$-DI : $^{16}O^{12}C$-ID in a simultaneous expansion has permitted determination of the isomerization energy for the former pair to be +2.8(1.0) and the latter to be -6.0(1.0) cm^{-1}. This last result is consistent with an average factor of 4.26(8) change in relative intensities for transitions given in Table 3. The former compares with the previously experimentally measured value of 3.4683(80) cm^{-1}, and

the latter with a value of -5.3(1.0) cm^{-1} predicted on the basis of a morphed potential of OC-HI.[96] It is pertinent to note that all these results do agree within estimated accuracy with the assumption that this complex has effectively equilibrated to an effective rotational temperature in both types of supersonic expansion and a value of 8 (+/-1) K in the current pulsed jet studies.

The current results confirm within the experimental error prediction of the phenomena of ground state deuterium isotopic isomerization predicted on the basis of the generated morphed potential in this complex.[96] The most desirable study would involve a direct analysis of the submillimeter transition between these isomeric forms, for that would completely specify the energy manifold in this energy regime. Unfortunately, the barrier between these isomeric forms has been shown to be approximately 418 cm^{-1}, consequently resulting in an unfavorable Franck-Condon factor for the cross-section between these states. This is further compounded by the low frequency and weak cross section of the transitions themselves. The necessity for the current intensity approach contrasts with Ar-HBr and Ar-DBr where the barrier is much lower, 54 cm^{-1}, and the wavefunctions of the Ar-H(D)Br and Ar-BrH(D) states are significantly more delocalized giving easily detectable transitions directly between these isomeric states or less directly through application of combination frequency difference methods.[100-102] The alternative approach of searching in the near infrared spectrum for a pair of transitions from the respective ground states of the isomers OC-HI and OC-IH to a common excited state also did not prove successful for the corresponding OC-DI and OC-ID isomers.[96] We were thus unable to make either type of frequency observations as

we did in Ar-HBr/ArDBr or use of infrared combinations differences as we did for OC-HI/OC-IH.[96,100,101] However, the intensity measurements that were made here in the pulsed slit jet expansion reflect a change in intensity measurements for the OC-HI : OC-IH isomer ratio to the OC-DI : OC-ID isomers by a factor of 4.26(8) that gives experimental verification of ground state isotopic isomerization upon deuteration.

Another interesting and related observation concerns the nature of isomerization on excitation of the HI and DI stretching vibrations of the complex, as seen in Table 4. In the case of the HI stretch, the red shifts for OC-HI and OC-IH are 1.26 cm^{-1} and 6.91 cm^{-1}, corresponding to respective increases in both of their excited state dissociation energies. However, unexpectedly in these excited HI stretches, the most stable isomeric form is OC-IH by 2.18 cm^{-1}, which differs from the ground state OC-HI isomer (Table 4). This is thus an example of vibrationally excited state isomerization from a ground state hydrogen bonded structure to the most stable halogen bonded isomeric structure in the HI stretching vibration. The corresponding red shift of OC-HI (-1.26 cm^{-1}) is less than that for OC-DI (-1.65 cm^{-1}) as the latter is again the stronger complex. However, in the case of OC-IH and OC-ID, the shifts of -6.91 cm^{-1} and of -5.09 cm^{-1} correlate with the fact that the ^{1}H and ^{2}H are each unencumbered by the CO molecule. The corresponding values associated with OC-IH and OC-ID indicate differences in X_{13} coupling constants in the HI and DI stretching vibrations of the complex. The red shift associated with OC-DI, however, quantitatively correlates with an even more strongly bound OC-DI complex in its vibrationally excited state. However, as discussed above, in the case of OC-IH, which occupies a local minimum in the ground vibrational state, the

opposite is true and in the vibrationally excited state, the OC-IH isomer is more stable than the corresponding ground state OC-HI isomer by 2.18 cm^{-1}. In contrast, in the DI stretching vibrations, the excited state isomerization increases by 3.44 cm^{-1} with the OC-ID being the most stable, correlating with its most stable isomeric form in the ground vibrational state. The frequency shifts in the CO stretch correlate with proper blue frequency shifts as given by work on the Badger-Bauer rule.[103] As expected for hydrogen bound OC-HI, the blue frequency shift of +5.28 cm^{-1} is less than the blue frequency shift of +5.99 cm^{-1} for the more strongly bound OC-DI complex. The corresponding shift of OC-IH (+3.41 cm^{-1}) is comparable as the OC-ID shift is +3.86 cm^{-1}. Interestingly, in the excited CO stretching vibration, the blue shifts of 5.28 cm^{-1} and 3.41 cm^{-1} for OC-HI and OC-IH correspond to a reduction in the isomerization energy by 1.60 cm^{-1} though the most stable isomer remains OC-HI. In contrast, the corresponding shifts in OC-DI and OC-ID are 5.99 cm^{-1} and 3.86 cm^{-1} and the OC-ID isomer becomes 5.09 cm^{-1} more stable in the excited state relative to the ground state isomer, OC-DI. Such measurements are thus a sensitive measure of the intricate isomerization and isotope effects in a weakly bound complex such as OC-HI. The complex should thus prove to be a very interesting prototype for investigation of infrared photodissociation dynamics and product distribution in a system that exhibits pronounced competing intermolecular effects associated with hydrogen and halogen bonding.

The spectroscopic rovibrational analyses of the ν_1 spectra of $^{16}O^{12}C$-DI and $^{16}O^{12}C$-ID, as well as ν_2 spectra of $^{16}O^{12}C$-DI, $^{16}O^{12}C$-ID have been completed using a

quantum cascade laser pulsed slit supersonic jet spectrometer centered with mode-hop free lasers centered around 4.57 and 6.26 mm respectively. Intensity measurements of the ν_2 $^{16}O^{12}C$-HI : $^{16}O^{12}C$-IH and ν_1 $^{16}O^{12}C$-DI : $^{16}O^{12}C$-ID in a simultaneous expansion has permitted determination of the isomerization for the former to be +2.8(1.0) cm^{-1} and the latter to be -6.0(1.0) cm^{-1}. The former compared with the previously experimentally measured value of 3.4683(80) cm^{-1} giving confidence in the accuracy of the intensity method utilized here. The latter value of -6.0(1.0) cm^{-1} compared with the value of -5.3(1.0) cm^{-1} previously predicted on the basis of a morphed potential for OC-HI.[101] These results thus confirm within experimental error the theoretical prediction of the phenomena of ground state deuterium isotopic isomerization predicted on the basis of the generated morphed potential in a simple prototypical system where the effect can be subject of in-depth investigation. This phenomenon is expected to influence the structure and dynamics of systems more generally, particularly in more complex environments such as those involving deuterated solvents in structural biology.

5. BADGER-BAUER REVISITED: A MODEL*

5.1 Background

Compiling some of the modeled data from the complexes investigated with the continuous wave QCL spectrometer, Figure 12 shows the linear relationship of hydrogen bonded species, specifically the relation between the frequency shift from the non-hydrogen bonded monomer and the dissociation energy. Furthermore, the predictive powers of this linear relationship are provided with the frequency shift estimated for the OC-H_2O from its dissociation energy.

The Badger–Bauer rule was initially applied to neutral closed shell hydrogen bonded complexes in 1937 following publication of the Badger rule for diatomic molecules.[104,105] In this paper, it was proposed that the enthalpy of formation of hydrogen bonds, ΔH, was linearly related to the infrared frequency shifts, Δv for hydroxylic electron acceptors involved in such hydrogen bonding.[104] Since this time, it has been extensively used to correlate experimentally determined red frequency shifts of B - HO- and related stretching vibrations with intermolecular binding strengths for a large range of hydrogen bonded acceptors, B.[106-108] A number of models have also been

---

* Adapted with permission from "The Badger–Bauer Rule Revisited: Correlation of Proper Blue Frequency Shifts in the OC Hydrogen Acceptor with Morphed Hydrogen Bond Dissociation Energies in OC–HX (X = F, Cl, Br, I, CN, CCH)" by L. A. Rivera-Rivera, B. A. McElmurry, K. W. Scott, R. R. Lucchese, and J. W. Bevan, *The Journal of Physical Chemistry A* Volume 117, Pages 8477- 8483. Copyright 2013 American Chemical Society.

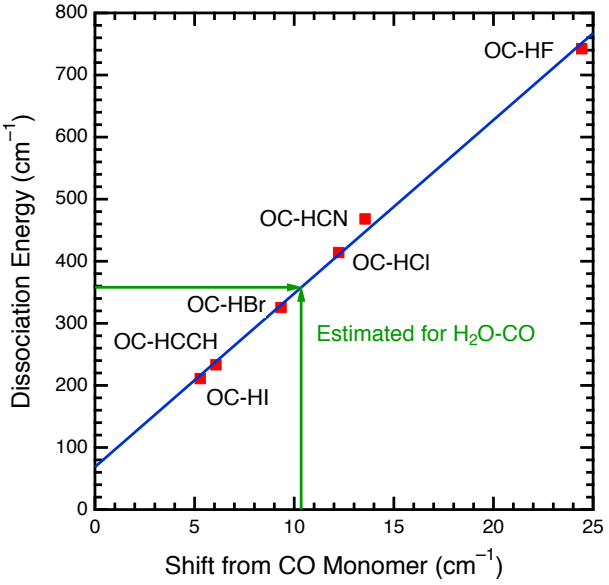

Figure 12. Correlation for blue shift of CO stretch and dissociation energy D_0 obtained from morphing. Interpolation gives D_0 for H_2O-CO to be 355(13) cm^{-1}.

developed theoretically to account for the basis of the Badger-Bauer relationship.[109-111] Further applications have, in addition, involved a wide range of studies including H-X red frequency shifts with force constants or bond length changes.[110-112] There have been varying degrees of success with such correlations, in part due to a number of factors such as solvent and steric effects in experimental studies and the influence of anharmonicity.[34,110,113-118] Despite these issues, Badger-Bauer relationships still continue to be invoked in a wide range of applications.[119-126] These have also included proton acceptor carbonyl frequency shifts because of the facility of experimental measurements.[127,128] In particular, spectroscopically determined frequency shifts on complexation are used as a means of qualitatively or quantitatively probing of the

strength of non-covalent interactions as well as the environment of hydrogen bonded interactions.

The accurate experimental determination of D_0 for neutral ground state isolated hydrogen bonded complexes has been and continues to be an active field of research.[129,130] Remarkably, such D_0 values have only been accurately determined for a relatively small number of systems under effectively isolated gas phase conditions or in supersonic molecular beams. In some respects, the Badger–Bauer relationship represents one of the earliest semi-empirical attempts to obtain quantitative binding energies for a wide range of hydrogen bonded complexes, especially in condensed phases and comparable investigations have continued since.[104]

Recently, morphing methods have been developed and applied to generate potential functions for hydrogen bonded complexes.[20,21,37,56,73,76,96,131,132] A primary objective of this work has been prediction of the properties of prototypical hydrogen bonded and halogen bonded complexes with significantly enhanced accuracy compared to standard *ab initio* calculations alone. Most importantly, this improvement in predictability should be relevant to determining either ground state D_0 or equilibrium D_e dissociation energies as well as frequency shifts of either intramolecular frequencies in hydrogen atom acceptors or donors that result from complexation of such dimers. Traditionally, for hydrogen bonded interactions these have involved correlation of binding energies of the dimer with red frequency shifts of the hydrogen donor using the widely applied Badger-Bauer rule or some closely related variant of it.[114] An alternative approach to be considered here, will investigate possible correlations of binding energies

predicted on the basis of potential morphing approaches with experimentally determined proper blue frequency shifts of the hydrogen acceptor. This is particularly so for hydrogen bond interactions that are free from matrix and solvent effects.[26,40,97,133] Recently, DFT calculations have been used to model the stretching frequency n_{CO} shifts within the protein matrices in which CO interacts with non-charged amino acids.[119,123] Certain of these calculations indicated blue frequency shifts on complexation, which the authors found consistent with the Badger rule.[105,119] Frequency shifts in CO associated with solute-solvent interactions have been the subject of previous theoretical treatment that also have direct relevance to the current work.[134]

A systematic investigation of the homologous series OC-HX (X=F, Cl, Br, I, CN, CCH) using both experimental and potential morphing approaches is presented here giving new insights into the applicability of tenets of the Badger-Bauer relationships.[20,21,37,56,73,76,96,131,132] In particular, a model has been developed that determines the requirements for such relationships and could result in further adaptions and extended applications through construction of a D_0 vs. $\Delta\nu_0$ calibration curve. An application is now reported for the systematic investigation of proper OC blue frequency shifts on complexation with hydrogen bond dissociation energy for the series considered. Such shifts are different from the improper blue shifts of H-X vibrations that have recently been the subject of considerable attention.[135-137] This series is selected in order to determine any correlations between D_0 and $\Delta\nu_0$ in this specified series and possible verification or otherwise of the Badger-Bauer rule to the observed proper blue frequency shifts.[104] The magnitude of hydrogen acceptor blue frequency shifts observed in this

series are frequently smaller in magnitude than corresponding HO-R and H-X stretching hydrogen bonded red shifts that have been measured.[26,39,126] However, in the context of the current studies, experimentally determined blue frequency shifts for intramolecular vibrations in hydrogen bond acceptors have been determined precisely. Here, rovibrational analysis using supersonic jet spectroscopic methods have been investigated under effectively collisionless conditions free from matrix or solvent effects.[26,40,97,133] In addition, prediction of zero-point energy corrected dissociation energies have been determined based on semi-empirically generated morphed potentials as are intramolecular harmonic frequency shifts giving the opportunity to investigate in detail the applicability of the Badger-Bauer rule to these types of systems.[56,104] The series chosen for investigation facilitates study because these complexes involve hydrogen bonded interactions that are linear or at least quasi-linear under conditions, free from solvent or matrix effects rendering simplification of both spectroscopic and computational treatments.[110] This is particularly so for correlating the results with both a model developed to account for the previously discussed observations and molecular calculations. Furthermore, the resulting linear correlation of D_0 with $\Delta\nu_0$ will be used to interpolate the dissociation energies of three other related hydrogen bonded complexes H_2O-CO, H_2S-CO and CH_3OH-CO not included in the prior analyses.[138-140] The results will also be correlated directly with DFT calculations that have been used to model the stretching frequency ν_{CO} shifts within the protein matrices where CO interacts with different non-charged amino acids.[119,121-123]

5.2 Impact and Application

The newly generated 5-D morphed potential for OC-HBr, $V^{(3)}_{\text{CMM-RC}}$, was obtained with the morphing parameters C_1 = 1.0945(19), C_2 = 0.1821(65), C_3 = 1.0, C_4 = 1.0 and C_5 = 0.00776(13). These parameters give a root mean square, RMS of G = 1.3. CO blue frequency shifts $\Delta\nu_0$ for OC-HX (X=F, Cl, Br, I, CN, CCH) have been measured experimentally previously and are given in Table 13 column 2 with the corresponding D_0 values in column 3.[21,73] Figure 10 shows the plot of D_0 against $\Delta\nu_0$ of a linear fit to these points giving the straight line plot $y = ax + b$ where a = 27.942 and b = 69.016 with R^2 = 0.9984. Using values of $\Delta\nu_0$ experimentally available for H_2O-CO, H_2S-CO and CH_3OH-CO, it is now possible to interpolate respective values of D_0 to be 355(13), 171(11) and 377(14) cm^{-1} under the assumption that the corresponding blue frequency shifts on complexation can be interpolated using the plot in Figure 10.[138-140] In order to obtain suitable data for development of the model described in Eq (19), the 1-D potentials in the intermolecular coordinate R and OC stretching coordinate r were generated from 5-D compound-model morphed potentials in OC-HX (X=F, Cl, Br, CN), and related data and parameters are given in Table 14. The other parameters, derived from the morphed potentials of the complexes considered are also given in Table 14. The corresponding plots for D_i against $\Delta\omega_{ei}$ for the model and potential are given in Figure 13.

Table 13. CO blue frequency shifts and dissociation energies from morphed potentials for OC-HX (X = F, Cl, Br, I, CN, CCH). All data in cm^{-1}.

Complex	$\Delta\nu_0$	D_0
$^{16}O^{12}C$-HF	24.42677	742.5(50)
$^{16}O^{12}C$-$H^{35}Cl$	12.22862	414.2
$^{16}O^{12}C$-$H^{79}Br$	9.33346	325.56
$^{16}O^{12}C$-HI	5.2775	210.99
$^{16}O^{12}C$-HCN	13.55011	468.26
$^{16}O^{12}C$-HCCH	6.0717	233.36

Table 14. Dissociation energies D_i, parameters g_i, dR_e/dr, and $\Delta\omega_e$ for model calculations on OC-HX (X = F, Cl, Br, CN). All data in cm^{-1}.

Complex	D_i	g_i	dR_e/dr	$\Delta\omega_e$ (Model)	$\Delta\omega_e$ (Potential)
$^{16}O^{12}C$-HF	1240.9	1.0774	0.9056	28.3986	29.6622
$^{16}O^{12}C$-$H^{35}Cl$	732.5	1	0.9965	16.9064	16.9064
$^{16}O^{12}C$-$H^{79}Br$	595.7	0.9861	1.0159	13.7787	13.3692
$^{16}O^{12}C$-HCN	656.3	0.9085	0.9841	14.5422	15.7238

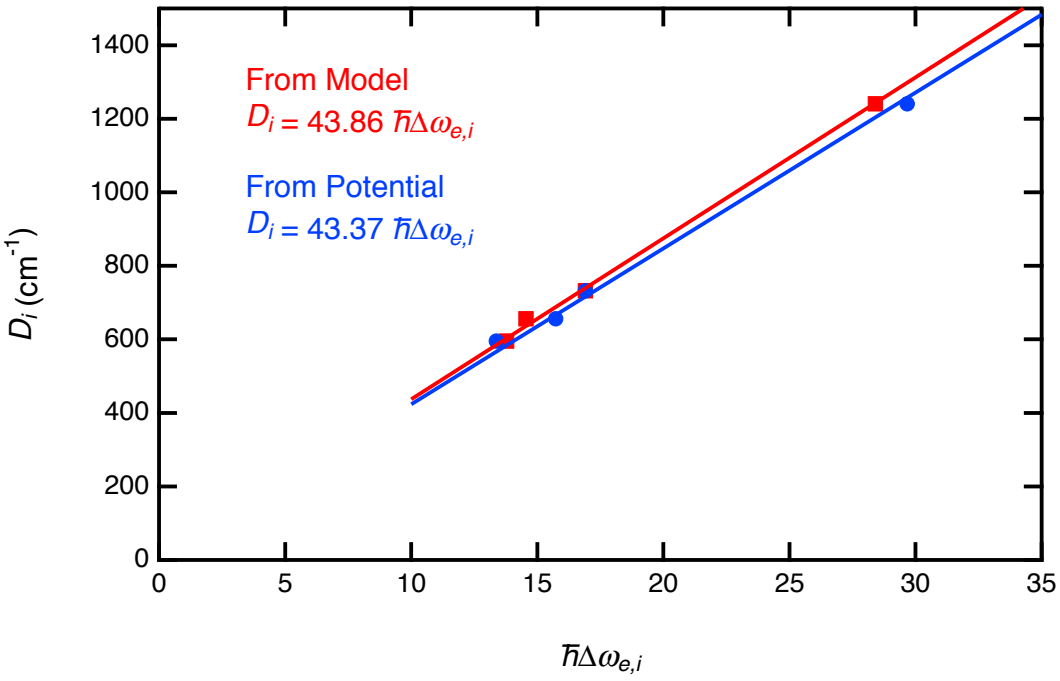

Figure 13. Correlation of D_i from *ab initio* morphed potentials and from the model with predicted harmonic frequency shifts in CO for OC-HX (X=F, Cl, Br, CN).

Table 15 contains data from CCSD(T)/aug-cc-pVQZ calculations for OC-HX (X = F, Cl, Br, I, CN, CCH, OH, SH) which are intended to supplement previous calculations and models.[119] Figure 12 shows a linearly dependent plot (R^2 = 0.9984) of D_0 against the experimentally determined blue shift $\Delta\nu_0$. This is indicative of a relationship that is consistent with the Badger-Bauer rule for the series investigated. This linear dependence, however, does not result in a straight line passing through the origin. This is not unexpected from a perspective based on the dissociation energies not being corrected for zero point energies and the frequency shifts in the different complexes not

Table 15. CO harmonic blue frequency shifts and dissociation energies from CCSD(T)/aug-cc-pVQZ calculations for OC-HX (X = F, Cl, Br, I, CN, CCH, OH, SH).

Complex	ω_e (cm^{-1})	$\Delta\omega_e$ (cm^{-1})	r_e(CO) (Å)	D_e (cm^{-1})
$^{16}O^{12}C$-HF	2189.76	30.43	1.128560	1211.36
$^{16}O^{12}C$-H^{35}Cl	2175.80	16.47	1.129993	686.19
$^{16}O^{12}C$-H^{79}Br	2172.51	13.18	1.130332	564.34
$^{16}O^{12}C$-HI	2167.52	8.19	1.130872	398.38
$^{16}O^{12}C$-HCN	2175.92	16.59	1.129959	600.02
$^{16}O^{12}C$-HCCH	2167.61	8.28	1.130903	367.14
$^{16}O^{12}C$-H_2O	2174.25	14.92	1.130207	618.32
$^{16}O^{12}C$-H_2S	2166.16	6.83	1.131052	326.18

The value ω_e for free CO is 2159.33 cm^{-1}.

being corrected for anharmonicity as these quantities are expected to differ significantly for the range of complexes considered in the plot. However, if an uncorrected plot of this kind can be used as a reliable calibrant for determination of ground dissociation of other complexes based on experimentally determined and comparable blue shifts, then the approach could have significant wider implications. In the case of the complexes under consideration, the frequency shift, however, is not the traditional red frequency shift dependence associated with the proton acceptor as proposed by Badger and Bauer.[104] Furthermore, a proper blue frequency shift of the hydrogen atom acceptor must also be

distinguished from corresponding HX improper blue frequency shifts.[134-136] Corresponding shifts associated with proton acceptors have been documented for carbonyl frequency shifts with change in enthalpy, ΔH , but in these cases such dependencies have been associated with red frequency shifts.[128]

Figure 13 is in many respects more meaningful than the variables, the dissociation energy D_e and the $\Delta\omega_e$ for the CO stretching vibration are corrected for zero point energy and anharmonicity in the complexes considered. This makes the results directly comparable with calculations based on standard *ab initio* packages. Two plots are presented in Figure 13. The first derived from morphed potential energy data and the second from this proposed model. Both plots give straight-line dependencies in complexes for which 5-D morphed potentials are available. The former has a slope of 43.37 blue frequency shift with $R^2 = 0.9997$, and the latter with a slope of 43.86 blue frequency shift and $R^2 = 0.9989$, each case giving a straight line through the origin. The former is interesting as it not only correlates with the linear dependence expected within the tenets of the original Badger–Bauer rule but corrections for anharmonicity and zero point energy effects giving a plot through the origin for the systems considered.[104] The characteristics of this plot including its slope has significance for future applications as it has been predicted from accurately determined semi-empirical compound morphed potentials generated from extensive high resolution spectroscopic data. Moreover, these results are also relevant to prior spectroscopic investigations that deviate from linear characteristics complicating application of the Badger-Bauer rule.[105-115] Specifically, they are indicative of the influence of anharmonicity as is apparent from the change in

slopes relative to Figure 12. Data specific to the validity of the assumptions made in its derivation and the effective independence of $f(r)$ are shown in Table 14. The terms in the expansion shown in Table 14 give the necessary requirements for the linear correlations associated with effective application of the Badger-Bauer rule. Clearly for the systems investigated and the range of binding energies involved, these requirements are met and can be compared with similar behavior observed in diatomic molecules.[105,141]

The harmonic corrected frequency shifts in CO that occur for the range of hydrogen bonded donors investigated are directly proportional to the equilibrium dissociation energies of the complexes. Furthermore, when their product is taken, it reflects the observed almost linear dependence. Of additional interest is how this derived relationship correlates with an equivalent approach invoked by Hermansson to explain certain frequency shifts on hydrogen bonding that are associated with $\Delta\nu_{\mathrm{OH}} \propto -\mathrm{E}_{\parallel}\cdot\left(\mathrm{d}\mu_{\parallel}^{free}/\mathrm{d}r_{\mathrm{OH}} + 1/2\cdot\mathrm{d}\mu_{\parallel}^{ind}/\mathrm{d}r_{\mathrm{OH}}\right)$.[136] The current model, however, goes further in order to explicitly consider the dependence on D_{e} and to include an additional term that influences frequency shifts. It is relevant to note that a plot of $\Delta\omega_e$ against D_{e} for modeling neutral amino-acid–CO interactions generated from B3LYP calculations also gives a straight line through the origin. However, the slope of 83 blue shift is significantly different from that presented in this work (43.25 blue shift). We attribute this difference as due to the former calculations, treating the interaction as primarily electrostatic with no contributions due to dispersive effects. A corresponding plot based on CCSD(T)/aug-cc-pVQZ calculations for the OC-HX series considered in this work

also gives a linear plot but in this case the gradient of 37.04 blue frequency shift is in better agreement with the plots more accurately determined in Figure 13. It is interesting also to consider applications of the results shown in the plot included in Figure 13. As an example the CO harmonic blue shift on complexation and its D_e calculated at the CCSD(T)/aug-cc-pVQZ level for the complex H_2O-CO can be compared with results interpolated from similar calculations to those used for the other OC-HX complexes considered as calibrants. Here the calculated value of $\Delta\omega_e$ for H_2O-CO gives an interpolated value of D_e = 615 cm^{-1} from that plot which can be compared with the directly calculated value of 618 cm^{-1} (Table 15). The corresponding values for H_2S-CO are 316 cm^{-1} and 326 cm^{-1}, respectively. These calculations thus support the conclusion that these complexes have similar blue frequency shift behavior to the hydrogen bonded series OC-HX (X=F, Cl, Br, I, CN, CCH) (Figure 12) and from a calibration perspective can be categorized in the same group interactions for application of the Badger-Bauer rule.

Experimentally observed proper blue shifts $\Delta\nu_0$ for the CO proton acceptor are demonstrated to have linear correlations with predicted hydrogen bonded dissociation energies D_0 based on accurate semi-empirical morphing methodologies. Such results are consistent with the original tenets of the Badger-Bauer rule.[104] In this series, such proper blue shifts contrast with traditionally directly measured H-X red shifts that frequently exhibit a corresponding non-linear dependence. A model has now been formulated to rationalize the intrinsic characteristics of the systems studied and associated blue frequency shifts on complexation, particularly with respect to the Badger-Bauer

relationship. Application of 5-D compound-model morphed potentials in formulating this model have provided criteria that correlate the linear dependence of $\Delta\omega_e$ with D_e and furthermore give insight into the influence of anharmonicity and zero point energy effects. In principle, similar approaches should be applicable to a range of hydrogen bonded interactions involving frequency shifts in acceptor vibrations including HCN, CH_3CN and NO. Results can also be compared with those previously generated in DFT calculations that asserts that the frequencies of ν_{CO} serve as a powerful tool to probe the surrounding environments of CO molecule inside protein matrices, as well as its orientations.[119] In these investigations of the weak interactions between non-charged amino acids and CO revealed the effects of the protein's micro-environments on the docked gas molecule, contributing insights into the accommodation and migration of small ligands within protein matrices. This in turn suggests the current studies of CO as hydrogen acceptor can provide quantitative information for using CO as a useful probe for delineating the structure–property–function relationship of heme-based sensors.[120]

6. INVESTIGATIONS INTO AR-NO AND NO-H_2O

6.1 Background for Ar-NO and NO-H_2O

The complex of Ar-NO is an excellent system that is prototypical of open shell complex systems. There has been much interest in it due to the nonadiabatic character of its dynamics. There have been numerous experimental and theoretical investigations into the Ar-NO system.[142-144] There have also been external cavity QCL investigations into NO monomer in the infrared region by means of Faraday rotation spectroscopy techniques.[13,145] The experimental investigations of the Ar-NO complex have ranged from the microwave and radio frequency regions to the mid-infrared with infrared resonance-enhanced multiphoton ionization (IR-REMPI) methods.[146-150] This last experimental work involving the IR-REMPI methods, generated some interesting results; Meyer's experimental work was combined with the theoretical efforts of Klos and Alexander resulting in what is shown in Figure 14.[150] The fact that it was a double resonance experiment provides the direction for our work in the lower state.

The investigation into the open shell complex Ar-NO to accurately measure spectroscopic data will be useful to analyzed to characterize the intermolecular interactions in a NO-H_2O complex. The experimental efforts resulted in rotationally resolved data. With this information the relative energies of structural isomers, dissociation energies, low frequency intermolecular transition energies and accurate predictions of thermodynamic properties can be determined.

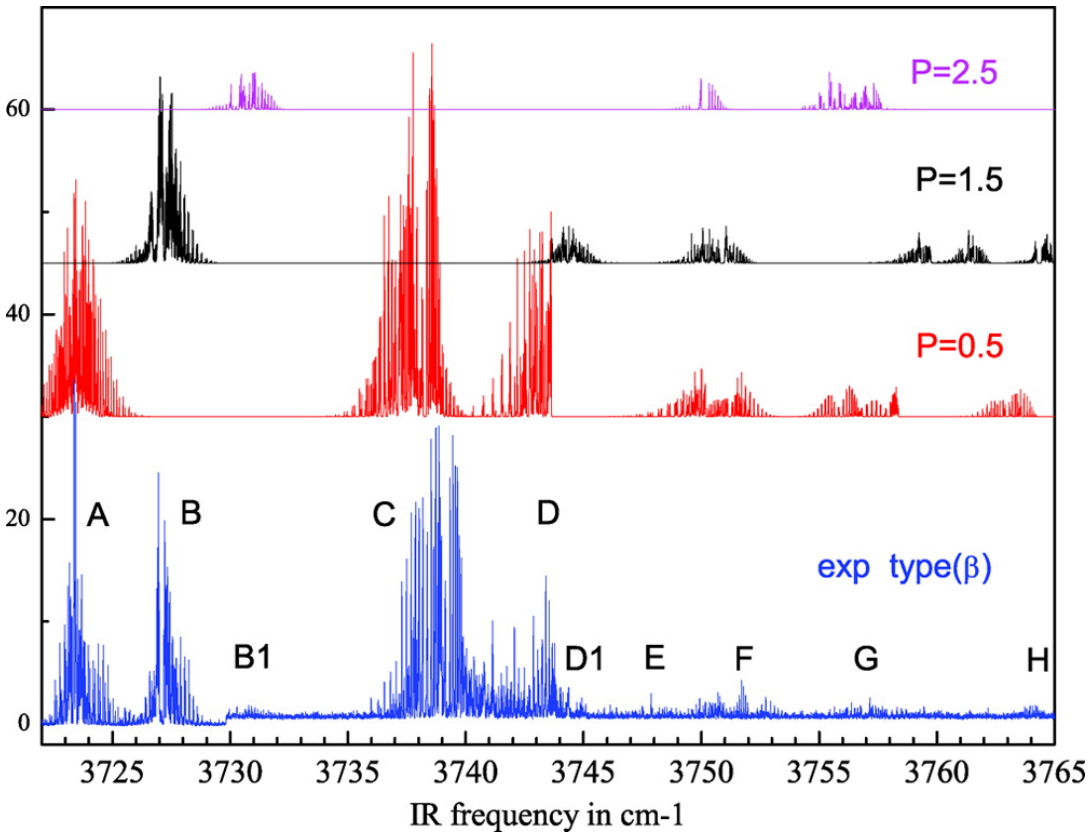

Figure 14. Meyer's experimental investigation of Ar-NO via IR-REMPI in the bottom spectrum, with calculated predictions from Klos and Alexander's theoretical studies visualized in the top three spectra.[150]

These studies of intermolecular interactions serve an important function as they can be applied to covalent or other categories of chemical bonds. Using this method will allow for the basis of modeling sophisticated biochemical, nanochemical, and material science interactions while encouraging future innovation. This research will institute

standards to increase the accuracy, when studying and modeling atmospheric chemical complexes and the role of NO in bioregulatory functions.

The NO-H_2O complex is one of interest for the part it plays in biological systems[1] due to the impact of NO in upper atmospheric chemistry.[151] The study of this complex serves as a prototype for future study of the interaction of water with open-shell molecules.

In order to better understand the role played by NO as an intracellular messenger molecule, with respect to its biological impact, the NO moiety modeled is dependent on its diffusion in water allowing for the determination of NO-H_2O potential interactions.[152]

The NO-H_2O complex has been the subject of several papers.[153-157] Ball studied the impact that bonding orientations would have on the complex and found that theoretically, whether bonded through the hydrogen or through the oxygen at ~0 K, the complex was weakly bound.[154] By using coupled-cluster spin-restricted R-CCSD(T) modeling as well as augmented correlation-consistent polarized-valence triple zeta basis set extended with a set of 3s3p2d1f1g mid-bond functions, the intermolecular potential energy surfaces of the two lowest energy levels of NO-H_2O could be determined, allowing for a comprehensive characterization of both the 2A′ and 2A″ electronic states in the C_s-symmetry configurations.

The global minimum for the 2A′ state represented by the lowest energy of −461.8 cm^{-1} is deeper than the global minimum in the 2A″ state with an energy of −435.2 cm^{-1}. The only vibrational spectrum recorded has been a Ar matrix isolation experiment in which bands have been recorded with shifts relative to monomers at ν_1

3660.9(-4.6) cm^{-1}, ν_2 1597.1(1.5) cm^{-1}, ν_3 3771.3(+10.2) cm^{-1} and ν_{NO} 1876.3(1.7) cm-^{1}, 1879.4 (1.9) cm^{-1}.[156] Interestingly, only the isomer with an HOH-ON intermolecular hydrogen bond was observed in the Ar matrix, with no evidence for the nitrogen bound isomer, despite the latter being calculated to be 0.2 eV more stable by DFT calculations.[156] There are no rovibrational analyses or rotational spectra for H_2O-NO under isolated conditions such as occur in static gas phase or supersonic jets. However, photoelectron–photofragment coincidence studies of NO-(H_2O), have been performed by dissociative photodetachment of an electron from the NO-$(H_2O)^-$ anion.[158] Companion calculations found minima in the PES for this complex with the N atom of NO interacting with the H_2O molecule. A binding energy of 411 cm^{-1} was predicted in agreement with earlier calculations.[159]

In the calculation by Cybulski, *et al.*, the lowest energy for the 2A′ state corresponds to the configuration with NO trans to the free OH geometry of R =3.66 Å, α=51.0°, and β=108.5° with an energy of −461.8 cm^{-1}.[159] For the 2A″ state the lowest minimum with an energy of −435.2 cm^{-1} is described by the following intermolecular parameters: R =3.08 Å, α=75.9°, and β=35.8°, and the bonding occurs between the nitrogen atom and the water molecule's oxygen.

In order to observe H_2O-NO rovibrational bands, the spectra obtained from the Ar-NO investigations served as a comparative baseline. In the future, through Faraday rotation spectroscopy in supersonic expansion, the 6.2 μm vibration and combination bands due to H_2O bend in the complex can be visualized. By using this technique, the sensitivity can potentially be improved by up to a factor of two from the present QCL

spectrometer setup. Furthermore, the Faraday rotation spectroscopy would filter closed-shell absorptions, increasing the desired signals' strength and providing a zero noise baseline. With the present data, it should be possible to map the structure and bonding energies of the complex, given full analysis.

6.2 Methods for Ar-NO Investigations

A schematic of the pulsed slit jet infrared QCL spectrometer is shown in Figure 2 and is a design incorporating an astigmatic AMAC-76LW absorption cell (Aerodyne Research) to create a multi-pass system within the vacuum chamber. The QCLs utilized in the current investigations were fabricated by Daylight Solutions (San Diego, California) having operational ranges from 1970 cm^{-1} to 2206 cm^{-1} (21047-MHF) and 1529 cm^{-1} to 1655 cm^{-1} (21062-MHF) respectively. The laser controller was connected via GPIB interface to the host computer and the output frequency and power of the laser head could be set by a custom LabVIEW program with integrated vi's from the manufacturer. Water cooling is supplied by a Thermo CUBE 200 Watt recirculating chiller (Solid State Cooling Systems, Wappingers Falls, NY). There are two ways to control the QCL's output frequency. This frequency is concurrently controlled by a stepping motor for coarse tuning and a piezo-electric micro-positioner (PZT) for fine-tuning through approximately 2 cm^{-1}. The voltage applied to the PZT was generated by a NI PCI-6251 analog output and MDT694A Piezo controller. Laser output powers of 80 to 100 mW are typical. Back reflections are known to produce etaloning and other

detrimental effects in the spectral baseline but was minimized using wedged optics. The output of the laser was first split by a CaF_2 wedge and split again twice more using beam splitters as shown in Figure 2. The total power used in the current experiment is estimated to be about 1 mW. The detectors used in the present study are two LN_2 cooled MCT detectors and preamplifiers having a 1MHz bandwidth. The output of the detectors are digitized and stored in the computer using the LabVIEW program and DAQ interface. The absolute frequency scale of the observed spectrum was determined by a combination of 500 MHz germanium etalon and reference lines from the HITRAN database of carbon monoxide (CO at 1 Torr, 30 cm path) and nitrous oxide (N_2O at 10 Torr, 10 cm path) and nitrogen dioxide (NO_2 at 1 Torr, 10 cm path). The 6 cm long slit jet expansion was formed from a reservoir sample maintained at a total pressure in the range 70 psi to 85 psi consisting of typically 0.5% to 1% DI (Cambridge Isotope Laboratories), 5% carbon monoxide mixed with 94% argon carrier and spectra recorded with a multi-pass path for the radiation source through the supersonic jet expansion. The AMAC-76LW multi-pass cell was composed of two astigmatic mirrors, one containing a center hole allowing the radiation to enter and exit the cavity. The vacuum chamber housing for the slit expansion and multi-pass cavity was pumped to 60 mTorr by an Edwards roughing pump (E2M275). A diffusion pump (VHS-400) obtained a vacuum pressure operating range of $2x10^{-6}$ to $5x10^{-4}$ Torr. The gas entry into the vacuum chamber was pulsed with a solenoid valve (Parker General Valve, Series 9) by an Iota One valve driver box triggered by the DAQ, allowing the LabVIEW program to be used to control both the length of the pulse during which the gas was allowed to enter the

chamber, and the timing of the pulsed gas expansion with the desired frequency position of the QCL range.

6.3 Methods for NO-H_2O Investigations

The NO-H_2O complex was found using a QCL spectrometer with a continuous wave supersonic jet expansion laser. The cw laser, made by Daylight solutions, is a QCL capable of covering a wavelength range from 1975-1849 cm^{-1} but for our research scanning was only over the range 1900-1850 cm^{-1}. Laser frequency was measured using a Bristol wavemeter and confirmed in the PGOPHER program. The laser passed through a series of beamsplitters and gold plated mirrors leading to an etalon, a reference cell, and an astigmatic multipass cell. The reference cell contained NO while the astigmatic cell was contained in a vacuum chamber into which Ar gas bubbled through H_2O and NO gas were allowed to expand via supersonic slit jet expansion. The multipass cell achieved over 100 passes, and the slit through which the gas expanded was 5 inches long and 25 microns wide. The sample is analyzed in a vacuum at low rotation temperatures in order to maintain a low collision environment.[100]

All beam paths from the QCL through the etalon, reference cell, and astigmatic cell were detected by liquid nitrogen-cooled MCT detectors. The experiment setup was identical to that seen in Figure 9, except for the addition to the sample gas line of a water bubbler.

6.4 Findings from Ar-NO and NO-H_2O Investigations

A range of 30.6 cm^{-1} was scanned in the investigation of Ar-NO. All of the spectra of the Ar-NO complex that were recorded over this range are shown in Figure 15. The Ar-NO spectrum is composed of the individual spectra combined over the region 1856.8 cm^{-1}–1887.4 cm^{-1}. The line list spectra of H_2O and NO transitions from the HITRAN database are also included as references with the Ar-NO spectrum. It is important to note that the intensity is relative only within each spectrum, respectively;

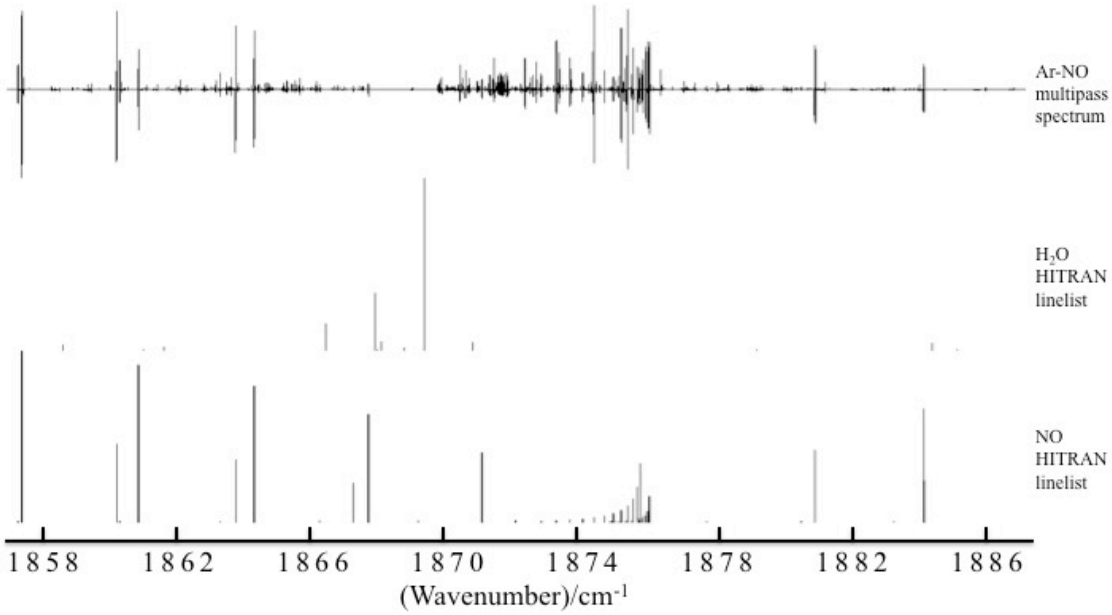

Figure 15. Full spectrum of Ar-NO over the region 1856.8 cm^{-1} to 1887.4 cm^{-1} investigated with the cw QCL supersonic slit jet spectrometer with an astigmatic multipass cell.

the intensities of the spectrum of Ar-NO and the line lists of NO and H_2O monomer from the HITRAN database are not on the same scale of intensity. This experimental investigation gives a spectral structure quite similar to the findings of Meyer in his IR-REMPI investigations, particularly in the band structure and separation.[150] Our band

Table 16. Observed Ar-NO complex band regions over the infrared frequency region of 1856.8 cm^{-1} to 1887.4 cm^{-1}.

Band	Region
pre-A	1859.13-1859.43 cm^{-1}
A	1861.68-1863.1 cm^{-1}
B	1863.28-1866.19 cm^{-1}
B1	1866.51-1867.55 cm^{-1}
C	1868.85-1870.75 cm^{-1}
D	1870.89-1872.25 cm^{-1}
E	1872.92-1874.95 cm^{-1}
F	1875.28-1877.32 cm^{-1}
G	1877.40-1880.82 cm^{-1}
H	1881.40-1884.04 cm^{-1}
I	1886.72-1887.26 cm^{-1}

structure and separation is equal to roughly half the frequency that Meyer reported, which is reasonable due to the double resonance experiments that they were conducting versus our direct investigation of the states. Table 16 gives a list of the bands that we have recorded, and uses the identification lettering of Meyer to describe the bands. The band seen in Figure 16, labeled "Band pre-A" has no corresponding band in the data that Meyer collected. Meyer did not report any data that would correspond to this frequency region in the IR-REMPI double resonance experiment that his group performed. It is important to note that the band seen in Figure 16 actually does match the

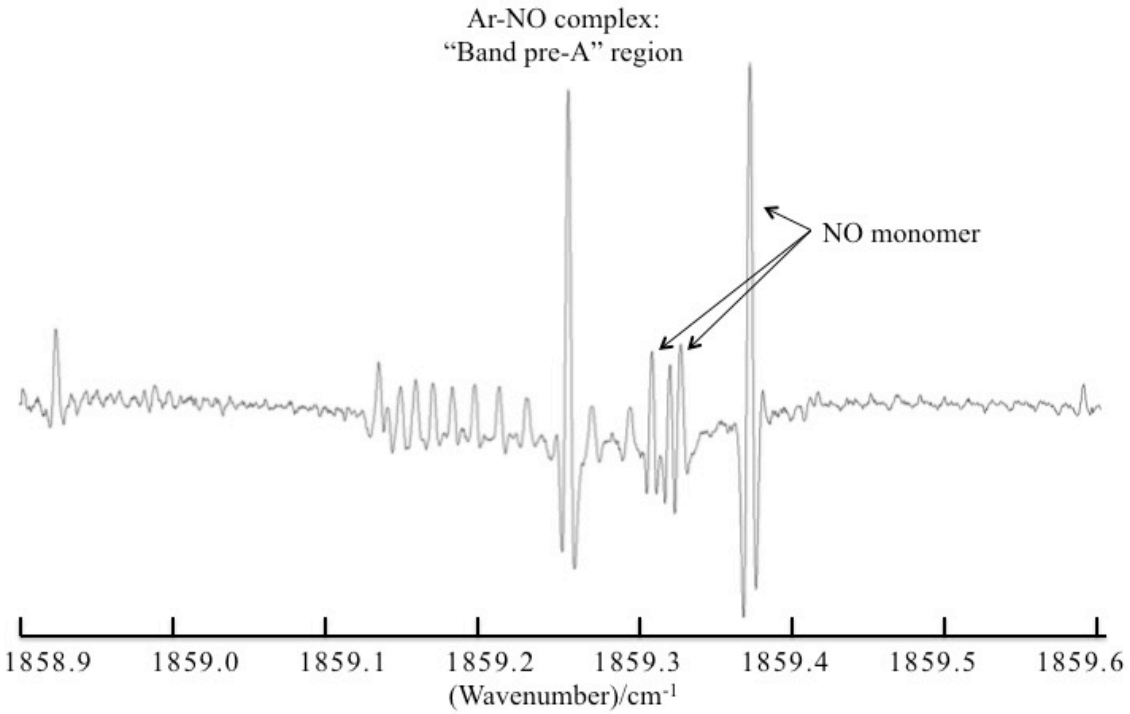

Figure 16. Segment of Ar-NO spectrum from 1858.9 cm^{-1} to 1859.6 cm^{-1} containing "Band pre-A."

structure of the band Meyer reported as “Band A” in Figure 14 with an intense central transition with supporting bands more noticeable to the low frequency side of the main transition. It should also be noted that in Table 16, the hot bands associated with a particular band are noted by a number following the band letter with which it is associated, such as is also observed in Figure 17. Upon similar grounds to the “pre-A” note, there is a “Band I” observed in Figure 18, which could possibly be a hot band for

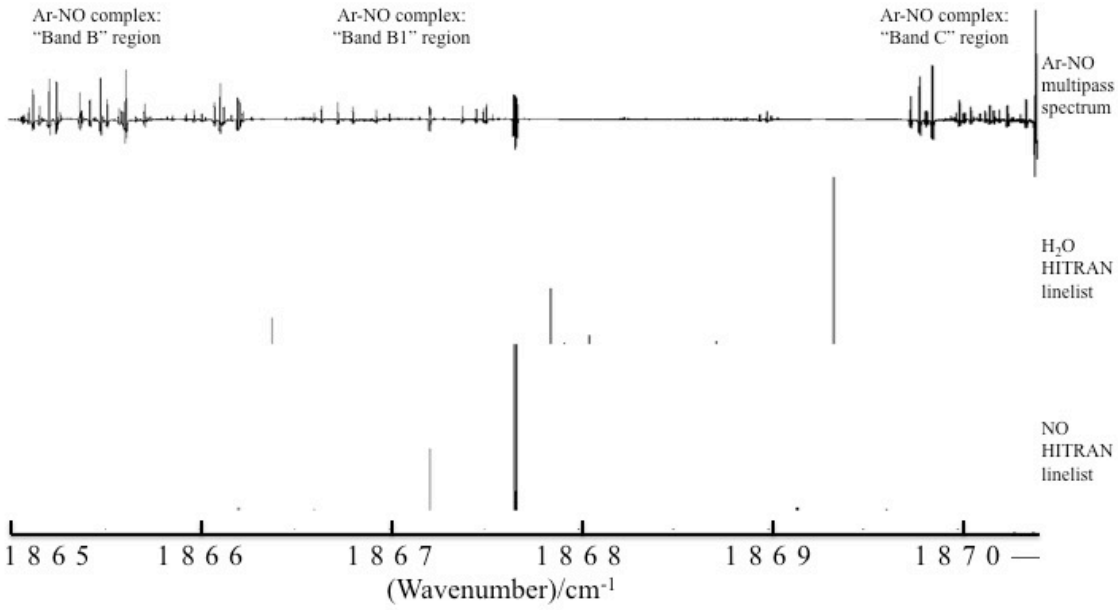

Figure 17. Ar-NO spectrum over the region 1865.0 cm^{-1} to 1870.4 cm^{-1} with three observed bands: “Band B,” hot band “Band B1,” and “Band C.”

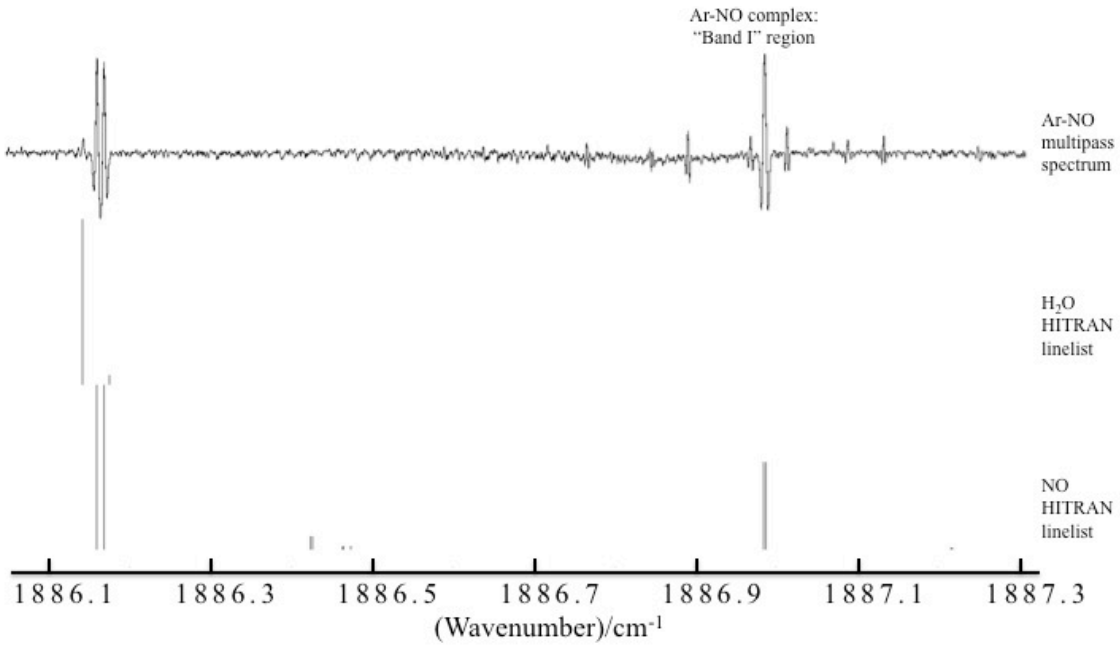

Figure 18. Segment of the Ar-NO spectrum over the region 1886.1 cm^{-1} to 1887.3 cm^{-1}, which includes "Band I."

"Band H," but which seems to exhibit the characteristics of an entirely new band, which was not observed by Meyer. Another explanation for the apparent difference in this data from that of Meyer's spectra, seen in Figure 14, might be that there is a red shift without the IR-REMPI double resonance. In the case of this investigation, the band referred to as "pre-A" may well end up being shifted band that corresponds to Meyer's "Band A." This remains to be determined with the current state of analysis. Issues certainly arise when attempting to make assignments with full certainty due to peak overlap with other bands and with those of the monomer, as well as atmospheric water, which is active over the recorded infrared region. Table 16 defines suggested regions that seem to correlate well

with Meyer's data for the double resonance higher frequency transitions; however, these very broad assignments are but an initial attempt at analyzing the spectrum of Ar-NO.

Further, analysis is desperately needed. The resolution of this work is superior to that of Meyer, and with the simpler, straightforward measurement of these transitions, this investigation of Ar-NO should shed light on the character of this prototypical open shell complex.

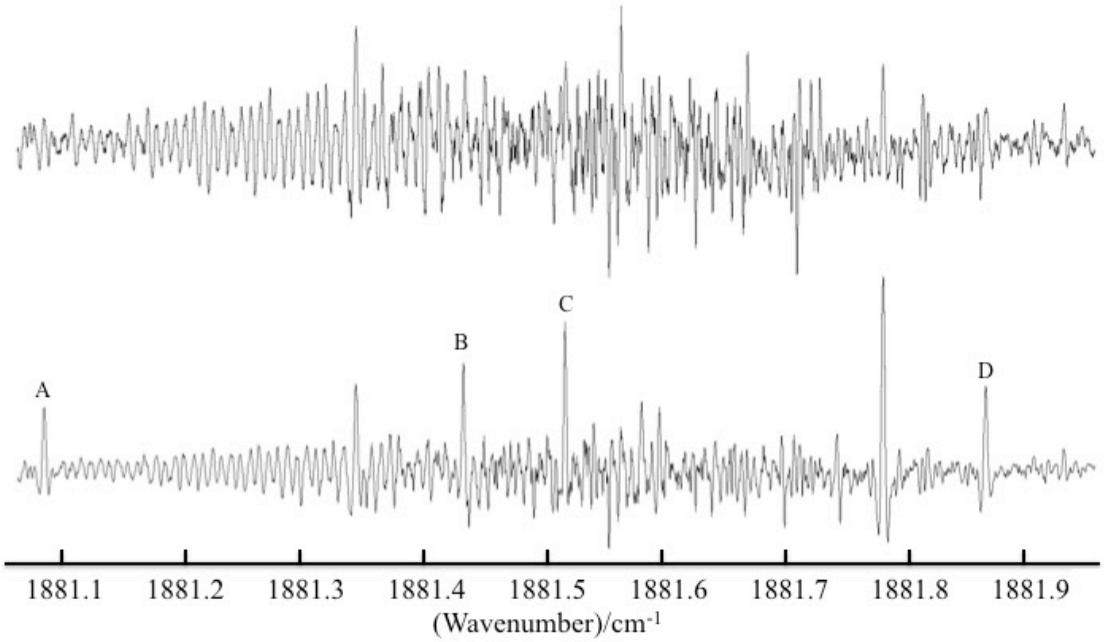

Figure 19. Experimental spectrum in the 1881.0 cm^{-1} to 1882.0 cm^{-1} range for NO-H_2O. Top spectra is Ar-NO complex serving as reference.

The data generated from the investigation of the Ar-NO complex was used subsequently in the corresponding investigation of NO-H_2O. The spectra obtained in from the Ar-NO investigation served as reference spectra in the NO-H_2O investigation. In a preliminary search, a total of 9 transitions were observed for NO-H_2O in the ν_{NO}, NO stretching region. These transitions are the labeled peaks in Figure 19 and Figure 20. Observation of these transitions should eventually allow for the determination of the rovibrational constants of NO-H_2O and the understanding of the stretching, rotating, and bending of the H_2O moiety. Transitions stemming from water being present can be

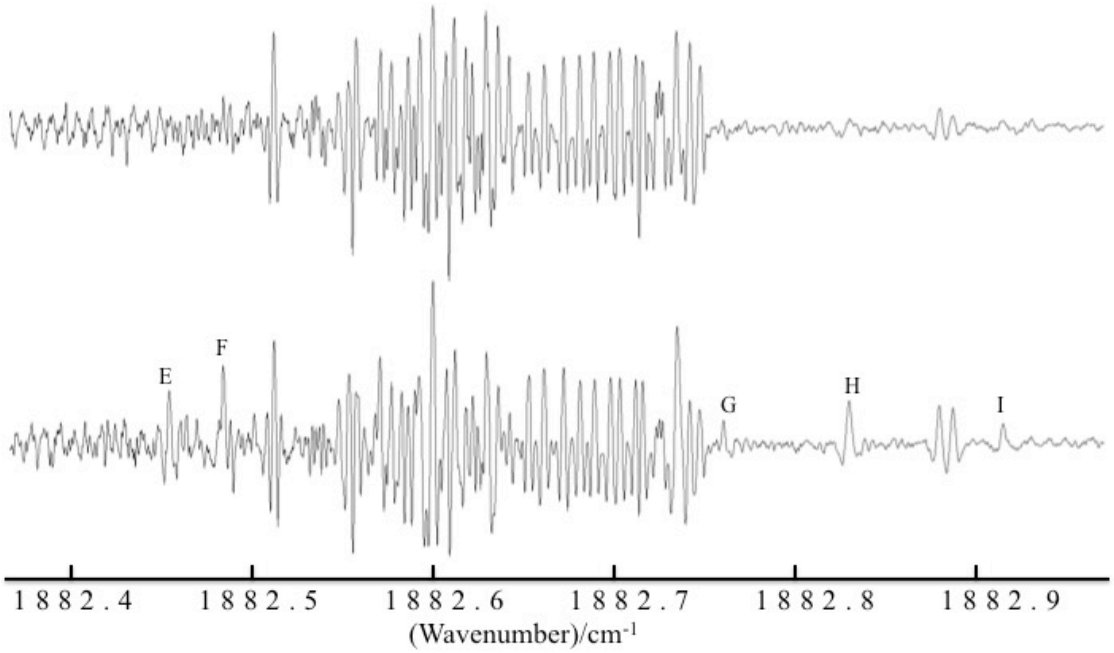

Figure 20. Experimental spectrum in the 1882.0 cm^{-1} to 1883.0 cm^{-1} range for NO-H_2O with the top spectrum of Ar-NO serving as a reference.

clearly seen as lone peaks appearing in the spectrum of NO-H_2O and not in the reference spectrum of Ar-NO such as those peaks labeled in Figure 20. There also is a reasonable probability that NO-H_2O peaks exist within the highly populated regions of the spectrum, but which are unable to be resolved by the present spectrometer. The presence of NO-H_2O can be immediately confirmed by comparing the intensities of the Ar-NO transitions. The peaks are not as intense in the sample spectra as the presence of water decreases the volume of the Ar-NO complex in the astigmatic cell by reacting forming complex with the NO.

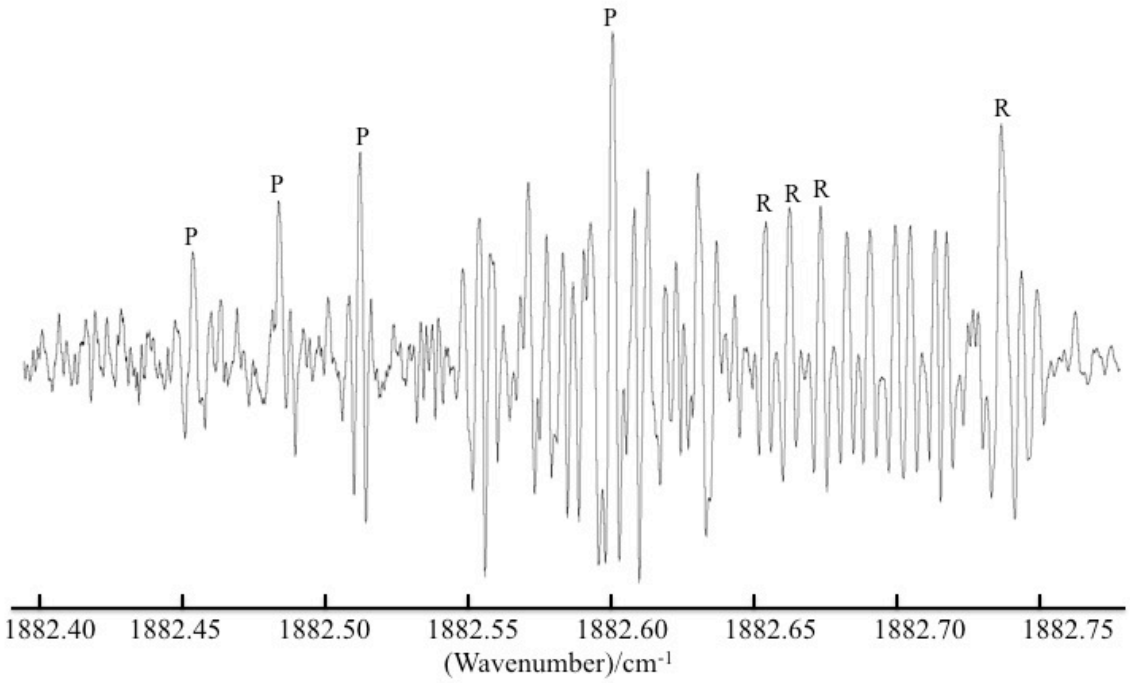

Figure 21. Spectrum of NO-H_2O complex with suspected P(J) and R(J) type transitions labeled.

As seen in Figure 21, P(J) and R(J) branches can be identified for the NO-H_2O complex by the previously described comparison with the pure Ar-NO spectra. The NO-H_2O complex stretch was found in the 1881-1883 cm^{-1} region. The presence of the water complex is further confirmed by the lowering in intensity of the Ar-NO peaks due to the population depletion of the Ar-NO with the rising population of the NO-H_2O complex. Both P and R branches were observed for the NO-H_2O, and confirmed based on the change in the spacing between transitions, but the need for further optimization is evident, due to the fact that true assignment is practically impossible, with the center of band so thoroughly obscured.

7. CONCLUSION

A continuous supersonic slit jet QCL spectrometer was constructed and successfully used to investigate the OC stretching vibrational bands and associated intermolecular hot and combination bands for several prototypical hydrogen and halogen bonded complexes, including OC-HCl, OC-HF, OC-HCN, OC-BrCl, and NO-H_2O. The QCL spectrometer has permitted the investigation of low frequency bridged intermolecular hydrogen bonded vibrations in all three of these complexes. In the case of OC-HF, it has allowed evaluation of the ν_5^1 band origin to be 81.96825(12) cm^{-1} above the ground state. With extension of the operating wavelength range of mode-hop free QCLs, this type of spectrometer was demonstrated to have extremely useful potential capabilities for investigation of low frequency vibrations in a wide range of non-covalent interactions. This research also permitted the first observation and ro-vibrational analysis of the ν_2 and intermolecular ν_7^1 hot and combinations bands in OC-HCN complex, as well as the first observation of mid-infrared frequency Ar-NO complex and NO-H_2O complex. The spectroscopic investigations enabled generation of a 5-D morphed potential for the OC-HCN complex. D_e of the OC-HCN complex (650(8) cm^{-1}) is between that predicted from morphed potentials for OC-HCl (725.6(50) cm^{-1}) and OC-HBr complex (564(5) cm^{-1}). The corresponding value of D_0, however, is predicted to be 463(8) cm^{-1} compared with 397(5) and 322(6) cm^{-1} for OC-HCl and OC-HBr respectively. The D_0 value thus lies between that of OC-HF (742.5(50)) cm^{-1} and that of OC-HCl. In addition, the OC-HCN complex has a predicted r_{C-H} value at its global

minimum of 2.572(2) Å, significantly larger than the corresponding predicted values of 2.061, 2.370 and 2.484 Å for OC-HF, OC-HCl and OC-HBr.

Infrared spectra of the halogen bonded complex OC-BrCl has been recorded in a QCL supersonic jet spectrometer and was combined with previously available microwave spectroscopic data to generate a 5-D compound model morphed potential of the complex. This potential predicts a D_0 of 605(70) cm^{-1} significantly larger than OC-Cl_2 and OC-HCl but less than OC-HF (732 cm^{-1}). This prediction is consistent with the magnitude of a proper ν_{CO} blue shift upon complexation, which increases from 6.252984(14) cm^{-1} to 12.89643(28) cm^{-1} for OC-Cl_2 and OC-BrCl respectively. Furthermore, the isomerization energy of the minimum for OC-BrCl to that in CO-BrCl is predicted to be 336(95) cm^{-1} with a barrier of 673(90) cm^{-1} and compares with corresponding isomerization energy of 215(10) cm^{-1} for OC-Cl_2, CO-Cl_2 isomerization.

Experimentally observed proper blue shifts $\Delta\nu_0$ for the CO proton acceptor were demonstrated to have linear correlations with predicted hydrogen bonded dissociation energies D_0 based on accurate semi-empirical morphing methodologies. Such results are consistent with the original tenets of the Badger-Bauer rule.[104] In this series, such proper blue shifts contrast with traditionally directly measured H-X red shifts that frequently exhibit a corresponding non-linear dependence. A model has now been formulated to rationalize the intrinsic characteristics of the systems studied and associated blue frequency shifts on complexation, particularly with respect to the Badger-Bauer relationship. Application of 5-D compound-model morphed potentials in formulating this model have provided criteria that correlate the linear dependence of $\Delta\omega_e$ with D_e

and furthermore give insight into the influence of anharmonicity and zero point energy effects. In principle, similar approaches should be applicable to a range of hydrogen bonded interactions involving frequency shifts in acceptor vibrations including HCN, CH_3CN and NO. Results can also be compared with those previously generated in DFT calculations that asserts that the frequencies of ν_{CO} serve as a powerful tool to probe the surrounding environments of CO molecule inside protein matrices, as well as its orientations.[119] In these investigations of the weak interactions between non-charged amino acids and CO, the affects of the protein's microenvironments were revealed on the docked gas molecule, which contributed insights into the accommodation and migration of small ligands within protein matrices. This in turn suggests the current studies of CO as a hydrogen acceptor can provide quantitative information in using CO as a useful probe for delineating the structure–property–function relationship of heme-based sensors.[120]

Furthermore, the spectroscopic rovibrational analyses of the n_1 spectra of $^{16}O^{12}C$-DI and $^{16}O^{12}C$-ID, as well as ν_2 spectra of $^{16}O^{12}C$-DI, $^{16}O^{12}C$-ID have been completed using a quantum cascade laser pulsed slit supersonic jet spectrometer with mode-hop free QCLs centered around 4.57 mm and 6.26 mm respectively. Intensity measurements of the ν_2 $^{16}O^{12}C$-HI : $^{16}O^{12}C$-IH and ν_1 $^{16}O^{12}C$-DI : $^{16}O^{12}C$-ID in a simultaneous expansion has permitted determination of the isomerization for the former to be +2.8(1.0) cm^{-1} and the latter to be -6.0(1.0) cm^{-1}. The former compared with the previously experimentally measured value of 3.4683(80) cm^{-1} giving confidence in the accuracy of the intensity method utilized here. The latter value of -6.0(1.0) cm^{-1}

compared with the value of -5.3(1.0) cm^{-1} previously predicted on the basis of a morphed potential for OC-HI.[130] These results thus confirm within experimental error the theoretical prediction of the phenomena of ground state deuterium isotopic isomerization predicted on the basis of the generated morphed potential in a simple prototypical system where the effect can be the subject of deeper investigation. This phenomenon is expected to influence the structure and dynamics of systems more generally, particularly in more complex environments such as those involving deuterated solvents in structural biology.

Finally, a novel spectrometer incorporating a cw supersonic slit jet expansion with a QCL and astigmatic multipass cell was designed and implemented in the investigation of the open shell complex of Ar-NO. This prototypical open shell system was investigated over the region 1856.8 cm^{-1} to 1887.4 cm^{-1}, yielding 11 unique bands. The transitions of the Ar-NO complex had previously been unreported in this region. The investigation of Ar-NO led naturally into the subsequent investigation of the NO-H_2O complex. This investigation led to the recording of 9 unique transitions. Unfortunately, an in-depth analysis is still required to achieve the most with the acquired data. Ideally, molecular parameters can be determined, and a better understanding into the nature of open shell complexes can be obtained.

REFERENCES

[1] McNaught, A. D. W., A. *IUPAC Compendium of Chemical Terminology*; 2nd ed ed.; Blackwell Scientific Publications: Oxford, 1997.

[2] Buckingham, A. D.; Utting, B. D. *Annu. Rev. Phys. Chem.* **1970**, *21*, 287-316.

[3] Faist, J.; Capasso, F.; Sivco, D. L.; Sirtori, C.; Hutchinson, A. L.; Cho, A. Y. *Science* **1994**, *264*, 553-556.

[4] Tanaka, K.; Harada, K.; Yamada, K. M. T. "Thz and Submillimeter-Wave Spectroscopy of Molecular Complexes." In *Handbook of High-Resolution Spectroscopy*; Quack, M., Merkt, F., Eds.; Wiley: Hoboken, NJ, 2011; pp 853-896.

[5] McIntosh, A. L.; Wang, Z.; Lucchese, R. R.; Bevan, J. W. *Infrared Phys. Techn.* **2004**, *45*, 301-314.

[6] Wysocki, G.; Lewicki, R.; Curl, R. F.; Tittel, F. K.; Diehl, L.; Capasso, F.; Troccoli, M.; Hofler, G.; Bour, D.; Corzine, S.; Maulini, R.; Giovannini, M.; Faist, J. *Appl. Phys. B-Lasers O.* **2008**, *92*, 305-311.

[7] Curl, R. F.; Capasso, F.; Gmachl, C.; Kosterev, A. A.; McManus, B.; Lewicki, R.; Pusharsky, M.; Wysocki, G.; Tittel, F. K. *Chem. Phys. Lett.* **2010**, *487*, 1-18.

[8] Borri, S.; Bartalini, S.; Cancio, P.; Galli, I.; Giusfredi, G.; Mazzotti, D.; De Natale, P. *Opt. Eng.* **2010**, *49*, 111-122.

[9] Trache, M. *Phil. Trans. Roy. Soc.* **2000**, *359*, 547.

[10] Myers, T. L.; Williams, R. M.; Taubman, M. S.; Gmachl, C.; Capasso, F.; Sivco, D. L.; Baillargeon, J. N.; Cho, A. Y. *Opt. Lett.* **2002**, *27*, 170-172.

[11] Tittel, F. K.; Richter, D.; Fried, A. "Mid-Infrared Laser Applications in Spectroscopy." In *Solid-State Mid-Infrared Laser Sources*; Sorokina, I., Vodopyanov, K., Eds.; Springer: Berlin Heidelberg, 2003; Vol. 89, pp 458-529.

[12] Borri, S.; Bartalini, S.; De Natale, P.; Inguscio, M.; Gmachl, C.; Capasso, F.; Sivco, D. L.; Cho, A. Y. *Appl. Phys. B-Lasers O.* **2006**, *85*, 223-229.

[13] Lewicki, R.; Doty, J. H., III; Curl, R. F.; Tittel, F. K.; Wysocki, G. *P. Natl. Acad. Sci. U.S.A.* **2009**, *106*, 12587-12592.

[14] Kluczynski, P.; Lundqvist, S.; Westberg, J.; Axner, O. *Appl. Phys. B* **2011**, *103*, 451-459.

[15] Liu, X.; Xu, Y. *Phys. Chem. Chem. Phys.* **2011**, *13*, 14235-14242.

[16] Liu, X.; Xu, Y.; Su, Z.; Tam, W. S.; Leonov, I. *Appl. Phys. B-Lasers O.* **2011**, *102*, 629-639.

[17] Xu, Y.; Liu, X.; Su, Z.; Kulkarni, R. M.; Tam, W. S.; Kang, C.; Leonov, I.; D'Agostino, L. *Proc. SPIE 7222, Quantum Sensing and Nanophotonic Devices VI* **2009**, *7222*, 722208-722208-11.

[18] Brumfield, B. E.; Stewart, J. T.; McCall, B. J. *J. Mol. Spectrosc.* **2011**, *266*, 57-62.

[19] Brumfield, B. E.; Stewart, J. T.; Weaver, S. L. W.; Escarra, M. D.; Howard, S. S.; Gmachl, C. F.; McCall, B. J. *Rev. Sci. Instrum.* **2010**, *81*, 063102.

[20] Springer, S. D.; Rivera-Rivera, L. A.; McElmurry, B. A.; Wang, Z.; Leonov, I. I.; Lucchese, R. R.; Legon, A. C.; Bevan, J. W. *J. Phys. Chem. A* **2012**, *116*, 1213-1223.

[21] Rivera-Rivera, L. A.; McElmurry, B. A.; Wang, Z. C.; Leonov, I. I.; Lucchese, R. R.; Bevan, J. W. *Chem. Phys. Lett.* **2012**, *522*, 17-22.

[22] Legon, A. C.; Soper, P. D.; Keenan, M. R.; Minton, T. K.; Balle, T. J.; Flygare, W. H. *J. Chem. Phys.* **1980**, *73*, 583-584.

[23] Soper, P. D.; Legon, A. C.; Flygare, W. H. *J. Chem. Phys.* **1981**, *74*, 2138-2142.

[24] Altman, R. S.; Marshall, M. D.; Klemperer, W.; Krupnov, A. *J. Chem. Phys.* **1983**, *79*, 52-56.

[25] Andrews, L.; Arlinghaus, R. T.; Johnson, G. L. *J. Chem. Phys.* **1983**, *78*, 6347-6352.

[26] Wang, Z. C.; Eliades, M.; Bevan, J. W. *Chem. Phys. Lett.* **1989**, *161*, 6-11.

[27] Meads, R. F.; Hartz, C. L.; Lucchese, R. R.; Bevan, J. W. *Chem. Phys. Lett.* **1993**, *206*, 488-492.

[28] McKellar, A. R. W.; Lu, Z. *J. Mol. Spectrosc.* **1993**, *161*, 542-551.

[29] Garnica, R.; McIntosh, A. L.; Wang, Z.; Lucchese, R. R.; Bevan, J. W.; McKellar, A. R. *Chem. Phys. Lett.* **1997**, *272*, 484-488.

[30] Larsen, R. W.; Hegelund, F.; Nelander, B. *J. Phys. Chem. A* **2004**, *108*, 1524-1530.

[31] Hinchliffe, A. *Adv. Mol. Relax. and Int. Pr.* **1981**, *21*, 151-157.

[32] Politzer, P.; Kammeyer, C. W.; Bauer, J.; Hedges, W. L. *J. Phys. Chem.* **1981**, *85*, 4057-4060.

[33] Rutkowski, K. S.; Melikova, S.; Shchepkin, D. N.; Lipkowski, P.; Koll, A. *Chem. Phys. Lett.* **2000**, *325*, 425-432.

[34] McDowell, S. A. C.; Buckingham, A. D. *J. Am. Chem. Soc.* **2005**, *127*, 15515-15520.

[35] Augspurger, J. D.; Dykstra, C. E. *Chem. Phys. Lett.* **1992**, *189*, 303-310.

[36] Rivera-Rivera, L. A.; Lucchese, R. R.; Bevan, J. W. *Chem. Phys. Lett.* **2006**, *429*, 68-76.

[37] Rivera-Rivera, L. A.; Lucchese, R. R.; Bevan, J. W. *Chem. Phys. Lett.* **2008**, *460*, 352-358.

[38] Legon, A. C.; Soper, P. D.; Flygare, W. H. *J. Chem. Phys.* **1981**, *74*, 4944-4950.

[39] Kyro, E. K.; Shojachaghervand, P.; McMillan, K.; Eliades, M.; Danzeiser, D.; Bevan, J. W. *J. Chem. Phys.* **1983**, *79*, 78-80.

[40] Wang, Z. C.; Bevan, J. W. *J. Chem. Phys.* **1989**, *91*, 3335-3339.

[41] Alberts, I. L.; Handy, N. C.; Simandiras, E. D. *Theor. Chimi. Acta* **1988**, *74*, 415-428.

[42] Yu, Z. H.; Chuang, C. C.; Medley, P.; Stone, T. A.; Klemperer, W. *J. Chem. Phys.* **2004**, *120*, 6922-6929.

[43] Benzel, M. A.; Dykstra, C. E. *Chem. Phys.* **1983**, *80*, 273-278.

[44] Benzel, M. A.; Dykstra, C. E. *J. Chem. Phys.* **1983**, *78*, 4052-4062.

[45] Benzel, M. A. *J. Chem. Phys.* **1984**, *80*, 3510-3511.

[46] Botschwina, P. *J. Chem. Soc. Farad. T. 2* **1988**, *84*, 1263-1276.

[47] Chen, C.; Chen, S. J.; Hong, Y. S. *J. Chin. Chem. Soc-Taip.* **2005**, *52*, 853-861.

[48] Chen, S. J.; Chen, C.; Hong, Y.-S. *J. Chin. Chem. Soc-Taip.* **2006**, *53*, 783-792.

[49] Civalleri, B.; Garrone, E.; Ugliengo, P. *Theochem-J. Mol. Struct.* **1997**, *419*, 227-238.

[50] Curtiss, L. A.; Pochatko, D. J.; Reed, A. E.; Weinhold, F. *J. Chem. Phys.* **1985**, *82*, 2679-2687.

[51] Parish, C. A.; Augspurger, J. D.; Dykstra, C. E. *J. Phys. Chem.* **1992**, *96*, 2069-2079.

[52] Reed, A. E.; Weinhold, F.; Curtiss, L. A.; Pochatko, D. J. *J. Chem. Phys.* **1986**, *84*, 5687-5705.

[53] Spackman, M. A. *J. Chem. Phys.* **1986**, *85*, 6587-6601.

[54] Tuma, C.; Boese, A. D.; Handy, N. C. *Phys. Chem. Chem. Phys.* **1999**, *1*, 3939-3947.

[55] Oudejans, L.; Miller, R. E. *J. Chem. Phys.* **2000**, *113*, 4581-4587.

[56] Rivera-Rivera, L. A.; Wang, Z.; McElmurry, B. A.; Lucchese, R. R.; Bevan, J. W.; Kanschat, G. *Chem. Phys.* **2011**, *390*, 42-50.

[57] Millar, L. J.; Ford, T. A. *J. Mol. Struct.* **2005**, *744*, 195-205.

[58] Goodwin, E. J.; Legon, A. C. *Chem. Phys.* **1984**, *87*, 81-92.

[59] Jucks, K. W.; Miller, R. E. *J. Chem. Phys.* **1988**, *89*, 1262-1267.

[60] Groenewegen, M. A. T.; Baas, F.; deJong, T.; Loup, C. *Astron. Astrophys.* **1996**, *306*, 241-254.

[61] Womack, M.; Stern, S. A.; Festou, M. C. *Planet. Space Sci.* **1997**, *45*, 711-715.

[62] Metrangolo, P.; Neukirch, H.; Pilati, T.; Resnati, G. *Accounts Chem. Res.* **2005**, *38*, 386-395.

[63] Metrangolo, P.; Meyer, F.; Pilati, T.; Resnati, G.; Terraneo, G. *Angew. Chem. Int. Ed.* **2008**, *47*, 6114-6127.

[64] Metrangolo, P.; Resnati, G.; Pilati, T.; Biella, S. "Halogen Bonding in Crystal Engineering." In *Halogen Bonding: Fundamentals and Applications*; Metrangolo, P., Resnati, G., Eds.; Springer: Berlin, 2008; Vol. 126, pp 105-136.

[65] Legon, A. C. *Phys. Chem. Chem. Phys.* **2010**, *12*, 7736-7747.

[66] Legon, A. C. "The Interaction of Dihalogens and Hydrogen Halides with Lewis Bases in the Gas Phase: An Experimental Comparison of the Halogen Bond and the Hydrogen Bond." In *Halogen Bonding: Fundamentals and Applications*; Metrangolo, P., Resnati, G., Eds.; Springer: Berlin, 2008; Vol. 126, pp 17-64.

[67] Legon, A. C. *Chem.-Eur. J.* **1998**, *4*, 1890-1897.

[68] Legon, A. C. *Angew. Chem. Int. Ed.* **1999**, *38*, 2686-2714.

[69] Blanco, S.; Legon, A. C.; Thorn, J. C. *J. Chem. Soc. Faraday T.* **1994**, *90*, 1365-1371.

[70] Schriver, A.; Schriver-Mazzuoli, L.; Chaquin, P.; Bahou, M. *J. Phys. Chem. A* **1999**, *103*, 2624-2631.

[71] Romano, R. M.; Downs, A. J. *J. Phys. Chem. A* **2003**, *107*, 5298-5305.

[72] Jager, W.; Xu, Y. J.; Gerry, M. C. L. *J. Phys. Chem.* **1993**, *97*, 3685-3689.

[73] McElmurry, B. A.; Rivera-Rivera, L. A.; Scott, K. W.; Wang, Z.; Leonov, I. I.; Lucchese, R. R.; Bevan, J. W. *Chem. Phys.* **2012**, *409*, 1-10.

[74] Western, C. M. PGOPHER, A Program for Simulating Rotational Structure, University of Bristol. 2013. http://pgopher.chm.bris.ac.uk.

[75] Rivera-Rivera, L. A.; Scott, K. W.; McElmurry, B. A.; Lucchese, R. R.; Bevan, J. W. *Chem. Phys.* **2013**, *425*, 162-169.

[76] Rivera-Rivera, L. A.; Lucchese, R. R.; Bevan, J. W. *Phys. Chem. Chem. Phys.* **2010**, *12*, 7258-7265.

[77] Kohen, A.; Limbach, H. H. *Isotope Effects in Chemistry and Biology*; CRC Press Taylor and Francis: Boca Raton, 2005.

[78] McMahon, M. I.; Nelmes, R. J.; Kuhs, W. F.; Dorwarth, R.; Piltz, R. O.; Tun, Z. *Nature* **1990**, *348*, 317-319.

[79] Koval, S.; Kohanoff, J.; Lasave, J.; Colizzi, G.; Migoni, R. L. *Phys. Rev. B* **2005**, *71*, 184102.

[80] Boudart, M. *Annu. Rev. Phys. Chem.* **1962**, *13*, 241-258.

[81] de Souza, J. M.; Freire, P. T. C.; Bordallo, H. N.; Argyriou, D. N. *J. Phys. Chem. B* **2007**, *111*, 5034-5039.

[82] Zhernov, A. P.; Inyushkin, A. V. *Phys.-Usp+* **2001**, *44*, 785-811.

[83] Williams, D. H.; Stephens, E.; O'Brien, D. P.; Zhou, M. *Angew. Chem. Int. Ed.* **2004**, *43*, 6596-6616.

[84] Guzzi, R.; Arcangeli, C.; Bizzarri, A. R. *Biophys. Chem.* **1999**, *82*, 9-22.

[85] Sugimoto, H. *J. Phys.-Condens. Mat.* **1998**, *10*, 1237-1246.

[86] Chan, S. I.; Lin, L.; Clutter, D.; Dea, P. *P. Natl. Acad. Sci. U.S.A.* **1970**, *65*, 816-822.

[87] Jaravine, V.; Cordier, F.; Grzesiek, S. *J. Biomol. NMR* **2004**, *29*, 309-318.

[88] Giese, K.; Petkovic, M.; Naundorf, H.; Kuehn, O. *Phys. Rep.* **2006**, *430*, 211-276.

[89] Choudhury, R. R.; Chitra, R.; Ramanadham, M. *Physica B* **2005**, *366*, 116-121.

[90] Robertson, J. M.; Ubbelohde, A. R. *P. Roy. Soc. Lond. A Mat.* **1939**, *170*, 222-240.

[91] Limbach, H. H.; Pietrzak, M.; Benedict, H.; Tolstoy, P. M.; Golubev, N. S.; Denisov, G. S. *J. Mol. Struct.* **2004**, *706*, 115-119.

[92] Singh, T. R.; Wood, J. L. *J. Chem. Phys.* **1969**, *50*, 3572.

[93] Zgierski, M. Z. *Phys. Lett. A* **1969**, *30*, 354-355.

[94] Legon, A. C.; Millen, D. J. *Chem. Phys. Lett.* **1988**, *147*, 484-489.

[95] Mootz, D.; Schilling, M. *J. Am. Chem. Soc.* **1992**, *114*, 7435-7439.

[96] Rivera-Rivera, L. A.; Wang, Z. C.; McElmurry, B. A.; Willaert, F. F.; Lucchese, R. R.; Bevan, J. W.; Suenram, R. D.; Lovas, F. J. *J. Chem. Phys.* **2010**, *133*, 184305.

[97] Wang, Z.; Lucchese, R. R.; Bevan, J. W.; Suckley, A. P.; Rego, C. A.; Legon, A. C. *J. Chem. Phys.* **1993**, *98*, 1761-1767.

[98] Guelachvili, G. *J. Mol. Spectrosc.* **1979**, *75*, 251-269.

[99] Hurlock, S. C.; Alexander, M.; Rao, K. N.; Dreska, N. *J. Mol. Spectrosc.* **1971**, *37*, 373-376.

[100] McElmurry, B. A.; Lucchese, R. R.; Bevan, J. W.; Leonov, II; Belov, S. P.; Legon, A. C. *J. Chem. Phys.* **2003**, *119*, 10687-10695.

[101] Willaert, F. F.; McElmurry, B. A.; Lucchese, R. R.; Bevan, J. W. *Chem. Phys. Lett.* **2008**, *460*, 525-530.

[102] Han, J.; McIntosh, A. L.; Wang, Z.; Lucchese, R. R.; Bevan, J. W. *Chem. Phys. Lett.* **1997**, *265*, 209-216.

[103] Rivera-Rivera, L.; McElmurry, B.; Scott, K.; Lucchese, R.; Bevan, J. *J. Phys. Chem. A* **2013**, *117*, 8477-8483.

[104] Badger, R. M.; Bauer, S. H. *J. Chem. Phys.* **1937**, *5*, 839-851.

[105] Badger, R. M. *J. Chem. Phys.* **1934**, *2*, 128.

[106] Pauling, L. *The Nature of the Chemical Bond*; 2nd ed.; Cornell University Press: Ithaca, 1960.

[107] Zeegershuyskens, T. *B. Soc. Chim. Belg.* **1977**, *86*, 823-832.

[108] Luck, W. A. P.; Wess, T. *Can. J. Chem.* **1991**, *69*, 1819-1826.

[109] Gould, I. R.; Hillier, I. H. *Theochem-J. Mol. Struc.* **1994**, *120*, 1-8.

[110] Pejov, L.; Ivanovski, G.; Petrusevski, V. M. *J. Math. Chem.* **1999**, *26*, 317-326.

[111] Kang, Y. K.; Jhon, M. S. *B. Kor. Chem. Soc.* **1981**, *2*, 8-11.

[112] Zhang, Y.; Ma, N.; Wang, W.-Z. *Acta Phys.-Chim. Sin.* **2012**, *28*, 499-503.

[113] Silvi, B.; Wieczorek, R.; Latajka, Z.; Alikhani, M. E.; Dkhissi, A.; Bouteiller, Y. *J. Chem. Phys.* **1999**, *111*, 6671-6678.

[114] Rao, C. N. R.; Dwivedi, P. C.; Ratajczak, H.; Orvillethomas, W. J. *J. Chem. Soc. Farad. T. 2* **1975**, *71*, 955-966.

[115] Arnett, E. M.; Joris, L.; Mitchell, E.; Murty, T.; Gorrie, T. M.; Schleyer, P. V. *J. Am. Chem. Soc.* **1970**, *92*, 2365-2377.

[116] Pimentel, G. C.; McClellan, A. L. *The Hydrogen Bond*; W.H. Freeman and Co: San Francisco, 1959.

[117] Marechal, Y. *Chem. Phys. Lett.* **1972**, *13*, 237-240.

[118] Sokolov, N. D.; Savelev, V. A. *Chem. Phys.* **1977**, *22*, 383-399.

[119] Lin, Y. W.; Nie, C. M.; Liao, L. F. *Chinese Chem. Lett.* **2008**, *19*, 119-122.

[120] Pinakoulaki, E.; Yoshimura, H.; Daskalakis, V.; Yoshioka, S.; Aono, S.; Varotsis, C. *P. Natl. Acad. Sci. U.S.A.* **2006**, *103*, 14796-14801.

[121] Nutt, D. R.; Meuwly, M. *Chemphyschem* **2004**, *5*, 1710-1718.

[122] Devereux, M.; Meuwly, M. *Biophys. J.* **2009**, *96*, 4363-4375.

[123] Daskalakis, V.; Varotsis, C. *Int. J. Mol. Sci.* **2009**, *10*, 4137-4156.

[124] Makshakova, O.; Chachkov, D.; Ermakova, E. *Int. J. Quantum Chem.* **2011**, *111*, 2525-2539.

[125] Dabo, I. *Phys. Rev. B* **2012**, *86*, 035139.

[126] Thijs, R.; Zeegershuyskens, T. *Spectroc. Acta Pt. A-Molec. Biomolec. Spectr.* **1984**, *40*, 307-313.

[127] Latajka, Z.; Scheiner, S. *Chem. Phys. Lett.* **1990**, *174*, 179-184.

[128] Drago, R. S.; Epley, T. D. *J. Am. Chem. Soc.* **1969**, *91*, 2883-2890.

[129] Casterline, B. E.; Mollner, A. K.; Ch'ng, L. C.; Reisler, H. *J. Phys. Chem. A* **2010**, *114*, 9774-9781.

[130] Oudejans, L.; Miller, R. E. *Annu. Rev. Phys. Chem.* **2001**, *52*, 607-637.

[131] Wang, Z.; McElmurry, B. A.; Lucchese, R. R.; Bevan, J. W.; Coudert, L. H. *J. Chem. Phys.* **2011**, *134*, 064317.

[132] Rivera-Rivera, L. A.; McElmurry, B. A.; Lucchese, R. R.; Bevan, J. W. *J. Mol. Struct.* **2012**, *1023*, 43-48.

[133] Anstey, J.; Brookes, M. D.; McKellar, A. R. W. *J. Mol. Spectrosc.* **1999**, *194*, 281-282.

[134] Buckingham, A. D. *T. Faraday Soc.* **1960**, *56*, 753-760.

[135] Trudeau, G.; Dumas, J. M.; Dupuis, P.; Guerin, M.; Sandorfy, C. *Top. Curr. Chem.* **1980**, *93*, 91-125.

[136] Hermansson, K. *Int. J. Quantum Chem.* **1993**, *45*, 747-758.

[137] Zierkiewicz, W.; Michalska, D.; Havlas, Z.; Hobza, P. *Chemphyschem* **2002**, *3*, 511.

[138] Brookes, M. D.; McKellar, A. R. W. *J. Chem. Phys.* **1998**, *109*, 5823-5829.

[139] Xia, C.; McKellar, A. R. W. *J. Mol. Spectrosc.* **2005**, *229*, 39-46.

[140] Xia, C. H.; McKellar, A. R. W. *Can. J. Phys.* **2001**, *79*, 461-466.

[141] Herschbach, D.; Laurie, V. W. *J. Chem. Phys.* **1961**, *35*, 458.

[142] Kim, Y.; Meyer, H. *Int. Rev. Phys. Chem.* **2001**, *20*, 219-282.

[143] Alexander, M. H. *J. Chem. Phys.* **1999**, *111*, 7435-7439.

[144] Alexander, M. H. *J. Chem. Phys.* **1999**, *111*, 7426-7434.

[145] Wysocki, G.; Lewicki, R.; Huang, X.; Curl, R. F.; Tittel, F. K. In *Conference on Quantum Sensing and Nanophotonic Devices VI* San Jose, CA, 2009; Vol. 7222.

[146] Mills, P. D. A.; Western, C. M.; Howard, B. J. *J. Phys. Chem.* **1986**, *90*, 4961-4969.

[147] Mills, P. D. A.; Western, C. M.; Howard, B. J. *J. Phys. Chem.* **1986**, *90*, 3331-3338.

[148] Sumiyoshi, Y.; Endo, Y. *J. Chem. Phys.* **2007**, *127*, 184309.

[149] Kim, Y.; Fleniken, J.; Meyer, H.; Alexander, M. H.; Dagdigian, P. J. *J. Chem. Phys.* **2000**, *113*, 73-85.

[150] Wen, B.; Kim, Y.; Meyer, H.; Klos, J.; Alexander, M. H. *J. Phys. Chem. A* **2008**, *112*, 9483-9493.

[151] Wayne, R. P. *Chemistry of Atmospheres : An Introduction to the Chemistry of the Atmospheres of Earth, the Planets, and their Satellites*; 2nd ed.; Oxford University Press: New York, 1991.

[152] Zhou, Z. W.; Todd, B. D.; Travis, K. P.; Sadus, R. J. *J. Chem. Phys.* **2005**, *123*, 054505.

[153] Fredin, L. *Chem. Scr.* **1973**, *4*, 97-102.

[154] Ball, D. W. *J. Phys. Chem. A* **1997**, *101*, 4835-4837.

[155] Myszkiewicz, G.; Sadlej, J. *Chem. Phys. Lett.* **2000**, *318*, 232-239.

[156] Dozova, N.; Krim, L.; Alikhani, M. E.; Lacome, N. *J. Phys. Chem. A* **2006**, *110*, 11617-11626.

[157] Gonzalez, M. M.; Bravo-Rodriguez, K.; Suardiaz, R.; de la Vega, J. M. G.; Montero, L. A.; Sanchez-Garcia, E.; Crespo-Otero, R. *Theor. Chem. Acc.* **2015**, *134*, 1-12.

[158] Poad, B. L. J.; Johnson, C. J.; Continetti, R. E. *Faraday Discuss.* **2011**, *150*, 481-492.

[159] Cybulski, H.; Zuchowski, P. S.; Fernandez, B.; Sadlej, J. *J. Chem. Phys.* **2009**, *130*, 104303.